REPORT DOCUMENTATION PAGE

Form Approved

AFRL-SR-BL-TR-98-

0413

1. AGENCY USE ONLY (Leave Blank)	2. REPORT DATE	3. REPORT
	1992	Final

4. TITLE AND SUBTITLE
Infrared Spectropolarimetry

5. FUNDING NUMBERS

6. AUTHORS
David Blair Chenault

7. PERFORMING ORGANIZATION NAME(S) AND ADDRESS(ES)
University of Alabama in Huntsville

8. PERFORMING ORGANIZATION REPORT NUMBER

9. SPONSORING/MONITORING AGENCY NAME(S) AND ADDRESS(ES)
AFOSR/NI
110 Duncan Avenue, Room B-115
Bolling Air Force Base, DC 20332-8080

10. SPONSORING/MONITORING AGENCY REPORT NUMBER

11. SUPPLEMENTARY NOTES

12a. DISTRIBUTION AVAILABILITY STATEMENT
Approved for Public Release

12b. DISTRIBUTION CODE

13. ABSTRACT *(Maximum 200 words)*
See attached.

14. SUBJECT TERMS

15. NUMBER OF PAGES

16. PRICE CODE

17. SECURITY CLASSIFICATION OF REPORT	18. SECURITY CLASSIFICATION OF THIS PAGE	19. SECURITY CLASSIFICATION OF ABSTRACT	20. LIMITATION OF ABSTRACT
Unclassified	Unclassified	Unclassified	UL

Infrared Spectropolarimetry

by

David Blair Chenault

A Dissertation

Submitted in partial fulfillment of the requirements
for the degree of Doctor of Philosophy in
The Department of Physics
of
The School of Graduate Studies

of

The University of Alabama in Huntsville

1992

ACKNOWLEDGEMENTS

The research described in this dissertation would not have been possible without the inspiration and direction of Dr. Russell A. Chipman. I am indebted to him for encouraging and guiding my professional development and the unique opportunities for learning he has provided me.

I am also grateful to Dr. Dennis H. Goldstein for his support and the many opportunities he and the Air Force have afforded me.

I would like to thank my committee for their encouragement and support:

Dr. J. Graeme Duthie, Dr. Lloyd W. Hillman, Dr. Don Gregory, Dr. C. C. Sung, and Dr. Mustafa Abushagur.

I wish to thank all those who have made contributions through the many useful discussions of polarimetry, proofreading, moral support, and other miscellaneous but much appreciated help:

J. Larry Pezzaniti, Dr. Steven C. McClain, Daniel J. Reiley, Shih-Yau Lu, Randy Gove, Rodney Fuller, Dan Brown, Dr. and Mrs. Michael Banish, and David Thigpen.

I must also thank my parents, Dr. and Mrs. Sidney Chenault, who encouraged and supported me throughout my education.

And last, but certainly not least, I thank my beautiful wife, Dawn, for supporting and encouraging me and for suffering the many long hours required to complete this work.

This research was sponsored in part by the Air Force Laboratory Graduate Fellowship Program contract F46920-86-C-0127/SB5861-0436, the Universal Energy Systems Graduate Student Research Program, contract F49620-88-C-0053, and the Universal Energy Systems Research Initiative Program, contract P.O. S-210-9MG-026 and the Air Force Office of Scientific Research, Bolling AFB, DC. Additional support was provided by the U.S. Army Missile Command.

To the memory of my mother,

Frances Gwaltney Chenault

ABSTRACT

A new instrument, a Fourier transform infrared (FTIR) spectropolarimeter, has been developed to characterize the elements of polarization critical optical systems. The rotating sample spectropolarimeter measures linear diattenuation (polarization) and linear retardance spectra of samples over a spectral range from 2.5 to 20 μm. The dual rotating retarder spectropolarimeter measures Mueller matrix spectra from 3 to 14 μm. This information provides essential data on the wavelength response of polarization elements and the modulation characteristics of spatial light modulators as a function of wavelength.

This dissertation describes data reduction algorithms for the rotating sample and dual rotating retarder polarimeters. The discussion includes description of common sources of systematic errors in polarimetric systems and how many of these errors are reduced or removed through the choice of appropriate measurement parameters and Fourier analysis of the polarimetric signal. The data reduction algorithms for spectropolarimetric measurements incorporate the wavelength dependence of the polarization elements. Self-calibration data reduction methods are also described.

Linear diattenuation, linear retardance, and linear birefringence spectra of cadmium sulfide and cadmium selenide multiple order waveplates and three liquid crystal materials are presented. Linear diattenuation and linear retardance calibration spectra of the polarization elements used in the spectropolarimeter, an infrared wire grid polarizer on a zinc selenide substrate and an infrared achromatic quarter

wave retarder, are also given. Mueller matrix spectra of a cadmium telluride modulator are given as a function of voltage. The electro-optic coefficient spectrum of cadmium telluride calculated from the Mueller matrix spectra is presented.

TABLE OF CONTENTS

LIST OF FIGURES

LIST OF TABLES

Chapter I

Introduction

This dissertation describes the development of the infrared spectropolarimeter, an instrument for the spectral characterization of the polarization properties of infrared materials and devices. The instrument is an FTIR spectrometer with a polarimeter placed in the sample compartment. The data reduction and instrumental configurations for the measurement of infrared polarization spectra, including Mueller matrix spectra, are described in this dissertation. The development of this metrology technique has included the calibration of the spectrometer, the polarimeter, and the polarization elements of the polarimeter. Calibration spectra have been made for each of these components and incorporated into the data reduction schemes for each of the various types of instrumental configurations.

The development of many infrared systems for optical computing, optical signal processing, optical interconnects, scene simulation, and neural networks is dependent on the spectral polarization characterization of two crucial components, polarization elements and spatial light modulators. Lack of spectral data on these

components has impeded and limited efforts to improve infrared instrumentation; this deficiency and the importance of these devices have been widely documented [1],[2],[3],[4].

Polarization data for polarization elements, polarizers and retardation devices, although partially characterized, remains incomplete. For example, the transmission spectrum for stock polarizers is available from most manufacturers; in some cases, spectra of extinction ratios are available [5]. However, complete polarization data -- such as retardance data for polarizers, and diattenuation data for retarders -- is not yet available.

Spatial light modulators (SLM's) have been characterized to even a lesser extent than polarization elements. SLM's are generally conceded to have less than desirable response in speed and contrast ratio [6],[7],[8]. Many of the materials traditionally used in these devices, such as cadmium telluride, cadmium sulfide, cadmium selenide, zinc selenide, and many others, have not been characterized as a function of wavelength. Continued spatial light modulator development requires systematic approaches to acquire further polarization data on existing SLM's and on potential SLM materials. A whole new class of potential modulator materials, liquid crystals, are still being characterized in the visible. Very little data has been collected in the technically more difficult infrared.

A new instrument, a Fourier transform infrared (FTIR) spectropolarimeter, has been developed to characterize the elements of these polarization critical optical systems. The spectral capability of the spectropolarimeter permits the investigation of the sample's polarization properties in all wavelength regions in the mid-infrared simultaneously. The spectropolarimeter produces calibration spectra

of the wavelength response of polarizing elements and provides essential data on the modulation characteristics of spatial light modulators as a function of wavelength.

In addition, extensions of the measurement techniques that were developed as part of this research are applicable to other parts of the spectrum and increase the flexibility of laser polarimeters. The spectropolarimeter's wide range of capability has resulted in a number of spectral polarization measurements -- Faraday rotation spectra of CdTe, used to demonstrate a quality control method for infrared detector fabrication; linear birefringence of CdS and CdSe waveplates, used to develop dispersion relations beyond the wavelength range of previously published relations; and linear diattenuation and linear birefringence data on liquid crystals, the first experimental data of its kind in the infrared.

The objectives of the research described in this dissertation are to develop a new class of instrumentation and measurement techniques to characterize the polarization properties of infrared samples. This development must include the calibration of the spectrometer, the polarimeter, and the polarization elements of the polarimeter. Calibration spectra must be made for each of these components and incorporated into the data reduction schemes for each of the various types of measurements. An estimate of the accuracy for each of the measurements must be made. Finally, measurements on samples of interest will be made to demonstrate the technique. The research should enable researchers to obtain new optical constants, a deeper understanding of polarization elements, and open the door for development of infrared polarizing optical systems.

This dissertation covers three topics of polarization spectroscopy or spectropolarimetry: the techniques, algorithms, and issues of spectropolarimetry that are

transportable to any wavelength band, the FTIR spectropolarimeter and the issues of infrared spectropolarimetry, and the results and interpretations obtained with the FTIR spectropolarimeter.

The first part of this dissertation is review and overview of spectropolarimetry. The first part of Chapter II gives definitions used in this dissertation and a brief review of the Mueller calculus and Jones calculus. The second part gives a brief review of some of the work in spectropolarimetry in all wavelength bands from the ultraviolet to the far infrared. Chapter III discusses basic concepts of polarimetry and introduces the important concept of Fourier analysis of polarimetric signals. The extension of polarimetry to many wavelengths with discussion of some of the issues and problems are also included in this Chapter. Chapter III also describes the instrument used to measure infrared spectra, the Fourier transform infrared spectrometer, and the polarization elements used in the spectropolarimeter.

The next several chapters describe the development of the Fourier transform infrared spectropolarimeter that is the subject of this dissertation. The rotating sample polarimeter and its application to the calibration of the retarders used in the Mueller matrix polarimeter are discussed in Chapter IV. Chapter V presents examples of data taken with the rotating sample spectropolarimeter including the birefringence for cadmium sulfide and cadmium selenide and birefringence and diattenuation of liquid crystals. Chapter VI describes the Mueller matrix spectropolarimeter and develops the data reduction equations that produce the measured Mueller matrix. The equations describing the ideal case assuming perfect polarization elements are developed first, followed by a discussion of how various systematic errors affect the results. The equations that eliminate the largest of these errors are then developed. The sources of the residual systematic errors in Mueller

matrix measurements are discussed in this Chapter. Measurements on a cadmium telluride electro-optic modulator using the data reduction equations developed in Chapter VI are described in Chapter VII. The electro-optic coefficient spectrum and the Mueller matrix spectra from which it is derived are shown.

Chapter VIII introduces a new formalism for describing polarimetric data reduction. A natural extension of this formalism allows for self-calibration of the polarimetric data reduction process. This formalism should allow a polarimeter to be calibrated for many polarimetric systematic errors without requiring a priori knowledge of the type of error and is proposed as the next step for improving the accuracy of polarimetric measurements.

The results and accomplishments of this doctoral research is summarized in Chapter IX. This Chapter also discusses future directions for research with the infrared spectropolarimeter.

Chapter II

Background

It is appropriate to define several terms that are used throughout this dissertation. Terminology describing polarization characteristics and elements, methods of measurement, and the mathematical systems that describe polarization are reviewed in the first half of this Chapter. A brief review of previous work is presented in the second half.

A. Definitions

1. Polarization Terminology

Polarimetry is the measurement of the state of polarization of optical radiation, or the measurement of the change of state of polarization by propagation through an optical material [1]. Polarimetry measures the complete state of polarization including any unpolarized component. Alternatively, polarimetry measures the polarizing characteristics of a sample as well as any change in the degree of polarization resulting from propagation through the sample.

Spectropolarimetry is an extension of polarimetry from a monochromatic or quasi-monochromatic wavelength to a spectrally resolved wavelength band or to several discrete wavelengths. Laser polarimetry at several discrete wavelengths could be termed spectropolarimetry, but for the present purpose spectropolarimetry

is defined as making polarimetric measurements as a continuous function of wavelength over a given spectral band. The techniques developed in this dissertation are applicable and useful in laser polarimeters [10].

The eigenpolarization states of a polarization element are useful when discussing polarization devices. Eigenpolarization states are defined to be the polarization states that are transmitted unchanged through a device or material except for overall amplitude and absolute phase changes. For every polarization element, there are two eigenpolarizations that define the fundamental polarization properties of the element. The eigenpolarizations of a polarization element are eigenvectors of its corresponding Mueller matrix. Further discussion of eigenpolarizations may be found in the references [11],[12],[13].

Multiple definitions of the words polarizer and polarization suggest the need for exact definitions of polarization elements. The following definitions will be used in this work [14]. A polarization element is defined as an optical element that alters the polarization state of light such as a dichroic polarizer, a retarder, a diffraction grating, or a thin film. A polarizer is an optical element that transmits a fixed polarization state independent of the incident polarization state. Although the polarization state of the transmitted light is independent of the incident polarization state, the intensity of the transmitted light does depend on the incident state. This merely describes formally, for example, the effect of changing the orientation of linearly polarized light incident on a linear polarizer. The uses of polarizer and analyzer in this dissertation follow common usage.

Diattenuation refers to different amounts of attenuation of the two eigenpolarization states. The transmitted intensity depends on the polarization state of the incident beam; the transmitted intensity is a maximum for one eigenpolarization

and a minimum for the other. Diattenuation is the more exact terminology for one common usage of the word polarization, that of the effect of a polarizer. The diattenuation $\mathcal{D}$ of an optical element ranges between 0 and 1 or between 0 and 100% and is defined

$$\mathcal{D} = \frac{I_1 - I_2}{I_1 + I_2}, \tag{2-1}$$

where I_1 and I_2 are the intensity transmittances of the eigenpolarizations (principal transmittances) of the element. A diattenuator is an optical element that exhibits diattenuation. A perfect polarizer has a diattenuation of 1 ; for a partial polarizer $0 < \mathcal{D} < 1$.

Retardance is the polarization dependent phase change associated with a polarization element or system. The transmitted phase is a maximum for one eigenpolarization state and a minimum for the other eigenpolarization. The difference in the phases for the two eigenpolarizations is the retardance. For an anisotropic material where the refractive indices for the two eigenpolarization states are n_1 and n_2 the retardance δ is given by

$$\delta = \frac{2\pi}{\lambda}(n_1 - n_2)d, \tag{2-2}$$

where the thickness is d, and λ is the wavelength.

The refractive indices of the two eigenpolarization are determined from the index ellipsoid of the medium and the direction of propagation through the medium [11],[15]. The birefringence Δn of the anisotropic medium is given by the difference of the indices

$$\Delta n = | n_1 - n_2 | . \tag{2-3}$$

For uniaxial media, the indices are the extraordinary n_e and ordinary n_o refractive indices.

A retarder is a polarization element with a phase difference between the output beams for incident eigenpolarization states. Many retarder designs utilize the phase difference accumulated in transmission through a birefringent medium and are called waveplates in common usage. Waveplates represent a subset of retarders. Modulation devices such as photo-elastic modulators (PEMs) [16],[17],[18], electro-optic modulators [18],[19], or magneto-optic modulators are adjustable or time varying retarders. These devices depend on a driving electric, magnetic, or acoustic signal to vary the retardance.

The most common configuration of retarder is the waveplate, a plane parallel plate of birefringent material, with the crystal axis oriented perpendicular to the propagation direction of light. An appropriate thickness plate d such that $\Delta n d = m\lambda/4$ (m odd) comprises a so called "quarter wave retarder." If m is one, the element truly is a quarter wave retarder and commercially is referred to as a "zero order" waveplate or retarder. The zero order waveplate may be inappropriately thin however. As the wavelength varies, the retardance of the zero order waveplate must also vary, unless by coincidence the birefringence were linearly proportional to wavelength. Since this doesn't occur in practice, the waveplate is only approximately quarter wave for a small wavelength range. For higher order waveplates, $m = 3, 5, \ldots$, the effective wavelength range for quarter wave retardance is even smaller.

2. The Mueller Calculus

Quantitative analysis of polarizing systems requires a mathematical formalism for describing the polarization state of a light beam and the polarization altering

properties of polarization elements. The two principal computational methods for treating polarization problems are the Jones calculus and the Mueller calculus. The Mueller calculus is used primarily in this dissertation and a summary of the Mueller calculus is given here. Further discussion of the Mueller calculus may be found in references [11],[15],[20],[21].

The polarization state of a light beam is described by the Stokes vector, a four element real vector $\vec{S}$

$$\vec{S} = \begin{pmatrix} S_0 \\ S_1 \\ S_2 \\ S_3 \end{pmatrix} = S_0 \begin{pmatrix} 1 \\ s_1 \\ s_2 \\ s_3 \end{pmatrix}, \tag{2-4}$$

where the lower case letters represent elements normalized by the first element of the vector S_0. The units of the Stokes vector are intensity. The first element of the Stokes vector S_0 gives the intensity of the beam and is the only element that is directly measurable by experiment. The other three elements of the Stokes vector describe the polarization state of the light and give the "preference" for horizontal, $+45°$, and right circular polarized light. Formally, the s_1 element represents the difference in intensities for horizontally and vertically polarized light, the s_2 element is the difference in intensities for light polarized along the $\pm 45°$ axes, and s_3 is the difference of right and left circularly polarized light. For the normalized Stokes vector, the elements range from 1 to -1. The s_1 element takes on a value of 1 for completely horizontally polarized light and is -1 for completely vertically polarized light. Similarly, the s_2 element is 1 and -1 for $+45°$ and $-45°$ polarized light, and for $s_3 = 1$ represents right circular light and $s_3 = -1$ is left circular. The degree of polarization is found from

$$\mathrm{DOP} = \frac{\sqrt{s_1^2 + s_2^2 + s_3^2}}{s_0}$$

$$\mathrm{DOLP} = \frac{\sqrt{s_1^2 + s_2^2}}{s_0} \tag{2-5}$$

$$\mathrm{DOCP} = \frac{|s_3|}{s_0},$$

where DOP is the degree of polarization including linear and circular polarization, DOLP is the degree of linear polarization, and DOCP is the degree of circular polarization. DOP = 1 represents totally polarized light, DOLP = 1 represents totally linear polarized light, and DOCP = 1 is totally circularly polarized light.

The transformation of the polarization state of a light beam incident on a polarization element to the output polarization state is described by the Mueller matrix M , a four by four real matrix

$$\mathrm{M} = \begin{pmatrix} m_{11} & m_{12} & m_{13} & m_{14} \\ m_{21} & m_{22} & m_{23} & m_{24} \\ m_{31} & m_{32} & m_{33} & m_{34} \\ m_{41} & m_{42} & m_{43} & m_{44} \end{pmatrix}. \tag{2-6}$$

The effect of an element or system on an incident polarization state $\vec{S}_{inc}$ is found by multiplying the Mueller matrix of the element or system M by the incident Stokes vector $\vec{S}_{inc}$

$$\vec{S}_{out} = \mathrm{M}_{sys}\vec{S}_{inc}. \tag{2-7}$$

The output intensity is given by the first element of the output Stokes vector $S_{out,0}$. The Mueller matrix itself is dimensionless but may be associated with an intensity transmittance [15].

The polarization properties of an optical train are found in the system matrix. The system matrix is formed by multiplying the Mueller matrices from the left in the order that the light encounters the elements

$$\mathbf{M}_{sys} = \mathbf{M}_Q \mathbf{M}_{Q-1} \cdots \mathbf{M}_2 \mathbf{M}_1 = \prod_{i=Q,-1}^{1} \mathbf{M}_i . \tag{2-8}$$

The Mueller matrix for a polarization element rotated by an angle θ perpendicular to the incident beam is given by the matrix coordinate transformation

$$\mathbf{M}(\theta) = \mathbf{R}(-\theta)\mathbf{M}\mathbf{R}(\theta)$$

where

$$\mathbf{R}(\theta) = \begin{pmatrix} 1 & 0 & 0 & 0 \\ 0 & \cos 2\theta & \sin 2\theta & 0 \\ 0 & -\sin 2\theta & \cos 2\theta & 0 \\ 0 & 0 & 0 & 1 \end{pmatrix}, \tag{2-9}$$

where $\mathbf{M}$ is the Mueller matrix for the element in its original coordinate basis. The identity matrix $\mathbf{I}$ represents a non polarizing element

$$\mathbf{I} = \begin{pmatrix} 1 & 0 & 0 & 0 \\ 0 & 1 & 0 & 0 \\ 0 & 0 & 1 & 0 \\ 0 & 0 & 0 & 1 \end{pmatrix}. \tag{2-10}$$

The Mueller matrices for some common polarization elements are given in the references [11],[15],[17].

3. The Jones Calculus

Although the Jones calculus is not used in this dissertation and will not be described further, it is worth justifying the choice of the Mueller calculus over the Jones calculus for this work. There are two chief reasons for using the Mueller calculus in experimental work. First, the Mueller calculus is an intensity calculus -- the first element of the Stokes vector is measured directly. In the Jones calculus

intensity is calculated from the sums of squares of the electric field. Second, the Mueller matrix treats partial polarization and depolarization -- the Jones calculus does not. Where Mueller matrices are being measured and are used to characterize a polarization element, depolarization should be included as part of the characterization. The Mueller calculus is thus more suitable for experimental work in which broad band, partially polarized radiation is incident on polarization elements. A depolarizer can be represented and measured in the Mueller calculus.

Further discussion of the Jones and Mueller calculi can be found in the references [11],[15],[22]. Conversion from Jones to Mueller calculus and back can also be found in the references [16],[20],[22].

4. Polarimeters

This section briefly describes and defines types of polarimeters and their classifications. Further information may be found in references [9],[11],[23].

A Stokes polarimeter consists of an appropriate combination of polarization elements that determines the polarization state of the light beam incident on the polarimeter. The Stokes polarimeter is called complete if it measures all four elements of the Stokes vector and is incomplete or partial otherwise. The total intensity S_0 may or may not be measured depending on whether the system has been calibrated for absolute radiometric measurements. There are a number of possible configurations for Stokes polarimeters -- some of these are reviewed in the second half of this Chapter and two others will be examined in Chapter III.

A Mueller matrix polarimeter consists of an appropriate combination of polarization elements that determines the polarization altering properties of a sample by measuring the Mueller matrix of the sample. A Mueller matrix polarimeter is complete only if it measures all sixteen elements of the Mueller matrix. If less than

the complete Mueller matrix of the sample is determined, the polarimeter is incomplete. An example of an incomplete Mueller matrix polarimeter is one that measures only linear diattenuation and linear retardance while circular diattenuation and circular retardance remain unknown. A complete Mueller matrix polarimeter measures both linear and circular diattenuation and retardance. In this dissertation, a polarimeter is called a Mueller matrix polarimeter if it measures some or all of the polarization properties of a sample, even if the output is not a Mueller matrix. For example, a particular polarimeter may measure linear diattenuation and retardation and thus be capable of measuring nine elements of the Mueller matrix although the output may not be in the form of a Mueller matrix.

The term "sample" as used in this dissertation refers to any material or optical element whose properties are under examination. This can include any polarization element, optical element, optical system or subsystem, or any bulk material.

B. Review of Spectropolarimetry

Significant development of spectropolarimetric instrumentation did not begin until the middle of the twentieth century. This section gives a brief review of some of the work in spectropolarimetry in the last forty years or so. This review does not include broadband measurements labeled as spectropolarimetry that do not resolve wavelength.

An examination of previous spectropolarimetric techniques reveals that the research falls into two major categories: applications of Stokes polarimeters, and applications of Mueller matrix polarimeters. Although other divisions are possible, such as the various techniques that resolve wavelength, the division by polarimeter type is used here. Stokes polarimeters measure the Stokes vectors and thus the

polarization state of the light incident on it. Stokes polarimeters measure properties of the source or the medium between the source and the polarimeter, as in astronomy. Mueller matrix polarimeters measure the polarization properties of samples.

Some good surveys of various classifications of polarimeters are given by Hauge [23], Azzam and Bashara [11] (with emphasis on ellipsometric applications), and by Nafie [24], Kliger [17], and Michl [25] (with emphasis on chemical analysis applications). Astronomical application surveys are given by Fymat [26], Stenflo [27] and Kemp [28].

1. Astronomy and Emission Spectropolarimetry

Stokes polarimetry has been used in astronomical applications to determine a variety of properties of the astronomical source. Discussions of instrument configurations for measuring complete Stokes polarimeters are given by Fymat [29] and Hodgon [30]. Wavelength resolution is accomplished by a two beam Fourier interferometer in Fymat's instrument, and a grating monochromator in Hodgon's instrument. They each note the difficulties associated with the wavelength dependence of the retardation devices that measure circular polarization. Hodgon solves the problem by using an achromatic quartz retarder available for the ultraviolet wavelength range in his study, while Fymat suggests using quasi-monochromatic light. Fymat later used his instrument [26] to study the linear polarization of Venus in the near infrared (0.8 to 2.7 μm).

A number of researchers, Baur [31], Kemp [28],[32], Stenflo [33],[34], and Lindgren and Tarbell [35], have used various configurations of polarimeters to determine the flux and strength of magnetic fields on the sun. Baur describes a spectrum scanning Stokes polarimeter using two KDP modulators and an achromatic quarter wave plate. This instrument measures all four Stokes parameters

from 390 to 700 nm using a high resolution (.001 nm) grating. Kemp describes a synchronous detection technique that encodes linear and circular diattenuation signals onto frequencies produced by photo-elastic modulators. Solar data was gathered from 400-700 nm. Stenflo used a Fourier transform spectrometer to measure complete Stokes vectors from 500-600 nm with a resolution of tens of milliangstroms. Full Stokes vectors were measured over small wavelength ranges using Pockels cells with a retarder. Lindgren and Tarbell resolve wavelength using a scan filter. Complete Stokes vectors are determined from 510-660 nm using a linear polarizer and a tunable birefringent filter.

Other extended astrophysical objects have been characterized through their polarization properties by researchers such as Fymat [26], Gonatas [36], and Goguen [37]. Fymat's study of Venus was mentioned previously. Gonatas describes instrumentation for far infrared measurements of the Orion nebula and other galactic clouds. Linear diattenuation was measured from 50-300 μm using a wire grid polarizer. Goguen used a narrow band pass filter and a linear polarizer in the near infrared to determine the amount and materials involved in Io's volcanic activity.

Stokes polarimetry can also provide information about sources in the laboratory. Elhanine [38] describes emission spectroscopy used to calculate the Zeeman splitting of paramagnetic NO and N_2O in plasma in an externally applied magnetic field. Complete Stokes vectors were measured from .88-6.5 μm using an achromatic CaF_2 modified Fresnel rhomb and linear polarizer. Hilbst [39] studied atomic and ionic structure with a uv grating spectrometer from 50-120 nm. Incomplete Stokes vectors were measured with a linear polarizer.

2. Mueller Matrix Spectropolarimetry

There is very little in the literature describing spectral measurements of a Mueller matrix of any kind. In general, researchers have in general measured the specific polarization property or properties they are trying to quantize rather than measuring the entire Mueller matrix. Although the data is not in the form of a Mueller matrix, the review of the research described in this section presents work in spectral polarization measurements or spectropolarimetry.

The magnetooptic Faraday and Kerr rotations were measured by Krumme [40] in liquid phase iron garnet films. A grating monochromator selects a single wavelength. Two polarizers and a photo-elastic modulators are used to measure the amount of rotation and ellipticity caused by the sample. The rotation and ellipticity are encoded on the fundamental frequency and the first harmonic of the PEM driving signal and are measured one after the other. The wavelength range was 0.26-1.8 μm.

Polarization labeling described by Teets [41] is a method for studying excited states of molecules. A polarized pump laser excites a gas mixture which is then probed by a broadband laser source. A probe laser analyzes the optical anisotropies induced by the polarized pump beam. Various pump polarization produce different anisotropies; a circularly polarized pump beam produces circular birefringence and dichroism. The beam is analyzed by a high resolution spectrograph. Results from the 474 - 498 nm wavelength band produced new spectroscopic constants for excited states of sodium.

One application of infrared spectropolarimetry is in chemistry, where molecular order can be investigated in a variety of ways. The order can be due to long range alignment of the molecules as in an oriented polymer film or a molecular

crystal, or due to a chirality or handedness in the sample. Nafie [24] and others [17],[25] describe several techniques that measure small amounts of linear and circular dichroism for investigating molecular structure of molecules having infrared transitions. A Michelson interferometer is used to resolve wavelength. An IR beam modulated in intensity at the Fourier frequency of the wavelengths present emerges from the interferometer and passes through a linear polarizer. The beam then passes through a PEM modulating at a frequency an order of magnitude higher than the highest Fourier frequency. The light, now oscillating between left and right elliptically polarized light, passes through the sample onto the detector. The spectrum taken with the sample present is ratioed to the spectrum without the sample present. This ratio, coupled with a calibration measurement that takes care of instrumental transmission, gives the circular dichroic ratios with a resolution of 10^{-4}. Nafie presented circular dichroism spectra from 6.3 to 10.6 μm.

Another method is the interferometric modulation or polarizing Michelson interferometer (PMI) technique [24],[42],[43]. In this case, the conventional beamsplitter in the interferometer is replaced by a polarizing beamsplitter. This produces a modulation in polarization rather than in intensity as in conventional interferometers. A polarizer is placed before the interferometer and measurements are made with and without an analyzer placed between the sample and PMI. These spectra are ratioed to give vibrational circular dichroism spectra. Linear dichroism can be detected by rotating the polarizer placed before the PMI and making a similar series of measurements.

Infrared spectral measurements on the birefringence of liquid crystals has been reported by Wu [44]. The intensities passed by parallel and perpendicular polarizers on either side of the sample were measured. The retardance of the sample is

calculated from the ratioed intensities to within an additive constant of π. One measurement at a laser wavelength is required to determine this constant. The birefringence can then be calculated from the retardance and Eq. 2-2. Wu presents results on several liquid crystals from 2 to 16 μm taken in an FTIR spectrometer.

Chapter III

Polarimetry and

Spectropolarimetry

Spectropolarimetry is the measurement of polarization properties and characteristics of materials as a function of wavelength. Consideration of the spectral nature of spectropolarimetric measurements is vital to making accurate polarimetric measurements of materials and devices. A discussion of polarimetry at a single wavelength and algorithms for data reduction can provide insight into many of the experimental issues of spectropolarimetry.

In this Chapter, a black box discussion of polarimetry and algorithms for data reduction is given. This discussion is intended to present the basics of polarimetry and to show the motivation for the particular polarimeter configurations and measurement sequences presented in later chapters. The Fourier analysis of polarimetric signals and the advantages of this method of data reduction for polarimetric measurements are presented. Procedures for developing the data reduction equations for specific polarimetric configurations and measurement sequences that exploit the advantages of the Fourier method of data reduction are given. A simple example is used to demonstrate and clarify these procedures.

The measurement of the wavelength dependent polarization properties of samples requires an instrument to measure intensity as a function of wavelength and appropriate polarization elements. This Chapter describes the Fourier transform infrared spectrometer and the infrared polarization elements used in the spectrometer for spectropolarimetric measurements.

A. Polarimetry

Polarimeters measure the polarization properties and characteristics of light and optical elements. Polarimeters can take many forms and measure some or all of the polarization properties of a sample. This section describes polarimeters and polarimetric data reduction for polarimetric measurements at a single wavelength.

1. Polarimeter Configurations

Polarimeters can be divided into five subsystems. Figure 3-1 shows the layout of the polarimetric configuration under consideration. It consists of a source, a polarization state generator (PSG), a sample, a polarization state analyzer (PSA), and a detector.

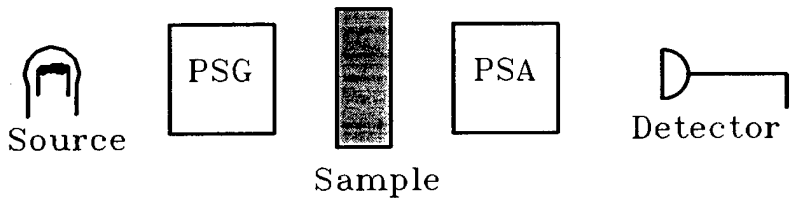

Figure 3-1 Block diagram of general polarimeter.

The polarization state generator contains a polarizing element or combination of polarizing elements that delivers a known polarization state to the sample. The polarization state analyzer consists of a combination of polarizing elements that determines the polarization state of the light incident on it. In the polarimeter of

Fig. 3-1, the polarization state analyzer measures the polarization state transmitted by the sample. With this configuration, the polarization properties of the sample are determined.

The operation of this polarimeter can be described as follows: the optical radiation from the source is polarized into a known polarization state by the polarization state generator. The polarization state is altered in some manner by the sample and is then analyzed by the polarization state analyzer. By changing the configuration of the polarization state analyzer, the response of the sample to the state delivered to the sample by the polarization state generator is completely characterized. By analyzing the interaction of the sample to various states generated by the polarization state generator, the sample's polarization properties are completely characterized.

Mueller matrix polarimetry may be understood in a fundamental way through the following quantitative argument. The polarization state analyzer analyzes the effect of the sample on a particular polarization state set up by the polarization state generator. If the polarization state analyzer is complete, one column of the sample Mueller matrix is determined. To determine the other columns, the sample's response to other incident polarization states must be measured, i.e measurements must be made for different states set up by the polarization state generator. The Mueller matrix is determined by choosing a combination of incident and analyzing polarization states such that the sample's response to a minimum set of basis states are spanned by the measurements. If a polarization state analyzer is incomplete, a row of the sample Mueller matrix is undetermined. Similarly a partial polarization state generator leaves a column of the sample Mueller matrix undetermined. A complete Mueller matrix can only be determined if both polarization state genera-

tor and polarization state analyzer are complete.

The Mueller matrix equation describing the polarimeter shown in Figure 3-1 is

$$\vec{S}' = \tau \mathbf{A} \mathbf{M}_{sample} \mathbf{G} \vec{S}_{inc}, \tag{3-1}$$

where $\vec{S}_{inc}$ is the Stokes vector of the light incident on the polarization state generator and τ is a factor including instrumental transmission and detector sensitivity. $\mathbf{G}$ is the Mueller matrix for the polarization state generator, $\mathbf{M}_{sample}$ is the Mueller matrix for the sample, and $\mathbf{A}$ is the Mueller matrix for the polarization state analyzer. The intensity i incident on the detector is given by the first element s_0' of the output Stokes vector $\vec{S}'$

$$i = s_0' = \tau(\mathbf{A} \mathbf{M}_{sample} \mathbf{G} \vec{S}_{inc})_0 \tag{3-2}$$

A Mueller matrix is determined by making a series of Q measurements with various configurations of the polarization state analyzer and generator. For the q'th measurement, $q = 0, 1, \ldots, Q-1$, the intensity i_q is

$$i_q = \tau(\mathbf{A}_q \mathbf{M}_{sample} \mathbf{G}_q \vec{S}_{inc})_0 . \tag{3-3}$$

Each intensity is a function of some of the Mueller matrix elements $i_q(m_{i,j})$. The set of $i_q(m_{i,j})$ represents a system of equations that must be solved for the elements $m_{i,j}$ in terms of the intensities. The specific polarimetric data reduction equations for calculating the sample Mueller matrix depend on the exact configuration of the elements of the polarization state generator and analyzer and how these elements are varied over the measurement sequence. Typically the response of the polarization state generator and analyzer and consequently the matrices $\mathbf{G}$ and $\mathbf{A}$ for each measurement are known. The analyzed states and generated states do not have to be the same and in general they are not.

2. Fourier Data Reduction of Polarimetric Signals

A common method of polarimetric data reduction is the Fourier analysis of polarimetric signals [23],[45],[46],[47]. The elements of the polarization state analyzer and generator are varied in a harmonic fashion. The polarization properties of the sample are encoded onto the harmonics of the detected signal. The polarization properties of the sample are then recovered from a Fourier transform of the measured data set.

Polarimeters with single and dual rotating polarizers have been used for measuring ellipsometric and scattering parameters [48],[49]. Ellipsometers and Mueller matrix polarimeters have used various combinations of rotating elements, including rotating polarizers [48], rotating the sample [50],[51], rotating polarizers and retarders [47],[52], and rotating two retarders [45],[46]. The rotating sample and dual rotating retarder methods used in this research will be described in greater detail in Chapters IV and VI.

This section introduces Fourier analysis of polarimetric signals. An example based on the Law of Malus is given. This example will be used throughout the rest of this Chapter to illustrate the extension of polarimetric signals to many wavelengths and to describe the noise and error analysis of polarimetric signals.

a. Fourier analysis of polarimetric signals

Consider a general polarimeter with a polarization state generator, a sample, and a polarization state analyzer as shown in Figure 3-1. A series of Q intensity measurements are made i_q for $q = 0, 1, \ldots Q-1$. The intensity incident on the detector for the q'th measurement i_q is

$$i_q = \tau(\mathbf{A}_q \mathbf{M}_{sample} \mathbf{G}_q \vec{S}_{inc})_0 . \tag{3-4}$$

The analyzed and generated polarization states are now modulated by varying the polarization elements of the analyzer and generator. A typical method of varying the polarization elements is by rotating some or all of the elements in discrete steps. If the angular increments of the polarization elements are constant, only discrete frequencies are generated in the detected intensity i. The detected signal can be written

$$i_q = \frac{b_0}{2} + \sum_{k=1}^{K} (b_k \cos k\theta_q + c_k \sin k\theta_q), \tag{3-5}$$

where K is the highest frequency component in the signal and $\theta_k = k\theta$ is proportional to the angular frequency of the polarization element. The elements of the sample Mueller matrix are encoded onto the various frequencies of the detected signal, i.e. the coefficients in the Fourier series expansion are functions of the sample Mueller matrix $b_k(m_{i,j})$ and $c_k(m_{i,j})$, where the subscripts i and j are the row and column indices of the Mueller matrix elements. These relations are inverted to give the Mueller matrix elements in terms of the Fourier coefficients $m_{i,j}(b_k, c_k)$. The contribution of the Fourier components to each Mueller matrix element is determined by the choice of polarization elements and measurement sequences. To determine all sixteen elements of the sample Mueller matrix, at least sixteen independent Fourier components should be produced by the modulation of the polarization elements. One configuration for measuring the complete Mueller matrix is given in Chapter VI.

The procedure for the Fourier analysis of polarimetric signals is as follows:

1) The configuration of the polarization state generator and analyzer are determined.

2) The Mueller matrix equation and intensity transmitted by the polarimeter are derived.
3) The intensity is written in the form of a Fourier series (Eq. 3-5) and the expressions for the coefficients in terms of the sample Mueller matrix elements are derived.
4) These expressions are inverted to give the Mueller matrix elements in terms of the Fourier coefficients.

The calculation of the Fourier coefficients from the measured data and the means to determine the best choice for rotation increments and total number of measurements are described in Section 3.

The Fourier analysis of polarimetric signals provides several significant advantages for data reduction. The calculation of the discrete Fourier transform automatically gives a least squares fit to the data [53]. A least squares fit is the best method to take advantage of all the data when the measurement is overdetermined. The discrete Fourier transform is also a useful analytical tool for investigating many types of systematic error such as beam wander and linear drift. The susceptibility to harmful noise sources can be reduced through adjusting the parameters of measurements and the corresponding Fourier transform. More details of the effect of noise and errors on the measurements and ways to compensate or negate these effects are given in Section B.

The magnitudes of the series coefficients in Eq. 3-5 are a function of the instrumental transmission τ. In polarimetry, however, the polarization properties of the sample should be independent of the absolute value of the intensity incident on it. Whenever possible, it is useful to express the data reduction equations in the form of ratios of the series coefficients so that the polarization properties are indepen-

dent of instrumental transmission. When it is not possible to construct ratios, it is necessary to normalize the coefficients by dividing all coefficients by the dc term b_0. Instrumental transmission is calibrated out in this manner. The factor τ will be omitted hereafter.

It should be noted that the sample Mueller matrix need not be completely arbitrary. If the polarization properties of the sample are known qualitatively and these polarization properties only need to be quantified, a physically reasonable model for the sample is chosen and the appropriate sample Mueller matrix is written in terms of this model. The arbitrary Mueller matrix is replaced by this Mueller matrix. The complexity of the data reduction is reduced since in many cases some of the sample Mueller matrix elements become zero. In this case the data reduction is developed in terms of the polarization properties modelled. The rotating sample polarimeter, in which the arbitrary sample Mueller matrix is replaced by the matrix for a sample with linear diattenuation and retardance, provides a good example and is presented in Chapter IV.

b. Example of Fourier analysis of polarimetric signals

A simple example will be examined to illustrate the Fourier analysis of polarimetric signals. In this example the Law of Malus is generalized. The diattenuation and initial orientation of a diattenuator rotated in front of an ideal polarizer are determined through the Fourier analysis of the detected polarimetric signal.

The Law of Malus is described in most basic optics texts. It describes the intensity of the light transmitted through a pair of polarizers whose principal axes are an angle θ apart (Figure 3-2). It was first described by Malus in the early 1800's [54],[55] and derived from observation. The (normalized) intensity i transmitted by the two polarizers with unpolarized incident light is given by

$$i(\theta) = \frac{i'(\theta)}{i_0} = \frac{1}{2}\cos^2\theta, \tag{3-6}$$

where i is the incident intensity.

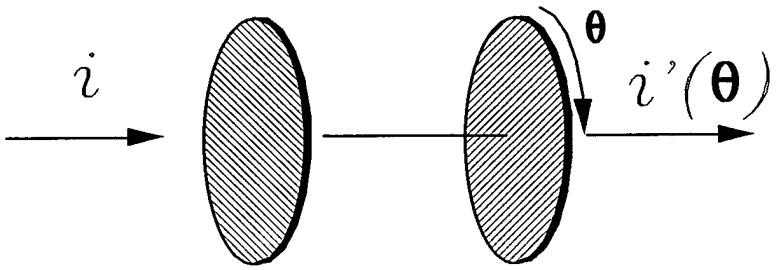

Figure 3-2 Fixed polarizer, rotating diattenuator polarimeter.

The Law of Malus is derived using the Mueller calculus. The Stokes vector transmitted through a polarizer $\mathbf{M}_p$ whose principal transmission axis is fixed along the x-axis, followed by a polarizer at angle θ to the x-axis $\mathbf{M}_p(\theta)$ is transformed according to

$$\vec{S}' = \mathbf{R}(-\theta)\mathbf{M}_p(0)\mathbf{R}(\theta)\mathbf{M}_p(0)\vec{S}_{inc} = \mathbf{M}_p(\theta)\mathbf{M}_p(0)\vec{S}_{inc}$$

or

$$\begin{pmatrix} S'_0 \\ S'_1 \\ S'_2 \\ S'_3 \end{pmatrix} = \frac{1}{4}\begin{pmatrix} 1 & \cos 2\theta & \sin 2\theta & 0 \\ \cos 2\theta & \cos^2 2\theta & \cos 2\theta \sin 2\theta & 0 \\ \sin 2\theta & \cos 2\theta \sin 2\theta & \sin^2 2\theta & 0 \\ 0 & 0 & 0 & 0 \end{pmatrix}\begin{pmatrix} 1 & 1 & 0 & 0 \\ 1 & 1 & 0 & 0 \\ 0 & 0 & 0 & 0 \\ 0 & 0 & 0 & 0 \end{pmatrix}\begin{pmatrix} 1 \\ s_1 \\ s_2 \\ s_3 \end{pmatrix}. \tag{3-7}$$

The normalized intensity for unpolarized incident light is

$$i(\theta) = \frac{1}{4}[1 + \cos 2\theta] \tag{3-8}$$

which is Malus' Law (Eq. 3-6).

The Law of Malus is now generalized. Consider the rotating diattenuator polarimeter of Fig. 3-2 where the second polarizer is replaced by a diattenuator whose diattenuation $\mathcal{D}$ and orientation θ_d with respect to the x-axis are unknown. The Mueller matrix of a diattenuator M_d is

$$\mathrm{M}_d(\mathcal{D}) = \frac{p_1 + p_2}{2}\begin{pmatrix} 1 & \mathcal{D} & 0 & 0 \\ \mathcal{D} & 1 & 0 & 0 \\ 0 & 0 & \sqrt{1-\mathcal{D}^2} & 0 \\ 0 & 0 & 0 & \sqrt{1-\mathcal{D}^2} \end{pmatrix} \tag{3-9}$$

where p_1 and p_2 are the principal intensity transmittances for the device and $\mathcal{D}$ is the diattenuation (Eq. 2-1). If the light incident on the polarizer is unpolarized, the normalized intensity of the light transmitted by the polarizer and diattenuator is

$$i(\theta) = \frac{1}{4}(p_1 + p_2)(1 + \mathcal{D}\cos 2\theta). \tag{3-10}$$

This can be considered a Fourier series of the form

$$i_q = \frac{b_0}{2} + \sum_k (b_k \cos k\theta_q + c_k \sin k\theta_q), \tag{3-11}$$

with one harmonic term. The coefficients are

$$\begin{aligned} b_0 &= \frac{p_1 + p_2}{2} \\ b_2 &= \frac{1}{4}(p_1 + p_2)\mathcal{D}\cos\theta_d \\ c_2 &= \frac{1}{4}(p_1 + p_2)\mathcal{D}\sin\theta_d \end{aligned} \tag{3-12}$$

where θ_d is the initial orientation of the principal transmission axis p_1. All other coefficients are zero. The diattenuation $\mathcal{D}$ and orientation of the principal axis θ_d of the diattenuator are then easily determined in terms of the Fourier coefficients,

$$\mathcal{D} = \frac{p_1 - p_2}{p_1 + p_2} = \frac{\sqrt{b_2^2 + c_2^2}}{b_0}\theta_d = \frac{1}{2}\tan^{-1}\left(\frac{c_2}{b_2}\right). \tag{3-13}$$

Figure 3-3 demonstrates these relationships. Figure 3-3(a) shows the intensity modulation when the second element is non-polarizing (i.e. $\mathcal{D} = 0$) there is no modulation. Figure 3-3(b) is the intensity modulation versus angle when $\mathcal{D} = 50\%$ and the initial orientation of the principal axis is θ_d. The third figure shows the intensity modulation for a perfect polarizer, $\mathcal{D} = 100\%$, where the depth of modulation is a maximum. It can thus be seen that the diattenuation of the partial polarizer is related to the depth of modulation of the polarimetric signal and the orientation is given by the phase of the modulated signal.

The rotating diattenuator polarimeter demonstrates the Fourier analysis of polarimetric signals that will be used in more complicated polarimetric systems where many Fourier frequencies and polarization properties may be present.

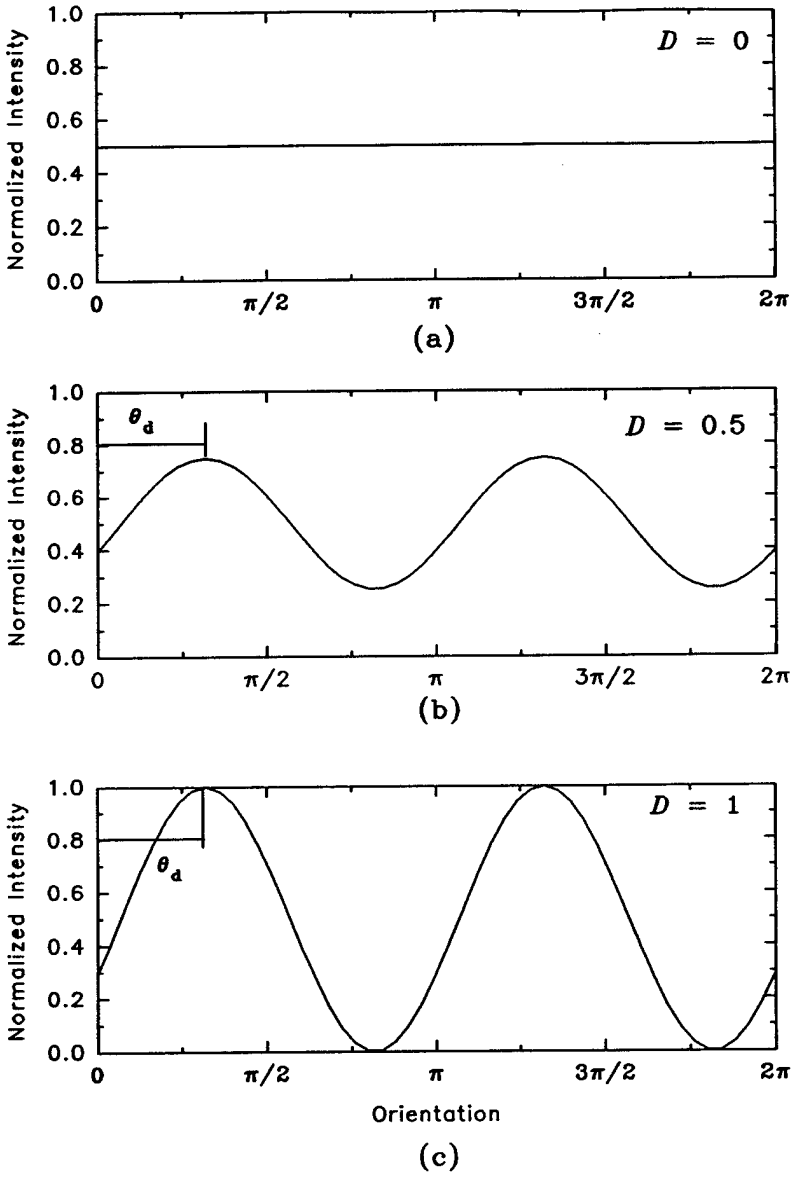

Figure 3-3 Intensity modulation of rotating diattenuator.

3. Fourier Analysis of Measured Data

The analytical expression for the polarization properties of the sample is determined in terms of the Fourier coefficients by the procedure described in the previous section. The values of the Fourier coefficients must now be calculated from the experimentally determined data set. This section describes the discrete Fourier transform and how the measurement parameters, such as angular increment and number of measurements, are determined for the measurement.

Consider a series of polarimetric measurements where an intensity measurement is made between discrete rotations of one or more of the polarization elements. The rotational increments are constant and generate a finite number of discrete frequencies in the detected signal. The set of Q intensities i_q, $q = 0, 1, 2, \ldots, Q-1$, may be expressed as a Fourier series

$$i_q = b_0 + \sum_{k=1}^{K} (b_k \cos k\theta_q + c_k \sin k\theta_q), \tag{3-14}$$

where K is the largest frequency present in the signal. The coefficients are determined from the set of intensities i_q by a discrete Fourier transform

$$b_0 = \frac{1}{Q}\sum_{q=0}^{Q-1} i_q$$

$$b_k = \frac{2}{Q}\sum_{q=0}^{Q-1} i_q \cos\left(\frac{2qk\pi}{Q}\right) = \frac{2}{Q}\sum_{q=0}^{Q-1} i_q \cos(k\theta_q) \tag{3-15}$$

$$c_k = \frac{2}{Q}\sum_{q=0}^{Q-1} i_q \sin\left(\frac{2qk\pi}{Q}\right) = \frac{2}{Q}\sum_{q=0}^{Q-1} i_q \sin(k\theta_q),$$

where k is the harmonic, $\theta_q = q\,\Delta\theta$, and $\Delta\theta$ is the angular increment of the polarization elements. For Q intensities, the coefficients for the $K = Q/2$ harmonics are found. The step size of the rotation $\Delta\theta$ of the polarization element is determined by the number of measurements $\Delta\theta = 2\pi/Q$.

The highest harmonic K in the polarimetric signal is known from the analytical expression for the intensity written as a Fourier series (Eq. 3-5). The minimum number of measurements Q_{min} required to calculate the dc term and all cosine and sine (real and imaginary) terms in the Fourier transform is $Q_{min} = 2K + 1$ [56]. It is often desirable to make more measurements than the minimum, or oversample, to help reduce the effects of noise. For oversampled data, the harmonics higher than the frequencies of the polarimetric signal are often used as a diagnostic tool to indicate sources of systematic error.

The procedure for making polarimetric measurements using Fourier analysis for data reduction is summarized as follows:

1) The highest frequency expected from the polarimetric signal K is determined from the analytical expression for the intensity.
2) The total number of measurements Q and angular increments for the rotation of the polarization elements $\Delta\theta$ are determined from the highest frequency and the measurement period T.
3) An intensity measurement i_0 is made with the polarization elements at the orientation θ_0.
4) The polarization elements are rotated by $\Delta\theta$ to θ_1 and another intensity measurement i_1 is made.
5) Step 4 is repeated until Q measurements are made.

6) The Fourier coefficients are calculated by a discrete Fourier transform of the set of intensities i_q.

7) The sample Mueller matrix elements are calculated by substituting the coefficients into the data reduction equations.

In the rotating diattenuator example of Section 2.b, the intensity is

$$i(\theta) = \frac{1}{4}(p_1 + p_2)(1 + \mathcal{D}\cos 2\theta). \tag{3-16}$$

and the highest harmonic is the second, $K = 2$. The minimum number of measurements $Q_{min} = 2K + 1 = 5$. If the diattenuator is rotated through a total of $360°$, the angular increment for rotation of the diattenuator is $\Delta\theta = 2\pi/Q_{min} = 72°$.

Polarimetric systems produce modulations periodic in π since the polarization state transmitted by an ideal polarization element oriented at 0° is equivalent to the state transmitted by the polarization element oriented at 180°. If the rotating elements rotate through a measurement period $T = 2\pi$ then the frequencies of the polarimetric signal fall only on the even harmonics and all odd harmonics are zero in a system without noise. If the elements are rotated through $T' = \pi$ the polarimetric signal falls on the odd and even harmonics. The angular increment $\Delta\theta$ remains the same, but the total number of measurements becomes $Q' = Q/2$ for $T' = \pi$. Care should be taken when the noise is not negligible since the noise that would fall on the odd coefficients will be distributed over the harmonics containing the polarimetric signal. Further discussion of the effects of various noise sources on measurement results and ways to compensate or remove these effects are given in Section B.

B. Systematic Error and Noise Considerations in Spectropolarimetry

Understanding systematic error and noise considerations is essential to improving the accuracy of spectropolarimetric measurements. In polarimetry appli-

cations there are a number of issues to consider beyond the normal radiometric issues found in other light measuring systems. This Section describes some of these issues and proposed solutions as they apply to polarimeters.

1. Random Errors

A polarimeter takes a series of intensity measurements from which specific polarization properties are calculated. Each measurement is a radiometric measurement and all standard precautions to reduce noise and error in radiometry are required for polarimetry. Random errors in radiometry that affect polarimetric measurements include spatial and temporal variations in the intensity of the source, detector noise, non-linearity in the detector, electronic noise, noise introduced in analog-to-digital conversion of electronic signals, and other less quantifiable sources such as vibration, changes in temperature and humidity, power fluctuation, and stray gases in the sample compartment. Random errors may be reduced by increasing the number of measurements, signal averaging, and intelligent data reduction. Radiometric noise issues have been well documented and further discussion of these issues is found in references [19],[57],[58].

2. Systematic Errors

Systematic errors are prominent in polarimetry and often swamp random noise. These errors include non-ideal polarization elements, drift in the radiometric signal, beam wander from rotating elements, alignment errors, and instrumental polarization. Many of these errors can be reduced or compensated through improvement in the instrument or in data reduction.

Non-ideal polarization elements can be one of the biggest sources of systematic error in polarimetry. Polarizers can have diattenuation less than one and retarders can have retardances that are unknown or unexpected values.

Polarization devices made up of more than one element such as multiple plate or Fresnel rhomb retarders or Wollaston prism polarizers can produce unexpected linear or elliptical polarization states if the components of the device are misaligned. Proper calibration of these devices is critical for making accurate polarimetric measurements.

Additional problems that involve the polarization elements include polarizers that contain retardance or retarders that contain diattenuation. Unexpected polarization effects can occur in devices that rely on birefringent devices if the birefringent crystal was improperly cut and the crystal axis is misaligned. These problems are much more difficult to correct, but in practice these effects are small compared to other systematic errors.

Some typical infrared polarization devices and their wavelength dependence are described in Section E. The effect of systematic errors due to the wavelength dependence of the polarizers and retarders used in this research and the removal of these systematic errors in data reduction are described at the appropriate point in later chapters.

The Fourier analysis of polarimetric signals offers a method to check the operation of the instrument and to determine the susceptibility of polarimetric data reduction to certain systematic errors in the measurements. For a given polarimeter configuration (rotating polarizer, dual rotating retarder, etc.) the frequency content of the polarimetric signal is fixed and known. Polarimetric measurements are susceptible to error when frequency components of the systematic error falls on the frequencies in the polarimetric signal. The frequencies of the polarimetric signal can be adjusted by judicious choices of the fundamental rotation period and number of measurements so that the effect of the systematic error on the polarimetric signal is

minimized.

To investigate the effect of various common systematic errors, consider the polarimetric signal of the rotating diattenuator polarimeter example of Section A.2.b. Let the diattenuation of the diattenuator be $\mathcal{D} = 0.5$ and assume intensity measurements are made at eight positions of the diattenuator. If eight measurements are made over a measurement period of $T = 180°$, the angular increment of the diattenuator is 22.5° and the polarimetric signal falls on the dc and first harmonic components. Figure 3-4 shows a typical polarimetric signal and the discrete Fourier transform (DFT) of the signal for $T = 180°$. If sixteen measurements are made over a complete rotation $T = 360°$, the polarimetric signal lies on the dc and 2nd harmonic. Similarly, 32 measurements over 720° constrain the polarimetric signal to the dc and fourth harmonic. Figures 3-5 and 3-6 show the polarimetric signals and DFT's for the 360° and 720° cases for this example.

Drift is the change in the response of the instrument that is not related to the polarimetric signal such as caused by a change in the output of the source or in the sensitivity of the detector. In many cases the drift is nearly linear over a measurement sequence. Linear drift over a measurement sequence will couple strongly into the lower harmonics and decreasingly into the higher harmonics. Presence of strong first, second, and third harmonics indicates the possible presence of drift. Figure 3-7 shows a 5% linear increase in sensitivity of the detector over the measurement interval and its Fourier transform. By comparing Figures 3-7 and 3-4, it becomes clear that a fundamental rotation period of 180° is more susceptible to linear drift since a substantial portion of the linear drift signal appears on the first harmonic.

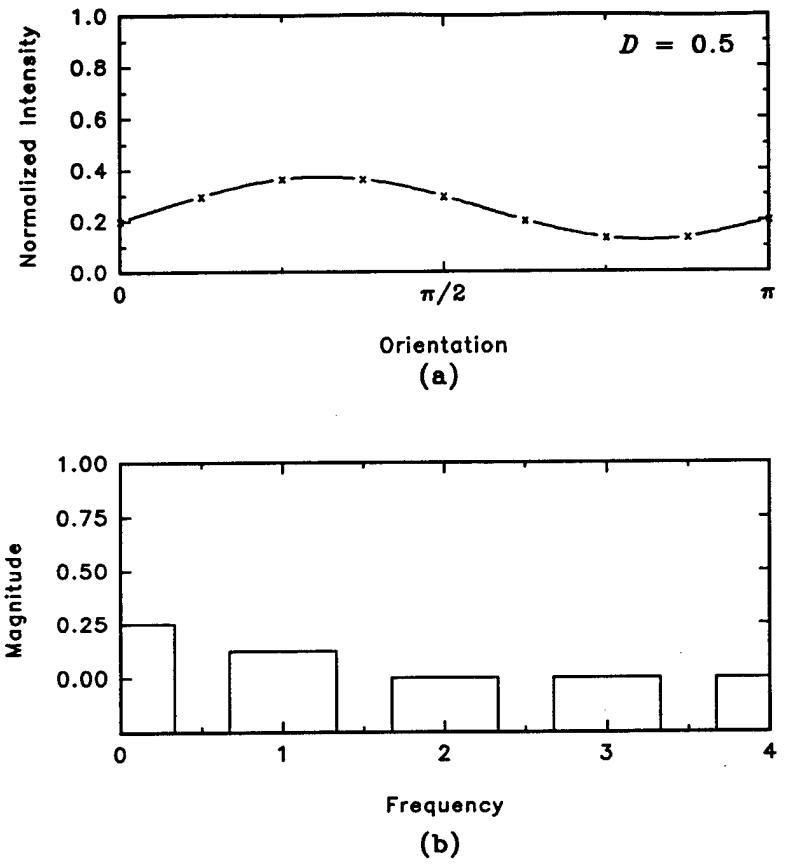

Figure 3-4 Polarimetric signal and Fourier transform of rotating diattenuator for $T = 180°$.

In polarimetric applications that utilize rotating polarization elements, beam wander becomes a problem if the rotating element has surfaces that are not plane parallel (Figure 3-8). The wedge causes a beam deviation that rotates with the element. The beam moves on the detector as the element rotates causing an intensity variation which depends on the shape of the detector, the distribution of light in the beam, and the beam path on the detector. Picture, for example, a beam moving onto and off of a detector. This intensity modulation can be mistaken as a polari-

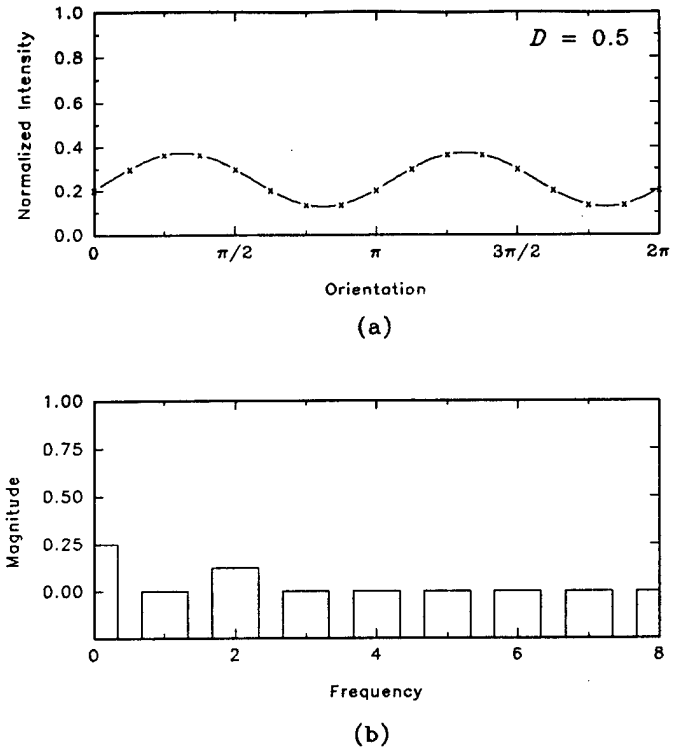

Figure 3-5 Polarimetric signal and Fourier transform of rotating diattenuator for $T = 360°$.

metric signal. However, the effect of beam wander can be minimized by choosing a measurement sequence such that the beam wander signal does not affect the polarimetric signal.

When an wedged element is rotated, the resulting beam wander signal couples most strongly into the first harmonic for a rotation of the element through 360°. Now consider a polarimeter which rotates elements through 360°. Since the polarimetric signal falls on the even frequencies for rotations through 360°, the first harmonic term in the beam wander does not overlap any polarimetric frequencies and isn't used in the polarimetric data reduction. Figure 3-9 shows the intensity

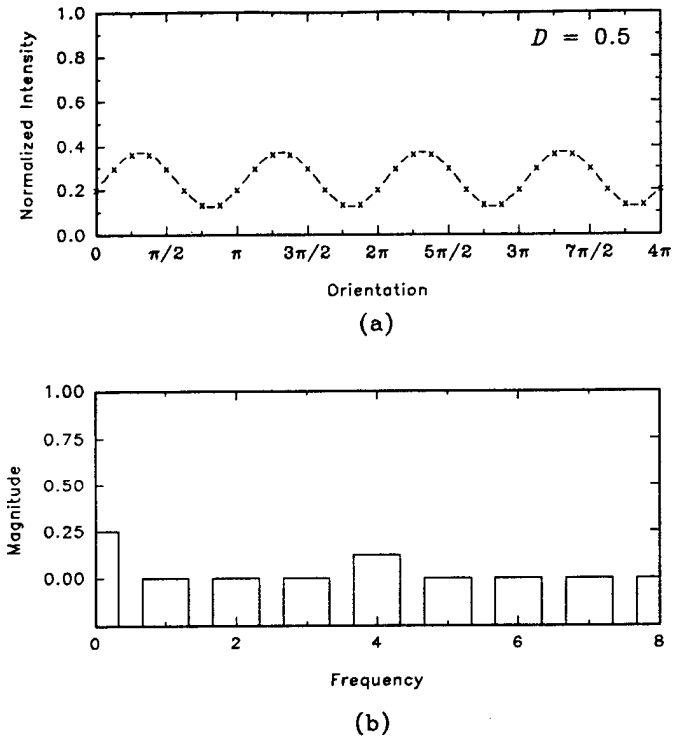

Figure 3-6 Polarimetric signal and Fourier transform of rotating diattenuator for $T = 720°$.

modulation as a function of orientation of the diattenuator ($\mathcal{D} = 0.5$) in the rotating diattenuator polarimeter with beam wander present. Figure 3-9(a) shows the polarimetric signal and Figure 3-9(b) shows the beam wander. Figure 3-9(c) shows the DFT for the sum of the two signals. The largest contribution of the beam wander falls on the first harmonic and the polarimetric signal is unaffected. This is also true if two polarization elements are rotated in a ratio of $2n + 1 : 1$ as in the dual rotating retarder polarimeter [10]. The rotation ratio is odd and the largest contribution of the beam wander signal is to odd frequencies. Since the frequency content of the polarimetric signal is even, the effect on the polarimetric signal by the beam wander generated by either rotating element is reduced. If, however, the polarization ele-

ment is rotated only through 180°, the "half harmonic" signal from the beam wander couples into the frequencies of the polarization signal. Figure 3-10(a) shows the beam wander signal and Figure 3-10(b) shows its Fourier transform for this situation. The proper measurement sequence and measurement period will reduce adverse effects of beam wander on the polarimetric signal.

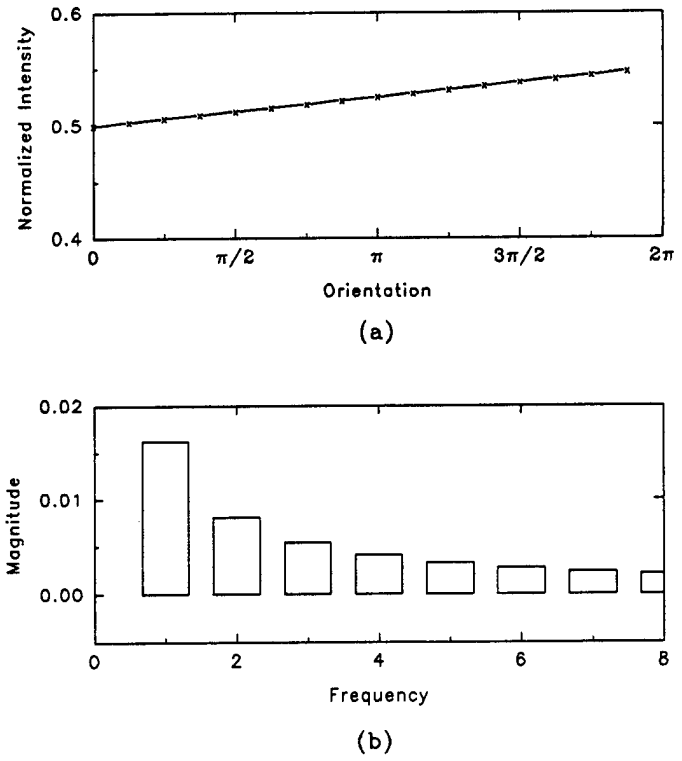

Figure 3-7 Linear drift and its Fourier transform.

A traditional difficulty in polarimetry is the accurate alignment of the polarization elements. Even small errors in the orientation of polarization elements can cause large errors in the measured results [46],[59]. An accurate means to determine the orientation is required. The polarization element can then be rotated to reduce the misalignment or the misalignment can be corrected in data reduction

or a combination of the two can be used. In broad band measurements the orientation of the diattenuation or retardance of the polarization elements can vary with wavelength. In this case the misalignment should be corrected in data reduction. Accurate measurement of the error is required to remove the systematic error. Chapter VI describes correction of these errors in the case of the spectropolarimeter.

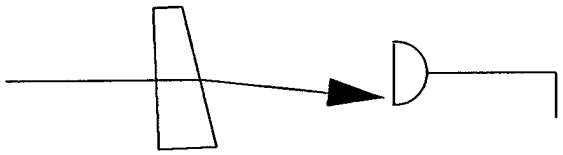

Figure 3-8 Beam wander caused by wedged rotating element.

Instrumental polarization is the additional polarization that may arise from components other than the polarization elements [12],[30],[60],[61],[62]. Some instrumental configurations require only a source and detector while others may include lenses, mirrors, beam splitters, and other components. Each of these components may change the desired polarization state or may affect the polarization signal in undesired ways. The intensity transmitted by a rotating polarizer will vary with rotation if the source is partially polarized, for example. Gratings produce large amounts of polarization. The Fresnel equations produce sources of instrumental polarization from large angles of incidence on mirrors or beamsplitters, or even in lenses. A detector may be more sensitive to one orientation of linear polarization than another and act as a partial polarizer.

One robust solution to instrumental polarization is to confine variation of polarization states between ideal polarizers that do not rotate as shown in Figure 3-11. The instrumental polarization does not usually change in time and the polar-

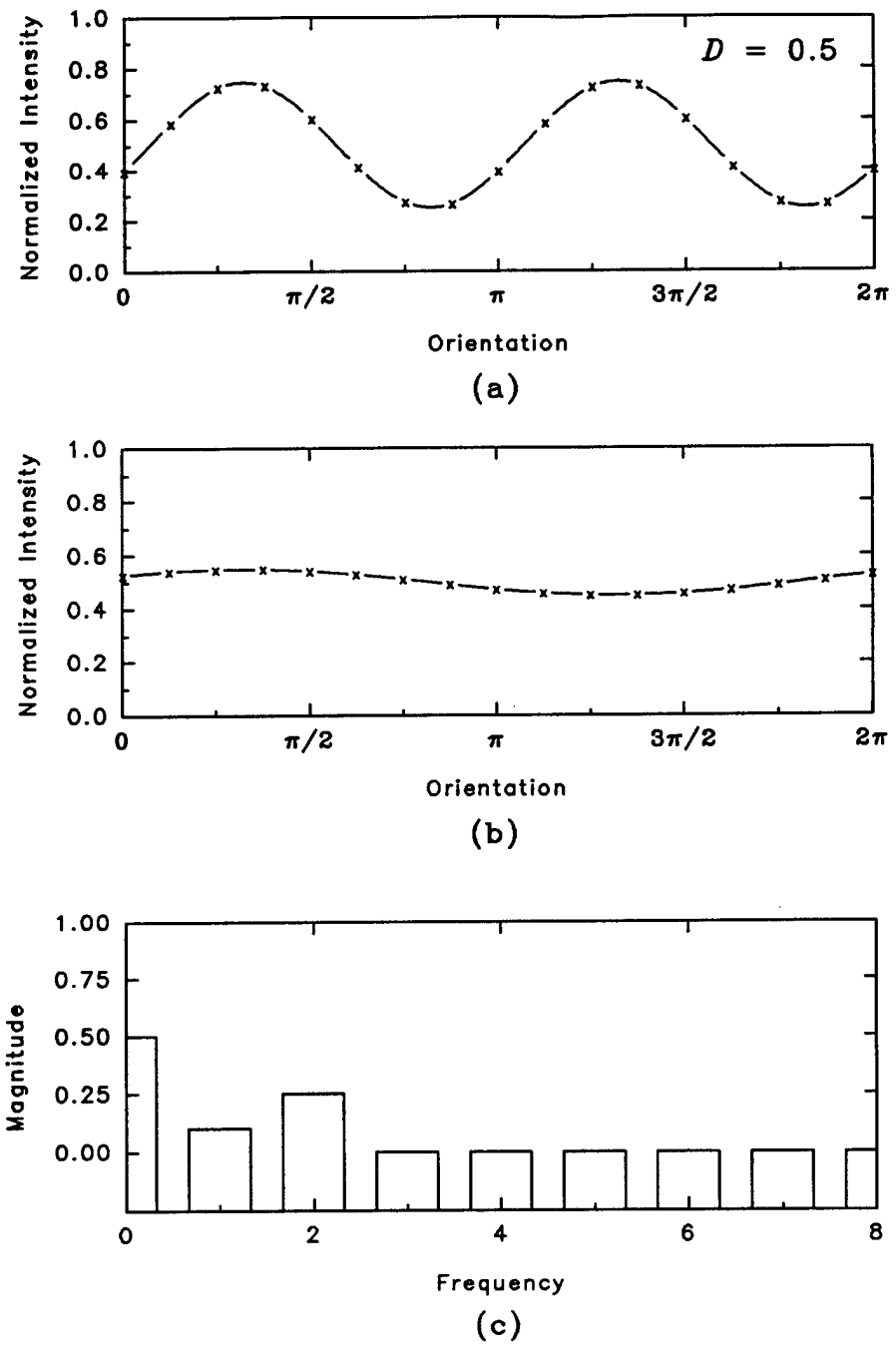

Figure 3-9 Intensity modulation of (a) the rotating diattenuator, and (b) beam wander, and (c) the combined Fourier transform.

ization state incident on the polarimeter remains the same. Since the first polarizer does not rotate, the polarization state and intensity transmitted by the first polarizer to the rest of the polarimeter remains constant. If the last polarization element in the polarimeter is a fixed ideal polarizer, the polarization state transmitted to the rest of the instrument remains constant. In this way, the effect of the instrumental polarization is constant and the intensity does not vary due to any instrumental polarization as polarization elements rotate. The chief disadvantage is that the outer polarization elements must remain fixed.

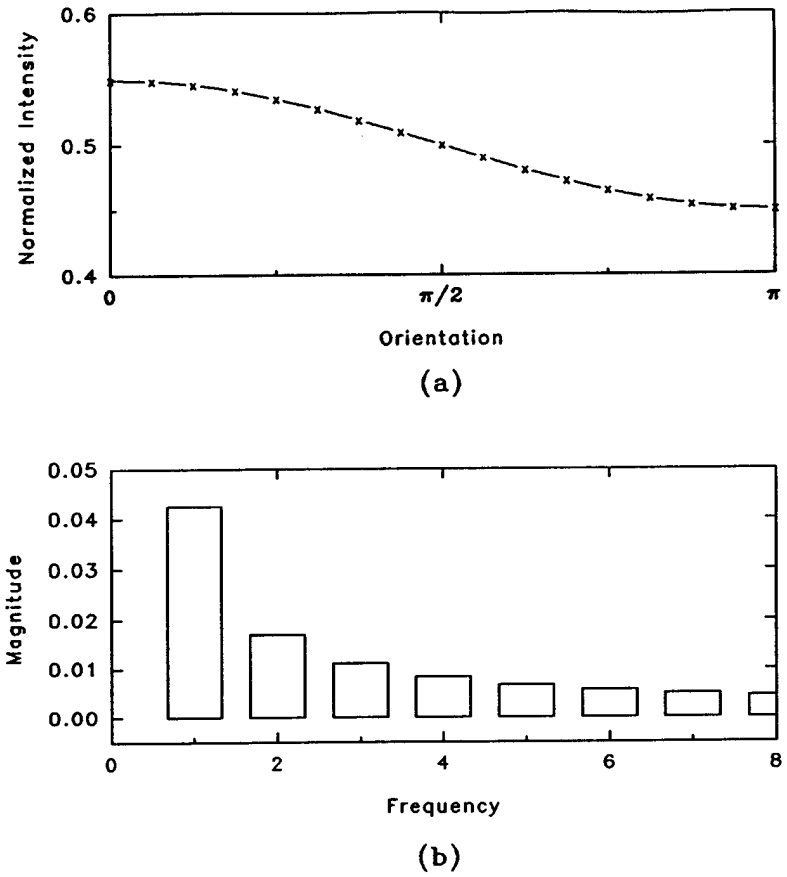

Figure 3-10 Intensity modulation of beam wander for $T = 180°$ and its Fourier transform.

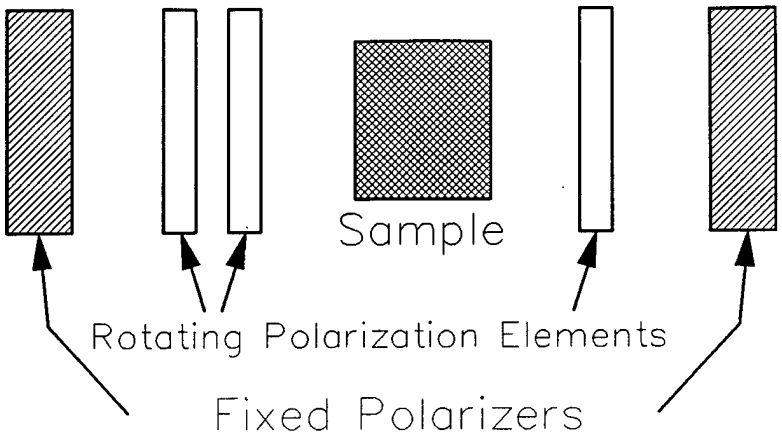

Figure 3-11 Polarimeter configuration for reducing instrumental polarization effects.

C. Spectral Extension of Polarimetric Data Reduction

The goal of this research is to make polarimetric measurements in a spectral instrument. Most polarizing samples display interesting wavelength dependence and polarization spectra can provide additional information and insight into the fundamental physical properties of samples. This section describes how polarimetry measurement techniques at single wavelengths are generalized for spectral instruments to produce polarization spectra.

Consider a spectrometer with a polarization state generator and polarization state analyzer in its sample compartment as shown in Figure 3-12. The Mueller matrix equation describing the system is

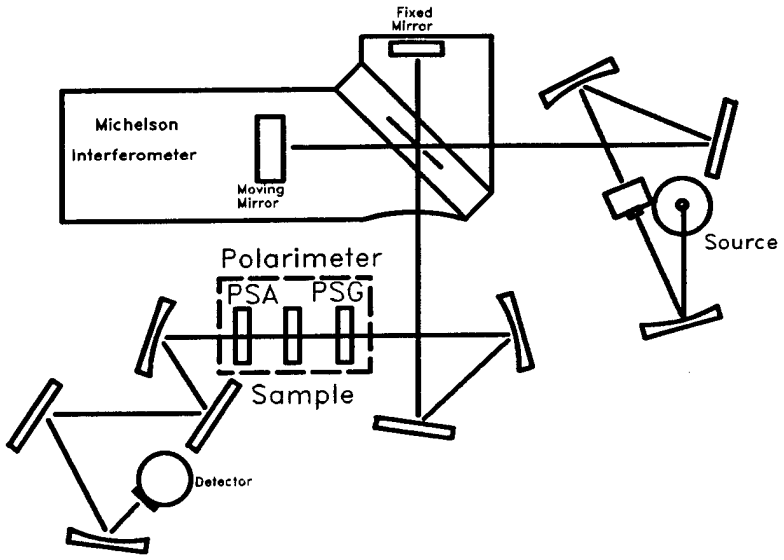

Figure 3-12 Nicolet FTIR spectrometer with polarimeter in sample compartment.

$$\vec{S}'(\lambda) = \mathbf{A}(\lambda)\mathbf{M}_{sample}(\lambda)\mathbf{G}(\lambda)\vec{S}_{inc}(\lambda). \tag{3-17}$$

The source is wavelength dependent and is characterized by the Stokes vector $\vec{S}_{inc}(\lambda)$. The polarization state generator, sample, and polarization state analyzer have wavelength dependent polarization properties and are denoted by $\mathbf{G}(\lambda)$, $\mathbf{M}_{sample}(\lambda)$, and $\mathbf{A}(\lambda)$ respectively. The intensity incident on the detector $i(\lambda)$, the first element of the Stokes vector $\vec{S}'(\lambda)$, is now an intensity spectrum. In a Mueller matrix measurement, Q spectra are measured and the intensity spectrum for the q'th measurement is written

$$i_q(\lambda) = [\mathbf{A}(\lambda)\mathbf{M}_{sample}(\lambda)\mathbf{G}(\lambda)\vec{S}_{inc}(\lambda)]_0. \tag{3-18}$$

The system of equations must be solved at each wavelength to determine the sample Mueller matrix spectrum. If the Fourier techniques described in Section A are used, the intensity can be written

$$i_q(\lambda) = \frac{1}{2} b_0(\lambda) + \sum_{k=1}^{K} [b_k(\lambda)\cos k\theta_q + c_k(\lambda)\sin\theta_q], \tag{3-19}$$

where the coefficients $b_k(\lambda) = b_k(m_{i,j}(\lambda))$ and $c_k(\lambda) = c_k(m_{i,j}(\lambda))$ are functions of the sample Mueller matrix elements. The subscripts i and j are the row and column indices of the Mueller matrix elements. The coefficients are calculated from the set of Q measured intensity spectra

$$b_0(\lambda) = \frac{1}{Q}\sum_{q=0}^{Q-1} i_q(\lambda)$$

$$b_k(\lambda) = \frac{2}{Q}\sum_{q=0}^{Q-1} i_q(\lambda)\cos\left(\frac{2qk\pi}{Q}\right) = \frac{2}{Q}\sum_{q=0}^{Q-1} i_q(\lambda)\cos(k\theta_q) \tag{3-20}$$

$$c_k(\lambda) = \frac{2}{Q}\sum_{q=0}^{Q-1} i_q(\lambda)\sin\left(\frac{2qk\pi}{Q}\right) = \frac{2}{Q}\sum_{q=0}^{Q-1} i_q(\lambda)\sin(k\theta_q).$$

These relations are inverted to give the sample Mueller matrix in terms of the wavelength dependent Fourier coefficients $m_{i,j}(\lambda) = m_{i,j}(b_k(\lambda), c_k(\lambda))$.

To summarize, the procedure for measuring polarimetric spectra using the Fourier analysis of polarimetric signals is as follows:

1) An intensity measurement $i_0(\lambda)$ is made with the polarization elements at the orientation θ_0.
2) The polarization elements are rotated by $\Delta\theta$ to θ_1 and another intensity measurement $i_1(\lambda)$ is made.
3) Step 2 is repeated until Q intensity spectra are acquired.

4) The Fourier coefficients $b_k(\lambda)$ and $c_k(\lambda)$ are calculated at each wavelength by a discrete Fourier transform of the set of intensities at each wavelength $i_q(\lambda)$.

5) Spectra of the sample Mueller matrix elements $m_{i,j}(\lambda)$ are calculated by substituting the wavelength dependent coefficients into the data reduction equations for each wavelength.

As an example, the rotating diattenuator configuration presented in Section A.2.b will be generalized to incorporate the wavelength dependence of the diattenuation. The intensity for the rotating diattenuator configuration (Eq. 3-10) becomes

$$i(\theta,\lambda)=\frac{1}{2}[p_1(\lambda)+p_2(\lambda)][1+\mathcal{D}(\lambda)\cos 2\theta]. \tag{3-21}$$

The Fourier coefficients are

$$\begin{aligned} b_0(\lambda)&=\frac{p_1(\lambda)+p_2(\lambda)}{2} \\ b_2(\lambda)&=\frac{1}{4}[p_1(\lambda)+p_2(\lambda)]\mathcal{D}(\lambda)\cos\theta_d(\lambda) \\ c_2(\lambda)&=\frac{1}{4}[p_1(\lambda)+p_2(\lambda)]\mathcal{D}(\lambda)\sin\theta_d(\lambda) \end{aligned} \tag{3-22}$$

and the diattenuation $\mathcal{D}(\lambda)$ and orientation $\theta_d(\lambda)$ are

$$\begin{aligned} \mathcal{D}(\lambda)&=\frac{p_1(\lambda)-p_2(\lambda)}{p_1(\lambda)+p_2(\lambda)}=\frac{\sqrt{b_2^2(\lambda)+c_2^2(\lambda)}}{b_0(\lambda)}=\frac{a_2(\lambda)}{a_0(\lambda)} \\ \theta_d(\lambda)&=\frac{1}{2}\tan^{-1}\left(\frac{c_2(\lambda)}{b_2(\lambda)}\right). \end{aligned} \tag{3-23}$$

This development has described the extension of the data reduction equations to many wavelengths. It has not addressed the wavelength dependence of the polarization elements. This is an issue that is addressed when the specific polarimeters and measurement sequences are introduced in later chapters.

D. Fourier Transform Infrared Spectroscopy

Spectroscopic measurements require some means to resolve wavelength, i.e. to obtain a plot of intensity versus frequency or wavelength. There are two chief approaches to this problem: dispersive spectrometers and Fourier transform spectrometers.

In the dispersive spectrometer, gratings or prisms spatially separate the various frequencies in the beam. In general, the beam is chopped, is transmitted through the sample, is dispersed by a dispersing element, and a spectrum is imaged onto a slit. The frequency of the light is scanned by mechanically rotating the dispersion element so that the appropriate frequency falls onto the slit. The wavelength resolution is determined by the width of the slit.

In Fourier transform (FT) spectroscopy, a Michelson interferometer generates an interferogram that contains intensity information at all frequencies simultaneously. The velocity of the moving mirror in the Michelson is set so the modulated frequencies fall within the appropriate frequency range for a particular detector. The interferogram is Fourier transformed to give the familiar intensity versus frequency spectrum.

There are several advantages of FT spectroscopy over dispersive spectroscopy for polarimetric applications. A comparison of dispersive and FT spectrometers is given in Table 3-1.

Table 3-1

Comparison of Dispersive and FT Infrared Spectrometers

Dispersive	Fourier Transform
Instrumental polarization effects from gratings can be significant and vary rapidly with wavelength.	Instrumental polarization is present but is generally smaller than the dispersive instrument.
A number of moving parts is required for moving gratings.	Moving mirror in Michelson is only moving part.
No internal reference for frequency. Calibration against reference spectra is required periodically.	A reference laser is used to provide frequency accuracy (Connes' advantage).
Smaller intensities are detected as the wavelength resolution increases (slit width decreases).	A much larger beam may be used. Intensity at the detector is greater since all frequencies are present (Jacquinot's and Felgett's advantages).
Stray light is not rejected and leads to spurious intensity readings.	Unmodulated stray light is rejected since only light modulated by the interferometer is detected.
The sample is at the focus of the beam and is subject to thermal effects.	Thermal effects of the sample are rejected since thermal changes are slow compared to detected frequencies.
Emission by the sample is detected.	Emission by the sample is rejected since only light modulated by the interferometer is detected.

The instrument used in the research described in this dissertation is a Nicolet 7199 FT infrared spectrometer. The various polarimeters described in the following Chapters are placed in the sample compartment shown in Figure 3-13. A brief description of the instrument is given here. A discussion of FTIR spectroscopy and further details of the hardware and software of the instrument are given in Appendix A and in the references [63],[64].

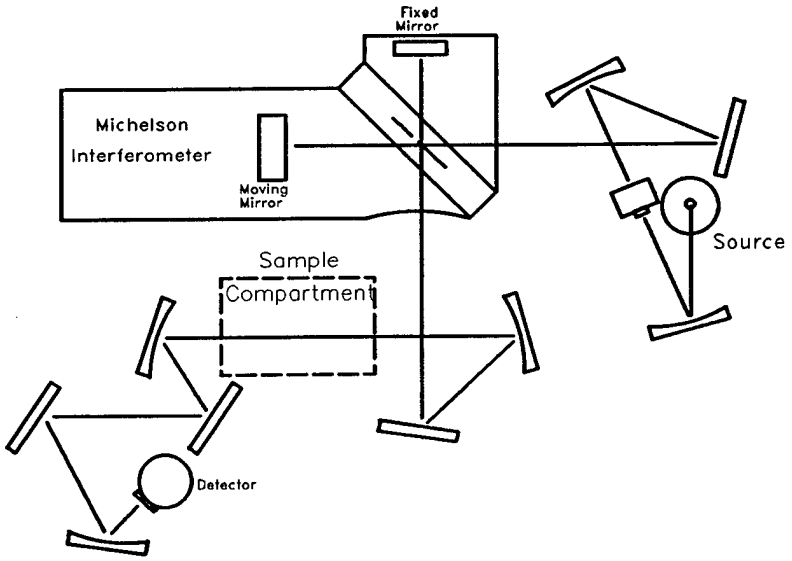

Figure 3-13 Nicolet FTIR spectrometer.

The Nicolet FTIR spectrometer is configured to acquire intensity spectra in transmission over the spectral range 2.5 to 25 μm. In this configuration, the source is a water cooled Globar filament, the beamsplitter substrate is potassium bromide, and the detector is a long wavelength liquid nitrogen cooled mercury cadmium telluride detector element. The two infrared beams from the beamsplitter are modulated by a high resolution Michelson interferometer consisting of a fixed mirror, moving mirror assembly, and the beamsplitter. The fixed mirror is mounted to

facilitate optimization of the IR signal. The moving mirror assembly is mounted on dual air bearings to reduce friction and the corresponding friction-induced fluctuations of velocity. The dual air bearings also prevent any appreciable mirror tilt allowing resolutions up to 0.06 cm^{-1}. In normal operation, the resolution used is 4 cm^{-1}. This corresponds to a resolution of 0.0001 μm at 2.5 μm, 0.02 μm at 10 μm, and 0.08 μm at 20 μm. A He-Ne reference laser runs the same path through the interferometer as the IR signal. The He-Ne interference pattern allows extremely accurate measurement of the distance traveled by the moving mirror. A closed servo loop uses the zero crossings of the laser interferogram to calculate and correct for variations in the velocity of the moving mirror assembly. These zero crossings are also used as a signal for the computer to take a data point. There is also a white light source whose interference pattern gives a spike at the point of zero optical path difference. This spike is used as a trigger to begin the sampling.

Data acquisition and manipulation parameters may be changed in the software that controls the spectrometer. Data acquisition parameters deal with such variables as resolution, bandwidth, spectral range, and gain levels. These may be varied to optimize signal-to-noise, increase resolution, or maximize file storage space. Data manipulation parameters deal with basic bookkeeping for the various data manipulation routines, such as plotting and displaying the data.

The Nicolet FTIR spectrometer has a 9.5 inch long sample compartment with a usable cross sectional area of 16 inches wide by 11 inches high. The baseplate is 35 by 45 inches. Rotation stages for the rotating polarization elements are Newport 495 stages with a resolution of 0.001°. The stages are computer controlled and are coordinated with data acquisition.

Software has been developed to operate the FT-IR spectrometer as a spectropolarimeter and process the resulting data. The configuration of the Nicolet control program, FTIR, allows macro control of hardware and operation of data processing and collection routines. FORTRAN programs are called from the macro as subroutines to advance the rotation stages in conjunction with data acquisition. Data files may also be managed from the macro, allowing the data to be stored on the Nicolet hard disk and later transferred to another computer (IBM-compatible) through an RS-232 port. The data collection software is maintained as a unit since, for a single polarization element setting, the spectropolarimeter operation is identical to that of the spectrometer.

The software operates as follows. Parameters and polarization element settings are initialized and the first spectrum is acquired. The appropriate polarization elements are then rotated. Another data set is taken, followed by another rotation of the elements and so on, until the required number of data sets is taken. The raw data is stored after each run for future use. After all data is taken, the set of spectra is transferred to the IBM-PC for data reduction.

E. Infrared Polarization Elements

Infrared spectral polarization measurements are made by placing a polarimeter in the sample compartment of the Fourier transform spectrometer described in the previous section. The elements of the polarimeter should be relatively achromatic over as much of the wavelength range of the spectrometer as possible. This section describes infrared polarization elements that are suitable for use in the spectropolarimeter in the 3 to 14 μm wavelength range of the mid-infrared.

Wavelength dependence of the polarization elements is perhaps the largest concern when extending the spectral range of polarization measurements from a single wavelength. Of the two classes of polarization elements, polarizers and retarders, polarizers present little difficulty. Linear polarizers of various types are available commercially that have fairly constant diattenuation over broad wavelength bands in the infrared. Wire grid polarizers are compact, have high transmission, and there is no beam offset or angular displacement at normal incidence. There is little polarization dependence of ray angle through the polarizer. Large clear aperture wire grid polarizers are readily available. Glan-Thompson polarizers have higher extinction ratios than wire grid polarizers but have constant diattenuation over a smaller wavelength range than wire grid polarizers. Figure 3-14 shows the principal transmittances of several wire grid polarizers in the infrared.

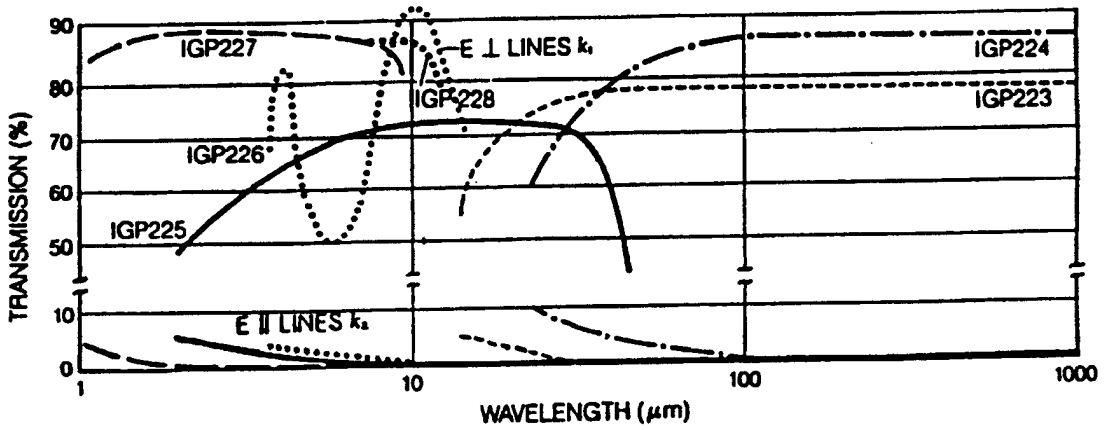

Figure 3-14 Principal transmittance spectra of IR wire grid polarizers. (Molectron Detector, Inc.)

Wire grid polarizers are composed of an infrared-transparent substrate onto which parallel lines of conducting material have been deposited. The polarization

parallel to the lines is absorbed, while the polarization perpendicular to the lines is transmitted with little attenuation. For the 3 to 14 micrometer spectral region, the grid spacing is on the order of 0.25 to 0.5 micrometers.

The wire grid polarizers used in this research were obtained from Molectron Detector Inc. They consist of gold wire grids with 0.25 μm spacing laid on a zinc selenide substrate. The diattenuation specified by the manufacturer is 85% at 2.5 μm and 95% at 10 μm.

Retarders are required to measure a complete Mueller matrix but present the most difficulty in terms of their wavelength dependence because they must have achromatic response. If the retarder is not achromatic the intensity is not modulated at points where the retardance is a multiple of 2π and polarization information is lost.

The most common configuration of retarder is the waveplate, a plane-parallel plate of birefringent material with the crystal axis oriented perpendicular to the propagation direction of light. As the wavelength varies, the retardance of the waveplate also varies and in practice the retardance of the waveplate is approximately achromatic for only a short wavelength range. One birefringent material commonly used for infrared waveplates is cadmium sulfide. Figure 3-15 shows the retardance measured as part of this dissertation for a cadmium sulfide (CdS) multiple order retarder that was designed to have $7\lambda/4$ waves of retardance at 10.6 μm. At the points where the retardance is a multiple of a wave of retardance, polarimetric information is lost. This occurs 8 times for CdS over the 2.5 - 11 μm range shown in the Figure. Zero order retarders have achromatic response over a limited wavelength band but are little better than multiple order retarders over a broad band such as shown in the Figure. Some achromatic retarder designs

[65],[66],[67],[68] that utilize multiple plates of birefringent materials have better achromatic characteristics, but the range of achromaticity is still limited to within 10% of the design wavelength [68].

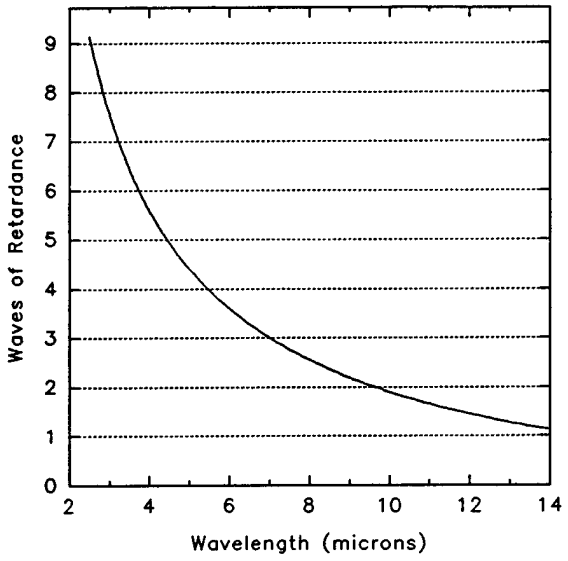

Figure 3-15 Retardance spectrum of cadmium sulfide retarder.

One exception to the class of retarder that uses multiple birefringent plates is an achromatic retarder composed of two birefringent plates of cadmium sulfide (CdS) and cadmium selenide (CdSe) [69]. For this design, the fast axes of the two plates lie in the plane of the plate and are perpendicular to each other. Since the fast axes are perpendicular, the effective retardance of the combination of plates is the difference of the retardances in the two plates. The birefringence dispersion for CdS and CdSe are similar enough that effective retardance remains fairly constant over a wavelength range from 3 to 14 μm. This achromatic retarder is used in the spectropolarimeter and is discussed in greater detail in Chapter IV.

The Fresnel rhomb gives the best achromatic response of achromatic retarder designs. Figure 3-16 shows a typical Fresnel rhomb designed for the visible. In the Fresnel rhomb, retardation occurs on total internal reflection. The amount of retardation depends solely on the refractive index which varies slowly with wavelength but is independent of optical path, unlike the waveplates based on birefringence. This design has the disadvantage of a beam offset which is unacceptable when the retarder must be rotated. A modified Fresnel rhomb corrects this problem and retains the achromatic response. Modified Fresnel rhombs have been designed for the visible [38],[70],[71] and the infrared [10]. The infrared design by Goldstein is shown in Figure 3-17. The theoretical retardance spectrum is shown in Figure 3-18.

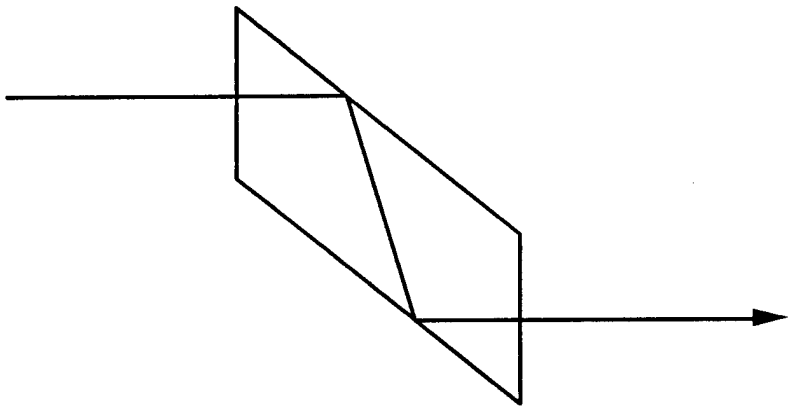

Figure 3-16 Fresnel rhomb achromatic retarder.

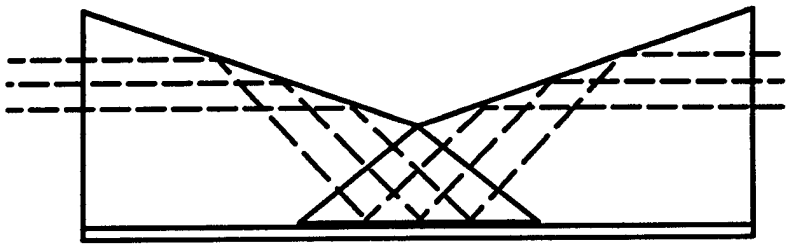

Figure 3-17 Modified Fresnel rhomb achromatic retarder.

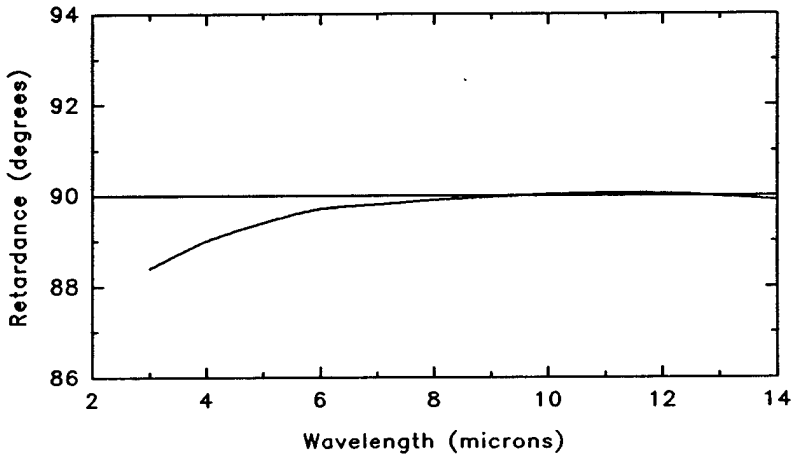

Figure 3-18 Retardance spectrum of modified Fresnel rhomb retarder.

Chapter IV

Rotating Sample Spectropolarimeter

The previous Chapters have provided an overview of polarimetric techniques and have discussed the application of these techniques to spectropolarimetry in a wavelength independent manner. The advantages of Fourier transform spectrometers as a method of wavelength resolution were described in the previous Chapter. The remainder of this dissertation describes application of these ideas to a Nicolet Fourier transform spectrometer configured for mid-infrared polarization measurements (hereafter "the spectropolarimeter") culminating in the measurement of the complete Mueller matrix as a function of wavelength.

This Chapter applies the Fourier analysis technique in describing the rotating sample polarimeter. A description of the retarders and their calibration required for the complete Mueller matrix polarimeter is also described in this Chapter. Chapter V gives additional examples of measurements using the rotating sample spectropolarimeter. Chapter VI describes the complete Mueller matrix polarimeter. Chapter VII gives examples of measurements using the Mueller matrix spectropolarimeter. Sources of systematic error in each of these techniques are described and resolved at the appropriate point in each of these Chapters.

A. Introduction

The precision calibration of polarizing elements is becoming more important as optical systems require greater accuracy and increased control over polarization [3],[4]. The rotating sample polarimeter presented here is used to measure the linear diattenuation and linear retardance spectra of a sample. These spectra are used for the calibration of polarization elements and the characterization of linear polarization properties of infrared materials. In our implementation, the polarimeter is placed in the sample compartment of a Fourier transform spectrometer [72],[73]. The rotating sample spectropolarimeter measures linear diattenuation and retardance spectra of transmissive samples from 2.5 - 16.5 μm.

Previous techniques have measured polarimetric and ellipsometric parameters of samples by rotating polarizers or retarders [23],[45],[47],[48],[50],[52]. The detected signal is modulated by the rotating polarization elements. The polarization properties of the sample are then determined from the detected signal's Fourier frequency components. In the rotating sample polarimeter presented here, modulation is produced by rotating the sample between fixed polarizers whose transmission axes are parallel, as shown in Figure 4-1. Any linear diattenuation or linear retardance present in the sample modulates the transmitted intensity as the sample rotates. The sample's linear diattenuation and linear retardance are determined by Fourier analysis of the detected signal.

The following three points summarize the conclusions of our analysis: the rotating sample polarimeter (1) is immune to instrumental polarization, (2) is immune to circular diattenuation and circular retardance, and (3) has increased accuracy relative to other more complete polarimeters. First, substantial instrumental polarization in spectrometers is caused by large angles of incidence on fold mir-

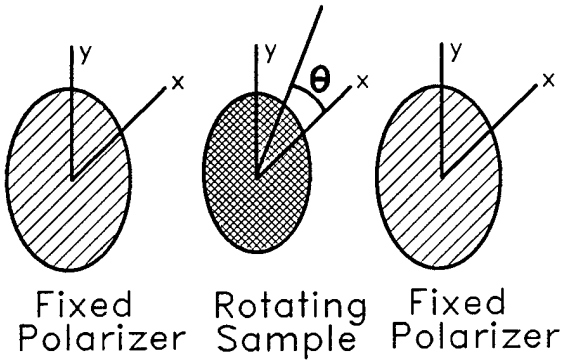

Figure 4-1: The rotating sample polarimeter configuration. The sample is rotated between two fixed linear polarizers.

rors and polarization of the beamsplitter or grating [12],[30]. It is necessary to either neutralize this instrumental polarization or perform complex data reduction to remove systematic errors introduced by the instrumental polarization. Fixing the orientation of the polarizers ensures that only one polarization state is transmitted to the sample and to the optics following the polarimeter [45]. The detected signal thus depends only on the linear diattenuation and retardance in the sample and not on the orientation of the polarizers in the instrument.

Second, the rotating sample polarimeter is immune to circular diattenuation (including circular dichroism) and circular retardance (including optical activity), i.e. any circular diattenuation or circular retardance in the sample changes the transmittance measured but does not influence the measured values of linear diattenuation or linear retardance. A circular diattenuator or circular retarder rotated between two fixed polarizers does not produce any intensity modulation.

Third, the rotating sample polarimeter is intrinsically more accurate than other more complex polarimeters which incorporate retarders. This configuration is best suited for the precision calibration of linear polarization elements.

The polarization spectra from the rotating sample polarimeter have been used for calibration of polarizing optical elements and for the bootstrap calibration of the dual rotating retarder polarimeter described in Chapter VI. The linear diattenuation and linear retardance spectra from the rotating sample spectropolarimeter have also been used to investigate potential modulator materials [74], and to confirm and extend the wavelength range of materials' optical constants. The calibration spectra of an achromatic retarder is included in this Chapter as an example of the data obtained by the rotating sample spectropolarimeter.

Section B describes the data reduction algorithms for the rotating sample polarimeter. The polarization elements and spectropolarimeter configuration and operation are described in Section C. Section D presents the linear diattenuation and linear retardance calibration spectra of an infrared achromatic retarder as an example of the data obtained by the rotating sample spectropolarimeter. Section E compares the rotating sample polarimeter to other polarimeter configurations. The terms diattenuation and retardance as used in the remainder of this Chapter refer to *linear* diattenuation and *linear* retardance unless specifically stated otherwise.

B. Theory

This section describes the data reduction method to find the diattenuation and retardance of a sample. The Mueller formalism [11] is used to model the rotating sample polarimeter and to relate the linear diattenuation and retardance of the sample to the output intensity. The diattenuation and retardance are derived in terms of the coefficients of the Fourier series which describe the intensity modulation of the polarimeter. Diattenuation and retardance spectra of the sample are obtained by calculating the Fourier series coefficients at a number of wavelengths and repeating the calculation for diattenuation and retardance with each of these

wavelength dependent coefficients. Since the diattenuation and retardance equations for each wavelength are the same, the wavelength dependence has been suppressed in the following derivation.

Many materials and optical devices simultaneously exhibit both retardance and diattenuation. For example, a birefringent material contains linear diattenuation due to the difference in its Fresnel coefficients for the ordinary and extraordinary refractive indices. A wire grid linear polarizer will exhibit some retardance. In such instances a sample acts simultaneously as a partial polarizer and a retarder [11]. In many cases, it may be assumed that the principal axes of linear diattenuation are coincident with the fast and slow axes of retardance. This occurs, for example, in a waveplate where the crystalline anisotropy that gives rise to the birefringence may cause differing amounts of attenuation of a beam linearly polarized parallel or perpendicular to the axis of the anisotropy [75]. The assumption that the axes are coincident is made in this development.

A sample with principal intensity transmittances k_1 and k_2 and retardance $\delta = |\delta_1 - \delta_2|$ and whose axes of diattenuation and retardance are coincident and aligned with the x and y axes is represented by the Mueller matrix $\mathbf{M}_S$

$$\mathbf{M}_S = \frac{1}{2}\begin{pmatrix} k_1 + k_2 & k_1 - k_2 & 0 & 0 \\ k_1 - k_2 & k_1 + k_2 & 0 & 0 \\ 0 & 0 & 2\sqrt{k_1 k_2}\cos\delta & 2\sqrt{k_1 k_2}\sin\delta \\ 0 & 0 & -2\sqrt{k_1 k_2}\sin\delta & 2\sqrt{k_1 k_2}\cos\delta \end{pmatrix}$$

$$= \tau_S \begin{pmatrix} 1 & \mathcal{D} & 0 & 0 \\ \mathcal{D} & 1 & 0 & 0 \\ 0 & 0 & \sqrt{1-\mathcal{D}^2}\cos\delta & \sqrt{1-\mathcal{D}^2}\sin\delta \\ 0 & 0 & -\sqrt{1-\mathcal{D}^2}\sin\delta & \sqrt{1-\mathcal{D}^2}\cos\delta \end{pmatrix}, \quad (4\text{-}1)$$

where

$$\mathcal{D} = \frac{k_1 - k_2}{k_1 + k_2} \quad \text{and} \quad \tau_S = \frac{1}{2}(k_1 + k_2). \tag{4-2}$$

are the linear diattenuation and the average transmission, and the axis of the principal transmittance k_1 is aligned with the x-axis [17].

This sample is placed between two linear polarizers whose transmission axes are parallel, as shown in Figure 4-1. For precision measurements, the polarizers cannot necessarily be assumed ideal. The linear polarizers are assumed to have diattenuation $\mathcal{D}_p$ and the systematic error introduced by the non-ideal diattenuation is corrected in the data reduction procedure. The system Mueller matrix $\mathbf{M}_{sys}$ for the polarimeter with the sample at an angle θ between parallel polarizers is

$$\begin{aligned}
\mathbf{M}_{sys} &= \mathbf{M}_{p2}(\mathcal{D}_2)\mathbf{R}(-\theta)\mathbf{M}_S\mathbf{R}(\theta)\mathbf{M}_{p1}(\mathcal{D}_1) \\
&= \tau_2 \begin{pmatrix} 1 & D_2 & 0 & 0 \\ D_2 & 1 & 0 & 0 \\ 0 & 0 & \sqrt{1-D_2^2} & 0 \\ 0 & 0 & 0 & \sqrt{1-D_2^2} \end{pmatrix} \begin{pmatrix} 1 & 0 & 0 & 0 \\ 0 & \cos 2\theta & -\sin 2\theta & 0 \\ 0 & \sin 2\theta & \cos 2\theta & 0 \\ 0 & 0 & 0 & 1 \end{pmatrix} \\
&\times \tau_S \begin{pmatrix} 1 & \mathcal{D} & 0 & 0 \\ \mathcal{D} & 1 & 0 & 0 \\ 0 & 0 & \sqrt{1-\mathcal{D}^2}\cos\delta & \sqrt{1-\mathcal{D}^2}\sin\delta \\ 0 & 0 & -\sqrt{1-\mathcal{D}^2}\sin\delta & \sqrt{1-\mathcal{D}^2}\cos\delta \end{pmatrix} \\
&\times \begin{pmatrix} 1 & 0 & 0 & 0 \\ 0 & \cos 2\theta & \sin 2\theta & 0 \\ 0 & -\sin 2\theta & \cos 2\theta & 0 \\ 0 & 0 & 0 & 1 \end{pmatrix} \tau_1 \begin{pmatrix} 1 & D_1 & 0 & 0 \\ D_1 & 1 & 0 & 0 \\ 0 & 0 & \sqrt{1-D_1^2} & 0 \\ 0 & 0 & 0 & \sqrt{1-D_1^2} \end{pmatrix},
\end{aligned} \tag{4-3}$$

where $\mathbf{R}(\theta)$ is the matrix for a rotational change of basis in the Mueller calculus [11]. $\mathbf{M}_{pi}(\mathcal{D}_i)$ represents the i th horizontal linear polarizer with diattenuation $\mathcal{D}_i$ and average transmission $\tau_i = \frac{1}{2}(k_{i,1} + k_{i,2})$.

The Stokes vector $\vec{S}'$ of the light transmitted by the polarimeter and incident on the detector is given by

$$\vec{S}' = \mathbf{M}_{sys}\vec{S}_{inc}. \tag{4-4}$$

The transmitted intensity is given by the first element of the transmitted Stokes vector. At each wavelength the intensity transmittance I as a function of sample orientation θ has the form

$$\begin{aligned} I(\theta) = \tau[1 &+ \frac{1}{2}\mathcal{D}_1\mathcal{D}_2(1+\sqrt{1-\mathcal{D}^2}\cos\delta) \\ &+ \mathcal{D}(\mathcal{D}_1+\mathcal{D}_2)\cos 2\theta \\ &+ \frac{1}{2}\mathcal{D}_1\mathcal{D}_2(1-\sqrt{1-\mathcal{D}^2}\cos\delta)\cos 4\theta] \\ = \tau(&a_0 + a_2\cos 2\theta + a_4\cos 4\theta). \end{aligned} \tag{4-5}$$

where τ is a normalization factor including the radiance of the source, the reponsivity of the detector, and the average transmission of the polarimeter. Equation 4-5 is a Fourier series in θ with coefficients a_0, a_2, and a_4. The diattenuation $\mathcal{D}$ and retardance δ of the sample expressed in terms of the Fourier coefficients are

$$\mathcal{D} = \frac{a_2}{a_0 + a_4}\left(\frac{1+D_1D_2}{D_1+D_2}\right), \tag{4-6}$$

$$\delta = \cos^{-1}\left(\frac{a_0 - a_4\left(1+\frac{2}{D_1D_2}\right)}{\left[(a_0+a_4)^2 - a_2^2\left(\frac{1+D_1D_2}{D_1+D_2}\right)^2\right]^{\frac{1}{2}}}\right). \tag{4-7}$$

For nearly ideal linear polarizers, $\mathcal{D}_1, \mathcal{D}_2 > 99\%$, the correction for nonideal polarizers is negligible and ideal diattenuations $\mathcal{D}_1 = \mathcal{D}_2 = 1$ can be assumed.

The quantities a_0, a_2, and a_4 are determined experimentally by rotating the sample in increments of $\Delta\theta$ to a set of N angles $\theta_n = n\Delta\theta$, where $n = 0, 1, 2, \ldots, N-1$. The number of measurements N and the increment $\Delta\theta$ must satisfy $N\Delta\theta = 360°$, where $N > 8$. An intensity measurement is made at each θ_n. At a particular wavelength, each set of N intensity measurements $I(\theta_n)$ may be expressed as a Fourier series

$$I(\theta_n) = \frac{b_0}{2} + \sum_{k=1}^{K} (b_k \cos k\theta_n + c_k \sin k\theta_n)$$
$$= \frac{a_0}{2} + \sum_{k=1}^{K} a_k \cos(k\theta_n - k\phi_k) \tag{4-8}$$

where $a_k^2 = b_k^2 + c_k^2$, $K \geq 4$, and $N \geq 2K$. The Fourier coefficients b_k and c_k are calculated from the set of measured intensities $I(\theta_n)$ by a discrete Fourier transform.

The phase of the Fourier frequencies ϕ_k is

$$\phi_k = \frac{1}{k}\arctan\left(\frac{c_k}{b_k}\right). \tag{4-9}$$

The phase of the second harmonic ϕ_2 gives the orientation of the sample's principal transmittance k_1 with respect to the x-axis. The phase of the fourth harmonic ϕ_4 gives the orientation of the phase delay δ_1 with respect to the x-axis within an integer multiple of $\pi/2$. The fast and slow axes of a device are not determined by this technique.

Only the Fourier coefficients a_0, a_2, and a_4 are used to determine the diattenuation and retardance spectra. The other Fourier coefficients, $a_1, a_3, a_5, a_6, a_7 \ldots$, which should be zero in the absence of noise and systematic

errors, provide valuable information on the operation of the polarimeter. For example, beam wander arising from the rotation of a sample with non-plane parallel surfaces couples strongly into the first harmonic a_1 and decreasingly into the higher harmonics. A nonzero value for a_1 suggests the presence of beam wander. Since significant beam wander also couples into a_2 and a_4, measurements on samples with non plane-parallel surfaces have reduced accuracy.

In our experience, there is a definite advantage to rotating the sample through 360°, rather than just 180°. The additional information acquired from 180° to 360° is not necessarily redundant. Doubling the rotation range from 180° to 360° moves the polarization information from the first and second to the second and fourth harmonics reducing the effects of systematic errors such as beam wander. Further discussion of the effects of choosing a particular rotation range is in reference [76].

Mathematical analysis of samples containing circular diattenuation and circular retardance shows that the rotating sample polarimeter is immune to these effects. Many other polarimetric configurations which measure only linear diattenuation and/or retardance have coupling between the linear and circular effects, i.e. the presence of circular diattenuation or circular retardance can affect the measured value of the linear diattenuation and linear retardance. This occurs, for example, if measurements are made with a fixed sample between polarizers that are rotated. With the rotating sample polarimeter there is complete immunity to the circular effects.

This immunity can be understood qualitatively by the following argument. If the sample contains circular diattenuation or circular retardance, the linearly polarized light from the first polarizer is elliptical or rotated linearly polarized light, which does not change with sample orientation. In the first case, the second

polarizer transmits the elliptically polarized light with a fixed attenuation. In the second case, the rotated light transmitted by the sample is partially attenuated by the polarizer according to the degree of linear polarization rotation, but the rotation and associated attenuation are independent of sample orientation. These effects occur for any orientation of the sample and produce no orientation-dependent modulation. The attenuation in both cases appears in the reduced data as simple absorption by the sample. Since the linear diattenuation and retardance are calculated from ratios which remove absorption effects, circular diattenuation and retardance do not affect measurement of the linear properties.

As a final note, we have described a polarimeter where the polarizers are parallel. Other relative orientations of the polarizers are viable, but parallel polarizers maximize the average throughput for a set of intensity measurements. Therefore the signal-to-noise ratio is optimized by parallel orientations of the transmission axes of the polarizers.

C. Experimental

Diattenuation and retardance spectra are obtained by making the intensity measurements as prescribed above but at a number of wavelengths. The data is reduced in like fashion, one wavelength at a time. The spectropolarimeter, an instrument capable of making polarimetric measurements at many wavelengths simultaneously, is described in this section.

Figure 4-2 shows the optical configuration of the spectropolarimeter. It is a Fourier transform infrared (FTIR) spectrometer modified by the addition of the rotating sample polarimeter of Figure 4-1 in the sample compartment.

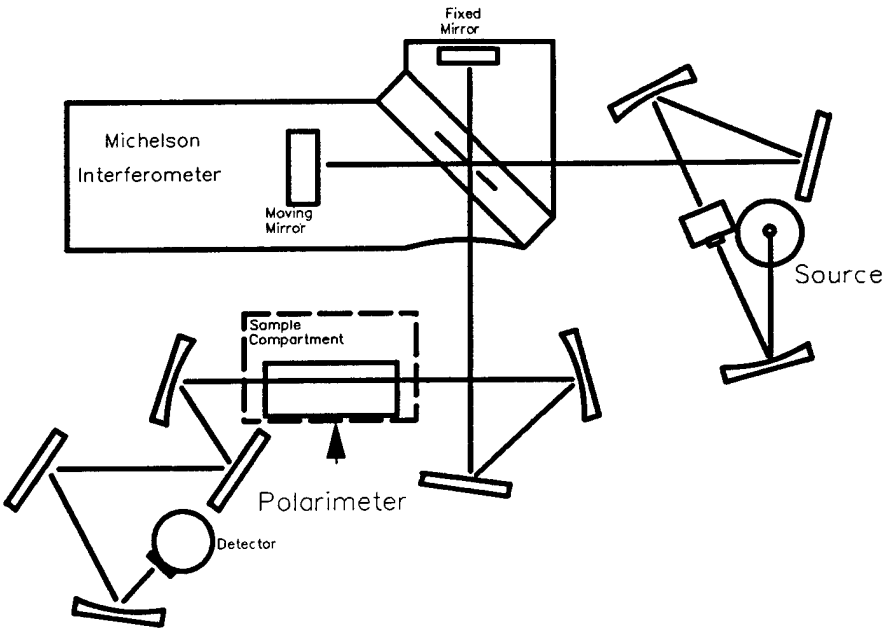

Figure 4-2: The Fourier transform infrared spectropolarimeter.

The polarimeter consists of two wire-grid polarizers whose orientations are fixed. The polarizers are aligned by rotating the second polarizer with no sample present. The second polarizer is aligned at the angle where the phase ϕ_2 of the second harmonic of the intensity modulation is zero. This aligns the transmission axes of the polarizers to within a tenth of a degree. Misalignment of the two polarizers by 0.1° introduces error in the retardance measurements of less than 0.4% and negligible error in the diattenuation measurements.

The operation of the spectropolarimeter proceeds as follows: The sample is placed in a computer-controlled rotary stage and a transmission spectrum $I_0(\lambda)$ is taken. The sample is then rotated by $\Delta\theta$ and a second spectrum $I_1(\lambda)$ is acquired. This process is repeated until the required set of N spectra is obtained. In the studies described here, $\Delta\theta = 22.5°$ and $N = 16$. The oversampling provides increased

signal-to-noise and allows for checks on instrument operation. The Fourier coefficients α_n are calculated at each wavelength from the N transmission spectra. Diattenuation and retardance spectra are then computed from the coefficients using Eqs. 4-6 and 4-7.

D. Example

In this section we demonstrate the utility of the rotating sample polarimeter by showing diattenuation and retardance spectra of a multiple plate achromatic retarder whose fast axis orientation oscillates. This example highlights the type of information which can be obtained, and demonstrates a defect in this particular polarization element which otherwise might escape notice. Figure 4-3 shows the achromatic retarder which consists of two plates of different birefringent materials whose crystal axes are orthogonal to each other [69]. The similarity in the dispersion curves of the two materials results in a net retardance of approximately one-quarter wave over the wavelength range 2.5 to 14 μm. Different materials have been used in similar designs in the visible and ultraviolet wavelength bands [65],[66],[67].

Figure 4-4 shows the measured retardance over the retarder's transmission band. The retardance remains largely achromatic out to 14.3 μm. Because of the small variation of retardance with wavelength, the retarder is superior to conventional single plate infrared retarder designs and is useful for many applications, particularly multi-wavelength [10] or broadband polarimetry. Figure 4-5 shows the diattenuation spectrum. The diattenuation is less than one half of one percent over most of the useful spectrum of the retarder.

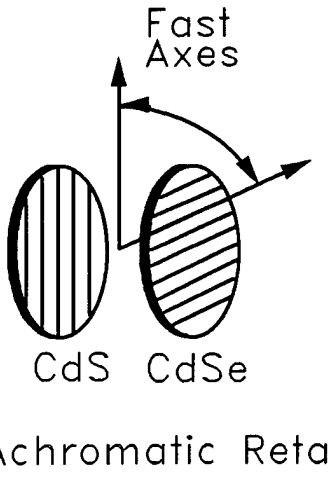

Figure 4-3: The configuration of the achromatic retarder. The angle between the fast axes of the two plates is ideally 90°.

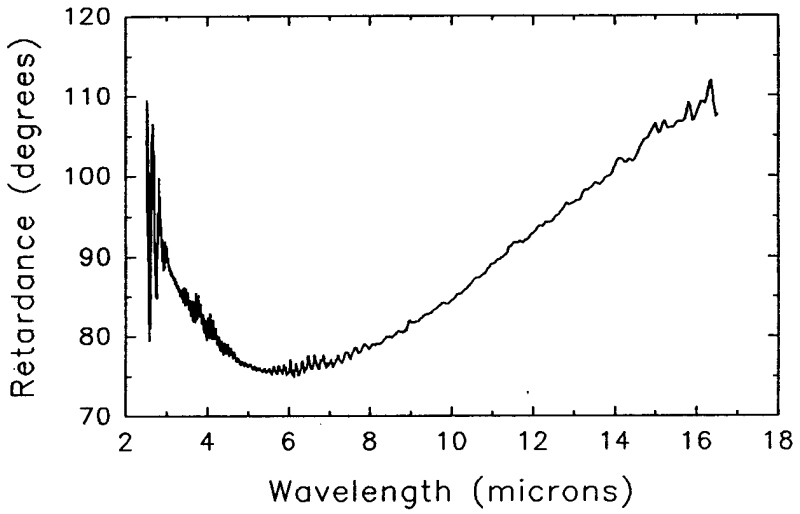

Figure 4-4: Retardance spectrum of the multiple plate achromatic retarder.

Figure 4-6 shows the variation of orientation of the fast axis as a function of wavelength. It oscillates by 5° seven times over the 2.5 to 16.5 μm wavelength band. The period of modulation increases as the wavelength increases. Investigation revealed that misalignment of the two plates comprising the retarder caused this oscillation of orientation with wavelength which was eventually corrected by realigning the plates. Ideally, the fast axes of the two plates are precisely 90° apart, but in this particular device the angle between the fast axes differed from 90° by the magnitude of the modulation, about 5°.

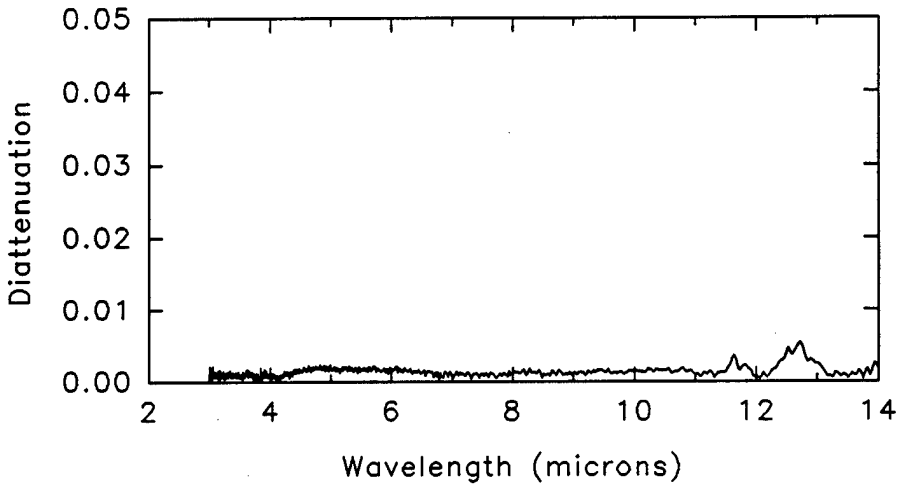

Figure 4-5: Diattenuation spectrum of the multiple plate achromatic retarder.

To understand this oscillation of the retarder's fast axis, consider a particular wavelength λ_1 where one plate has $2\pi n$ retardance and contributes no net retardance. At this same wavelength the second plate acts as a net one quarter wave retarder whose orientation is that of the second plate. At some λ_3 different from λ_1 the second plate has zero net retardance and the first plate contributes the net quarter wave of retardance at the orientation of the first plate. At λ_2 between λ_1 and λ_3

both plates contribute to the quarter wave of retardance at the average orientation of the two plates. (Actually the two plates produce retardation that is slightly elliptical at this point, a more subtle reason to measure and correct the misalignment.) By rotating one plate with respect to the other by the misalignment indicated in the figure, the two plates are made perpendicular and the orientation becomes constant with wavelength. If this misalignment is less than 8°, it affects only the orientation of the achromatic retarder and has negligible effect on the magnitude of the retardance (the retardance in Figure 4-4 remains the same).

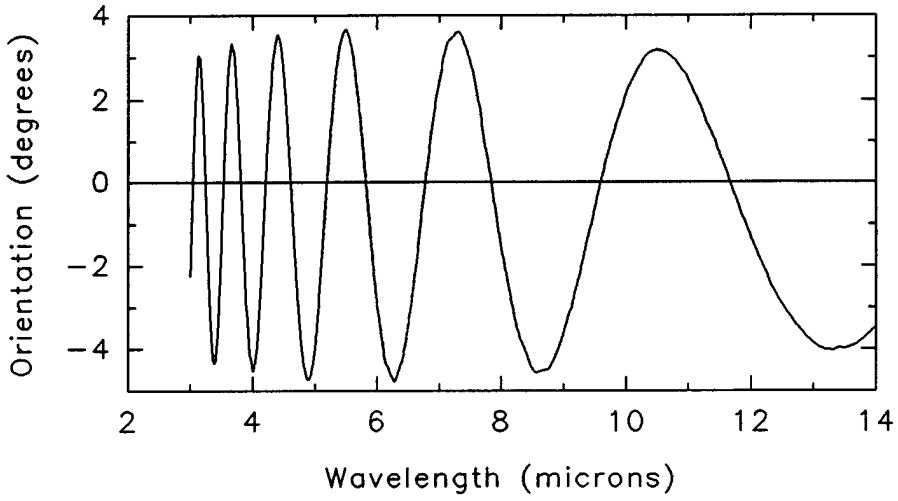

Figure 4-6: The orientation of the fast axis as a function of wavelength of the achromatic retarder.

This example has demonstrated the usefulness of the rotating sample spectropolarimeter not only through the calibration of the diattenuation and retardance but also through the additional information contained in the spectra of the orientation of polarization properties.

E. Conclusion and Comparison to Other Polarimetric Configurations

It is helpful to compare the rotating sample polarimeter to other types of polarimeters in order to understand the usefulness of the rotating sample polarimeter. One of the most common and popular polarimeters for the characterization of samples is the dual rotating retarder polarimeter first described by Azzam [45], and analyzed by others [46],[59]. Table 4-1 lists advantages and disadvantages of both types of polarimeters. The dual rotating retarder polarimeter is complete, i.e. it measures all sixteen elements of the Mueller matrix including linear polarization, circular polarization, and depolarization. For circular polarization, Mueller matrix, or depolarization measurements a rotating retarder is required.

However, calibration and operation of a dual rotating retarder is far more complex than for the rotating sample polarimeter and there are many more potential sources of error. Based on our experience, we feel the dual rotating retarder is less accurate because of greater complexity of data reduction, calibration, and systematic error removal. For spectral measurements, calibration and data reduction of the rotating sample polarimeter is much easier since wavelength dependence of retarders is generally much stronger than the wavelength dependence of polarizers.

Both types of polarimeters are operated on the same mechanical platform. The rotating sample polarimeter is used for greater accuracy and for the calibration of linear elements. The dual rotating retarder polarimeter is used on samples that are difficult to rotate, and to measure Mueller matrices, circular polarization elements, and depolarization.

Table 4-1: Comparison of the Rotating Sample Polarimeter to Rotating Retarder Polarimeters.

	Rotating Sample Polarimeter	Rotating Retarder Polarimeters
1	Requires only polarizers	Requires polarizers and retarders
2	Only polarizers need to be calibrated (bootstrap calibration quickly converges)	Calibration must include retarders (which requires calibrated elements)
3	Easily extendable to many wavelengths	Wavelength dependence of retarders is critical
4	Requires only one rotating stage	Requires two rotating stages for dual rotating retarders
5	Immune to instrumental polarization	Immune to instrumental polarization (if polarizers don't rotate)
6	Immune to circular polarization effects	Measures circular polarization effects
7	Results are in terms of diattenuation and retardance	Diattenuation and retardance must be extracted from Mueller matrix (for Mueller matrix polarimeters)

Chapter V

Rotating Sample

Spectropolarimeter Results

This Chapter describes several examples of measurements using the rotating sample spectropolarimeter described in the previous Chapter. The first three materials examined in the rotating sample spectropolarimeter were ferroelectric liquid crystal materials. The linear diattenuation and linear birefringence for the liquid crystals are presented. The samples described in Section B are the cadmium sulfide and cadmium selenide waveplates that comprise the infrared achromatic retarder used in the dual rotating retarder spectropolarimeter. Linear retardance, linear birefringence, and linear diattenuation are given. In addition, dispersion relations for the linear birefringence and refractive indices for these two materials are given.

A. Liquid Crystals

The interest in ferroelectric liquid crystals as spatial light modulators for the visible and near infrared has grown recently due to their high switching speed, substantial birefringence, and low power requirements [6],[7],[8],[77]. In this Section linear birefringence and linear diattenuation spectra from 2.5 to 12 μm for the BDH 764E smectic A^* electroclinic and BDH SCE4 and SCE9 smectic C^* ferroelectric

liquid crystals [78] are presented. The results presented here indicate that the large birefringence ($\Delta n > 0.1$) and the small linear diattenuation ($\mathcal{D} < 2\%$ in non-absorbing regions) warrant investigation of these liquid crystalline materials for use as spatial light modulators in the mid-infrared.

Wu [79] gives an overview of previous measurements of the birefringence of liquid crystals. Many of these techniques are suitable only for discrete wavelengths, or require theoretical interpolation [80],[81]. The birefringence spectra of nematic liquid crystals from 2 to 16 μm have been estimated using theoretical models and through measurements in an FTIR spectrometer [44],[82]. The previous techniques do not measure the linear diattenuation of the liquid crystal, however. The spectro-polarimetric technique applied here combines polarimetric techniques [10],[45],[47] with Fourier transform spectroscopy [72] to produce linear diattenuation and linear birefringence spectra.

The linear retardance δ of the liquid crystal sample is defined as the difference between the phase change for the extraordinary wave δ_e and the phase change for the ordinary wave δ_o of the two linear eigenpolarizations of a sample $\delta = |\delta_e - \delta_o|$ upon transmission through the sample. The linear birefringence $\Delta n = |n_e - n_o|$, the linear retardance δ, and the sample thickness d are related by

$$\Delta n(\lambda) = \frac{\lambda}{2\pi d}\delta(\lambda). \tag{5-1}$$

Larger birefringence is desirable for liquid crystal devices, since the resulting device can be fabricated thinner and will switch faster.

Linear diattenuation is a measure of the tendency of a sample to linearly polarize incident light which is unpolarized. The linear diattenuation $\mathcal{D}$ [12] is defined as

$$\mathcal{D} = \frac{|T_e - T_o|}{T_e + T_o}, \tag{5-2}$$

where T_e and T_o are the principal intensity transmittances associated with the extraordinary and ordinary rays of a material with linear eigenpolarizations. For an ideal polarizer $\mathcal{D} = 1$, while for a purely retarding sample $\mathcal{D} = 0$. Diattenuation is undesirable in an electrooptical modulator. The presence of linear diattenuation prevents a half wave retardance modulator from switching exactly between the two circular polarization states, or two orthogonal linearly polarized states. The larger the linear diattenuation, the further from orthogonal the initial and final polarization states are.

The liquid crystal samples were prepared at the University of Colorado in Boulder and measured in a spectropolarimeter developed at the University of Alabama in Huntsville [72]. The spectropolarimeter utilizes a rotating sample polarimeter [50],[51] located in the sample compartment of a Fourier transform infrared spectrometer (Figure 5-1). In this configuration the measurements of linear diattenuation and linear retardance are immune to crosstalk from circular diattenuation (circular dichroism) and circular retardance (optical activity); i. e. circular diattenuation or circular retardance do not influence the measured values of the linear diattenuation or the linear retardance.

The three liquid crystals investigated in this study were the British Drug House mixtures 764E, SCE4, and SCE9. The 764E mixture is an electroclinic mixture at elevated temperatures [83] while the latter two are broad temperature smectic C^* ferroelectric liquid crystals. All three samples were in the SMC^* phase at the measurement temperature 25°C. The samples were mounted between two uncoated CaF_2 windows with 50 μm spacing.

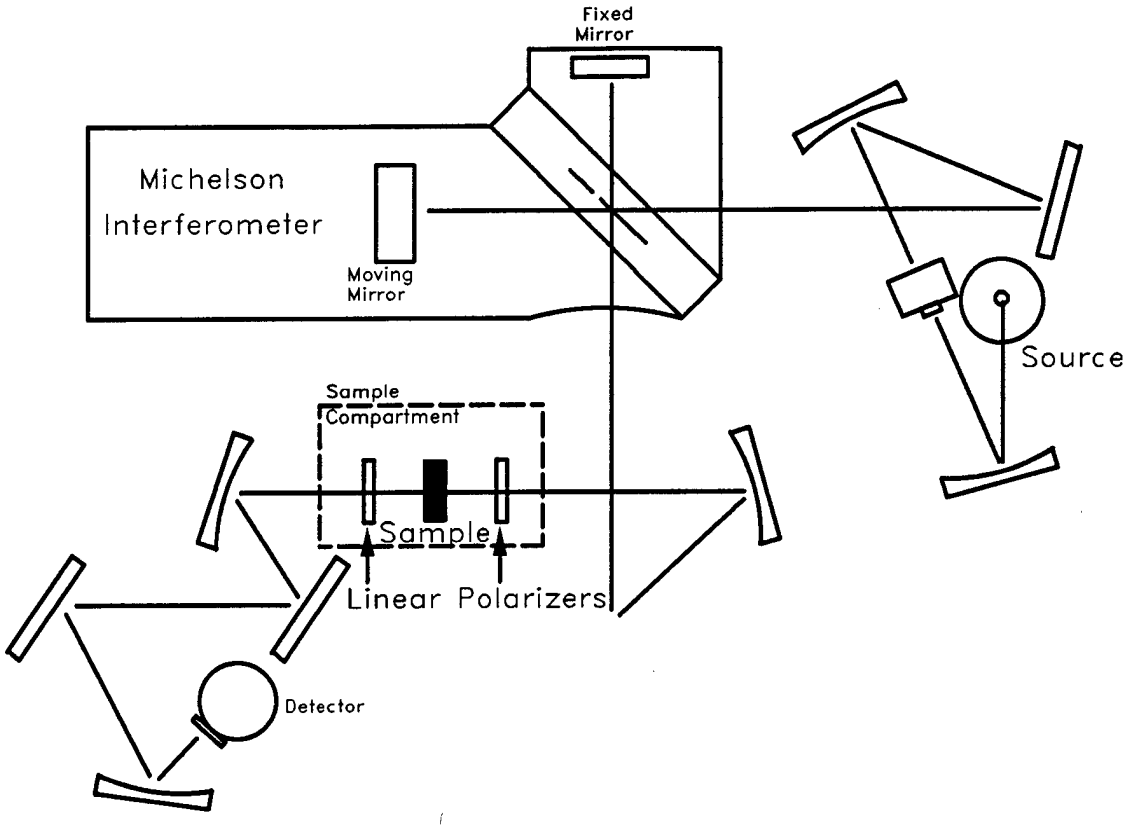

Figure 5-1: The Fourier transform infrared spectropolarimeter. The rotating sample polarimeter is placed in the sample compartment.

Figure 5-2 shows the transmission, linear diattenuation, and linear birefringence spectra of the 764E liquid crystal material. Figure 5-3 shows the spectra for the SCE4 material and Figure 5-4 for the SCE9 material. Table 5-1 gives the numerical values for the transmission, linear diattenuation, and linear birefringence for the 5.5 μm laser line and the 9.6 μm and 10.6 μm CO_2 laser lines. The transmission spectra include absorption by the CaF_2 windows. CaF_2 is completely absorbing beyond 12 μm.

Gaps have been introduced in the diattenuation and birefringence spectra where the transmission is less than 2%. In these regions, the spectropolarimeter cannot determine accurate values of the diattenuation and retardance because there is not enough light. In the absorption bands, the magnitudes of the Fourier componenents of the polarimetric signal become small and noisy and the resulting quantities are consequently less accurate.

Table 5-1: Transmission, linear diattenuation, and linear birefringence of the liquid crystals LCE4, LCE9, and 764E at the 5.5 μm CO and the 9.6 μm and 10.6 μm CO_2 laser lines.

Wavelength (μm)	Transmission (%)	Linear Diattenuation (%)	Linear Bire-fringence Δn
	LCE4		
5.5	73.7	1.1	0.138
9.6	4.7	5.2	0.56
10.6	5.5	0.8	0.21
	LCE9		
5.5	72.3	13.4	0.095
9.6	13.3	1.8	0.37
10.6	4.4	30.8	0.30
	764E		
5.5	57.0	1.6	0.178
9.6	7.4	0.6	0.39
10.6	3.7	3.8	0.589

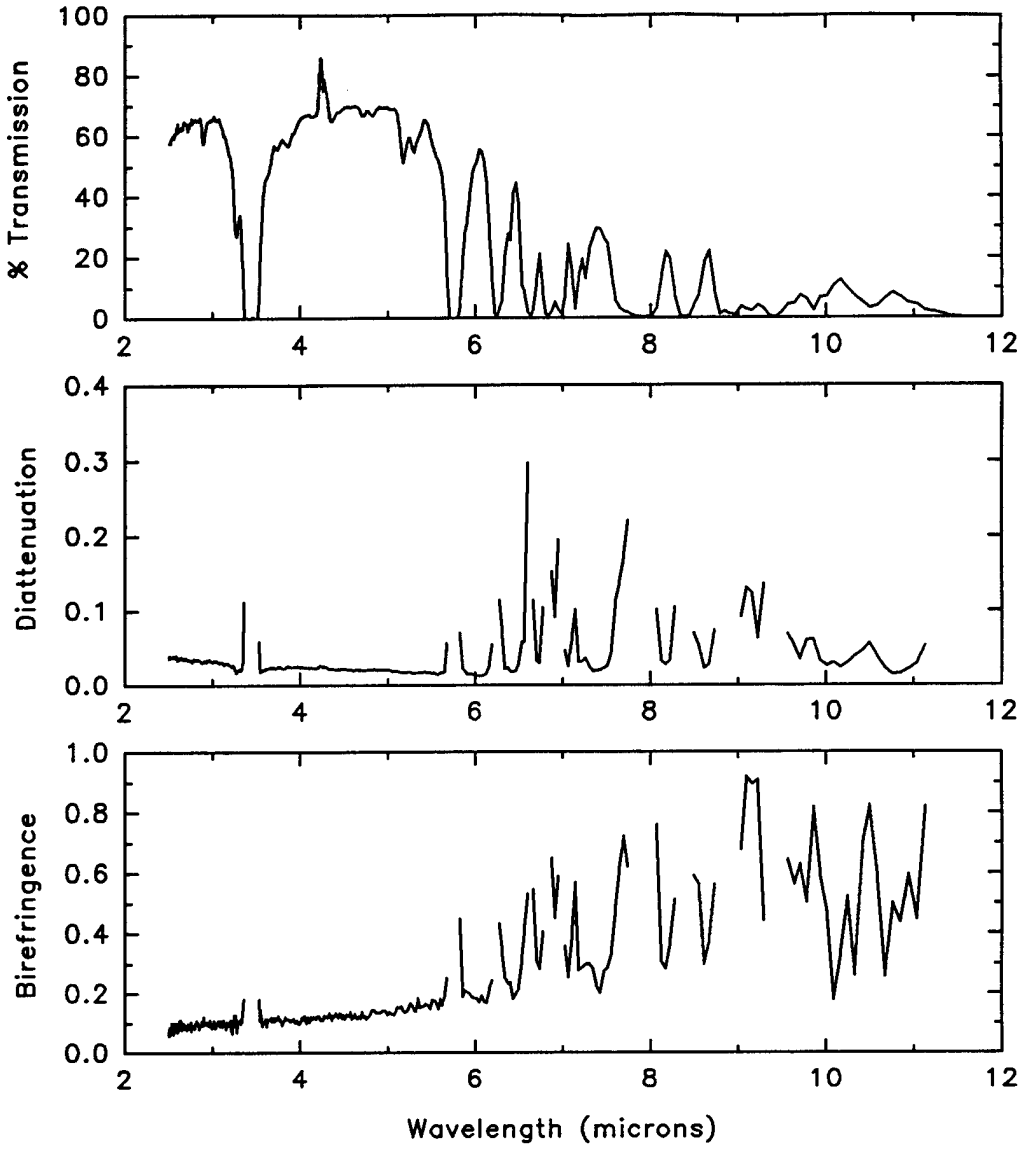

Figure 5-2: The transmission, linear diattenuation, and linear birefringence of the BDH 764E liquid crystal.

Remarkably large values of linear birefringence are seen near the absorption bands; values of $\Delta n > 0.2$ occur at points of small but non-zero transmission. The diattenuation is also large at these points relative to the diattenuation in the non-absorbing regions. Although the large birefringence is potentially useful for a modulation device at these wavelengths, a high throughput, purely retarding device could not be constructed due to the low transmission and substantial diattenuation.

Diattenuation and birefringence fundamentally result from a difference between the complex refractive indices for the two eigenpolarization states of the sample [84],[85]. Further, when the corresponding absorption bands of the two eigenpolarizations are shifted in wavelength, then the diattenuation spectra and the retardance spectra show anomalous dispersion, as these spectra do.

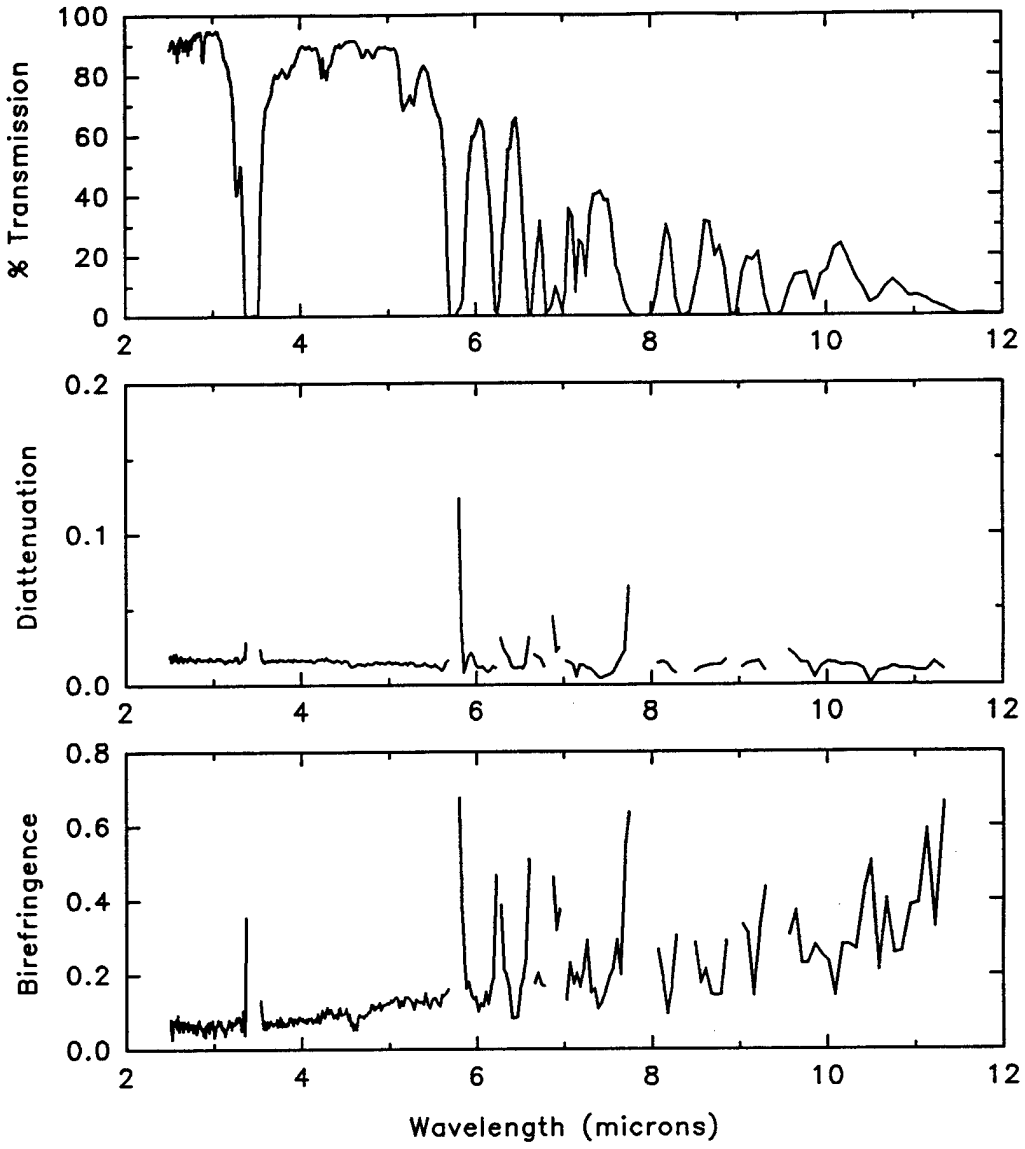

Figure 5-3: The transmission, linear diattenuation, and linear birefringence of the BDH SCE4 liquid crystal.

For all three samples, the 3.5 μm to 5.5 μm band is suitable for broad band modulation. In this region, the birefringence is nearly proportional to wavelength (the best fit line to the birefringence crosses the axis near $\lambda = 0 \mu m$.) Thus, the linear retardance across this waveband is nearly constant. The resulting modulator would be achromatic, working with high efficiency with monochromatic or broadband illumination. The small linear diattenuation in this band (less than 2%) is of little concern. The relatively high birefringence $\Delta n \geq 0.1$ enables a relatively thin infrared modulation devices, with a correspondingly fast response time.

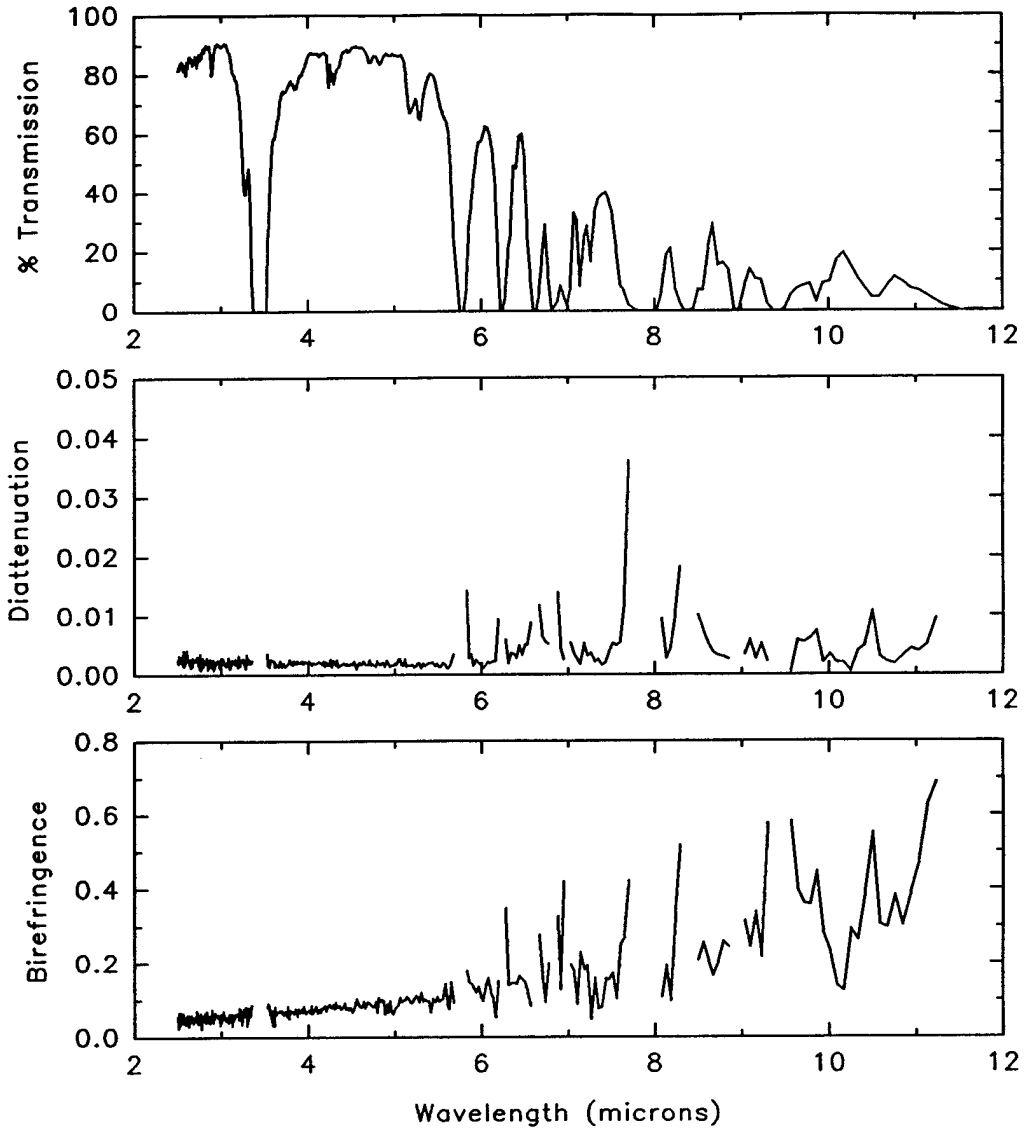

Figure 5-4: The transmission, linear diattenuation, and linear birefringence of the BDH SCE9 liquid crystal.

Further work remains to be performed in measuring the infrared polarizing properties of liquid crystals as a function of applied electric field. Also, knowledge of the depolarization spectra (i. e. the tendency to couple polarized light into unpolarized light) will be useful. Liquid crystals are expected to display measurable depolarization due to the size of the molecules, and the imperfect arrangement of these molecules in devices.

B. Cadmium Sulfide and Cadmium Selenide

This section presents measurements of the birefringence for cadmium sulfide (CdS) and cadmium selenide (CdSe) from 2.5 to 16.5 μm. This wavelength range includes the region from 10.6 to 16.5 μm for which no birefringence measurements have been previously reported. Previous researchers have measured the birefringence and dispersion of CdS and CdSe throughout the visible and mid-infrared using interferometric techniques [86] and by the method of minimum deviation from a prism [87],[88]. Our birefringence measurements utilize a rotating sample polarimeter [50],[51],[74] operating in the sample compartment of a Fourier transform spectrometer.

Section 1 contains the birefringence spectra of CdS and CdSe from 2.5 to 16.5 μm. Section 2 describes the theory of our rotating sample spectropolarimeter measurement technique and data reduction procedures. Section 3 presents estimates to the ordinary and extraordinary refractive indices obtained from an extrapolation of previously published dispersion relations combined with our experimentally determined birefringence. The application of these materials to an achromatic infrared retarder is discussed in the conclusion.

1. Dispersion of Birefringence of Cadmium Sulfide and Cadmium Selenide

Cadmium sulfide and cadmium selenide are positive uniaxial crystals which display linear birefringence. The linear birefringence (henceforth just "birefringence") Δn is defined as the difference between the extraordinary refractive index n_e and the ordinary refractive index n_o. We measured single crystal samples of CdS and CdSe whose faces were polished and plane parallel. The samples were grown by vapor deposition and cut so that the crystal axes lie in the plane of the plate, the common configuration of plates for use in linear retarders. Both faces of both plates had broad-band anti-reflection coatings. The plates were illuminated at normal incidence. The CdS sample was 1.295± 0.010 mm thick and the CdSe plate was 1.100± 0.010 mm thick.

Figure 5-5 shows the birefringence for CdS and CdSe from 2.5 to 16.5 μm as measured in the rotating sample spectropolarimeter. The data from 10.6 μm to 16.5 μm extends the range of previously published birefringence data. Table 5-2 contains tabulated values for the birefringence in columns two and five. We estimate the uncertainty in this data as ± 0.0002 based upon studies of our systematic errors [89].

The linear diattenuation [12] of both samples was also measured and found to be less than 0.2% over most of the 2.5 to 16.5 μm wavelength range, rising to less than 0.5% at either end of this range. The linear diattenuation describes the degree of linear polarization of the transmitted light when unpolarized light is incident.

This birefringence data is now compared to previously reported birefringence data. Previously published refractive index data for CdS and CdSe [90],[91],[92],[93] over the spectral region 1.0 μm to 10.6 μm are given in the form of Sellmeier disper-

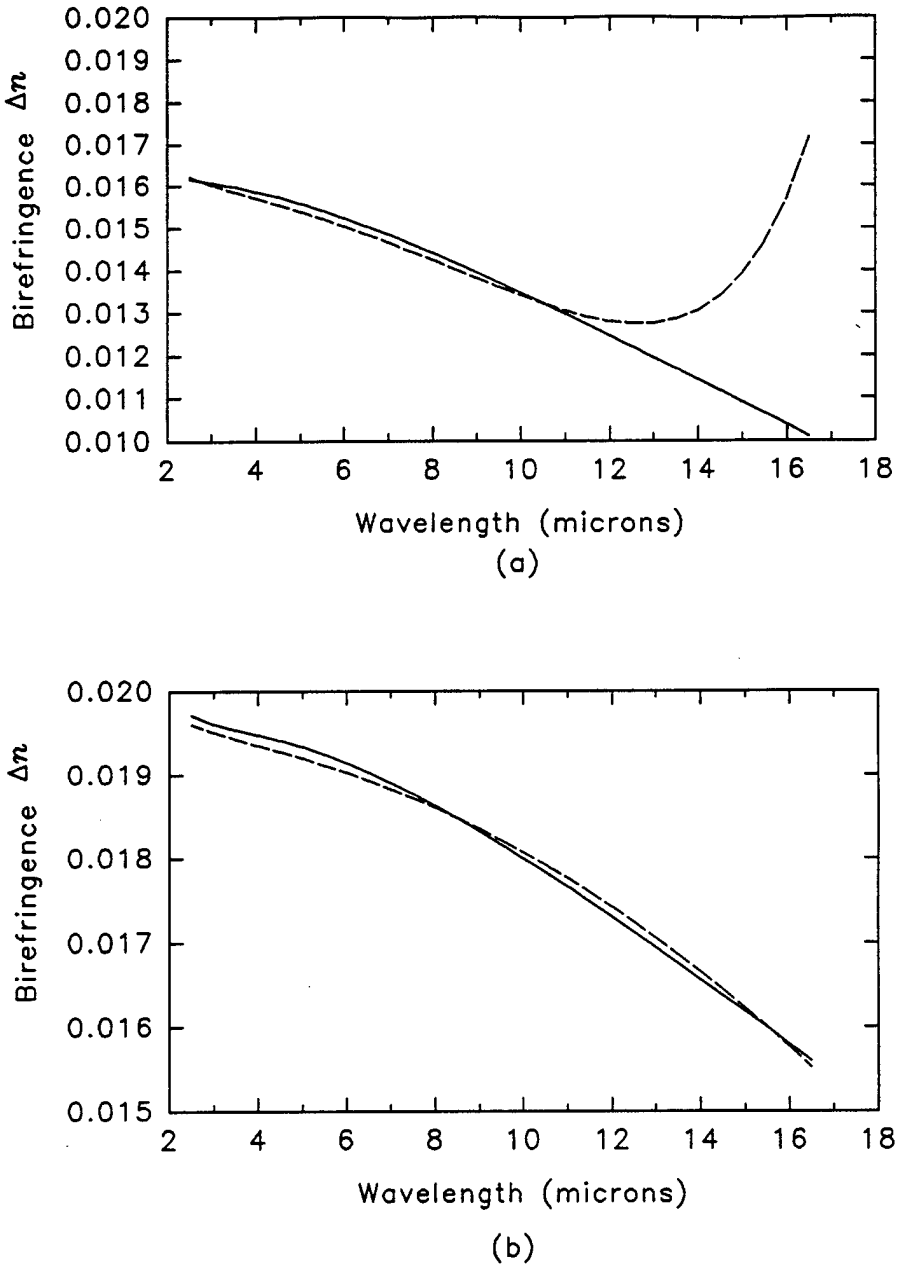

Figure 5-5: The birefringence of (a) CdS and (b) CdSe. The solid line shows the experimental data and the dashed line shows the birefringence predicted by previous dispersion relations.

sion equations. Fig. 5-5a (CdS) and 5-5b (CdSe) compares our measurements (solid lines) with the birefringence computed from previous dispersion relations (dotted lines) [89]. These dispersion relations were not intended for use beyond 10.6 μm but are shown here to demonstrate the need for data at longer wavelengths. Over the 2.5 to 10.6 μm range of the previously published data, the agreement between the previously published data and our experimental results is better than 1.3% for the CdS sample and better than 0.7% for CdSe.

Table 5-2: Birefringence and refractive indices from 2.5 to 16.5 μm for CdS and CdSe.

	CdS			CdSe		
λ	Δn	n_o	n_e	Δn	n_o	n_e
2.5	0.0162	2.2809	2.2969	0.0197	2.4601	2.4798
3.0	0.0161	2.2772	2.2932	0.0196	2.4553	2.4749
3.39	0.0160	2.2749	2.2909	0.0196	2.4527	2.4723
3.5	0.0160	2.2744	2.2903	0.0195	2.4521	2.4716
4.0	0.0159	2.2719	2.2878	0.0195	2.4497	2.4692
4.5	0.0157	2.2695	2.2853	0.0194	2.4478	2.4672
5.0	0.0156	2.2671	2.2827	0.0193	2.4460	2.4654
5.5	0.0154	2.2645	2.2800	0.0192	2.4444	2.4637
6.0	0.0152	2.2619	2.2772	0.0191	2.4429	2.4620
6.5	0.0150	2.2590	2.2742	0.0190	2.4413	2.4603
7.0	0.0148	2.2559	2.2709	0.0189	2.4397	2.4586
7.5	0.0146	2.2525	2.2673	0.0188	2.4380	2.4568
8.0	0.0144	2.2489	2.2634	0.0186	2.4363	2.4549
8.5	0.0142	2.2450	2.2593	0.0185	2.4345	2.4530
9.0	0.0139	2.2407	2.2547	0.0183	2.4326	2.4509
9.5	0.0137	2.2361	2.2498	0.0182	2.4306	2.4488
9.6	0.0137	2.2351	2.2488	0.0181	2.4302	2.4483
10.0	0.0135	2.2311	2.2445	0.0180	2.4285	2.4465
10.5	0.0132	2.2256	2.2388	0.0178	2.4263	2.4442
10.6	0.0132	2.2245	2.2376	0.0178	2.4258	2.4437
11.0	0.0130	2.2197	2.2326	0.0177	2.4240	2.4417
11.5	0.0127	2.2133	2.2259	0.0175	2.4216	2.4391
12.0	0.0125	2.2063	2.2186	0.0173	2.4190	2.4363
12.5	0.0122	2.1987	2.2107	0.0171	2.4163	2.4335
13.0	0.0120	2.1905	2.2021	0.0169	2.4135	2.4305
13.5	0.0117	2.1814	2.1928	0.0168	2.4106	2.4274
14.0	0.0114	2.1715	2.1827	0.0166	2.4075	2.4241
14.5	0.0112	2.1607	2.1716	0.0164	2.4043	2.4207
15.0	0.0109	2.1488	2.1595	0.0162	2.4010	2.4171
15.5	0.0106			0.0160	2.3974	2.4134
16.0	0.0104			0.0158	2.3938	2.4095
16.5	0.0101			0.0156	2.3899	2.4055

2. Measurement and Data Reduction

This section describes the measurement technique and the data reduction procedures used to measure birefringence spectra. We briefly describe the rotating sample spectropolarimeter, the wavelength dependent signal from the polarimeter, and the relation of the sample's birefringence to the polarimetric signal. Finally the curve fit procedure used to calculate the birefringence spectrum is discussed.

The rotating sample spectropolarimeter shown in Figure 5-1 is used to measure linear diattenuation and retardance spectra of infrared samples. The linear retardance δ and linear diattenuation $\mathcal{D}$ present in the sample induce a wavelength dependent modulation in the detected signal as the sample rotates. The spectral transmittance $I(\theta,\lambda)$ of the rotating sample spectropolarimeter [51] as a function of the sample's retardance $\delta(\lambda)$, the sample's diattenuation $\mathcal{D}(\lambda)$, the sample's orientation θ, and the wavelength λ is

$$\begin{aligned} I(\theta,\lambda) &= 1+\frac{1}{2}\left[1+\sqrt{1-\mathcal{D}^2(\lambda)}\cos\delta(\lambda)\right] \\ &\quad +\mathcal{D}(\lambda)\cos 2\theta \\ &\quad +\frac{1}{2}\left[1-\sqrt{1-\mathcal{D}^2(\lambda)}\cos\delta(\lambda)\right]\cos 4\theta \\ &= a_0(\lambda)+a_2(\lambda)\cos 2\theta + a_4(\lambda)\cos 4\theta . \end{aligned} \tag{5-3}$$

This is a Fourier series in θ with coefficients a_0, a_2, and a_4. If the linear diattenuation $\mathcal{D}$ of the sample is nearly zero as is the case for CdS and CdSe, the fourth harmonic coefficient becomes

$$a_4(\lambda)=\frac{1}{2}-\frac{1}{2}\cos\delta(\lambda). \tag{5-4}$$

The retardance of the sample is directly related to the phase of the oscillations of the fourth harmonic. Figure 5-6 shows, for example, the spectrum of the fourth harmonic coefficient $a_4(\lambda)$ for CdS. This spectrum includes the wavelength dependent transmission of the sample and instrument. The $a_4(\lambda)$ spectrum undergoes a series of maxima and minima as the retardance varies with wavelength. At wavelengths where $a_4(\lambda)$ is a maximum, the retardance is an odd multiple of π. The retardance is an even multiple of π when $a_4(\lambda)$ is a minimum. As the wavelength decreases, each minimum represents an additional wave (2π radians) of retardance. The absolute retardance for the spectrum is determined from prior knowledge of the proper order of retardance at a single wavelength.

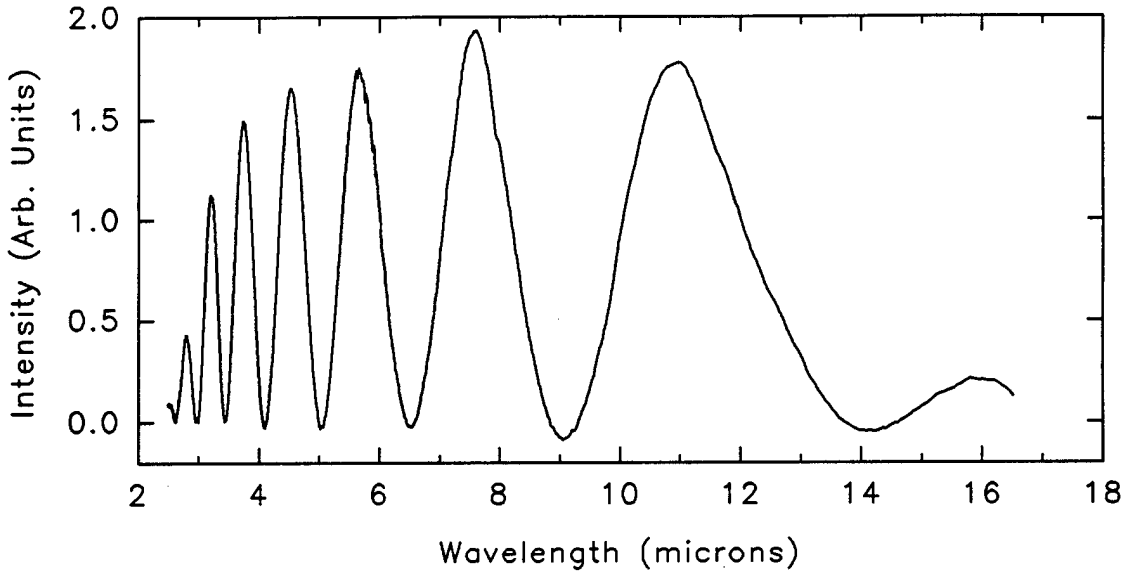

Figure 5-6: The fourth harmonic coefficient spectrum of the output intensity from the rotating sample spectropolarimeter for the CdS sample. The phase of the signal is related to the retardance of the sample at each wavelength.

The Fourier amplitudes $a_k(\lambda)$ are determined experimentally by a discrete Fourier transform of a set of sixteen intensity spectra taken every 22.5° of sample orientation. The magnitude of the retardance $|\delta(\lambda)|$ is determined by an appropriate curve fit to the signal of Fig. 5-6. The sign of the retardance, which determines whether the fast axis of the retarder is horizontal or vertical, is not determined by this method, but was previously known.

We choose to fit the fourth harmonic spectrum of Fig. 5-6 to an equation of the form

$$a_4(\lambda) = \alpha_0 + \alpha_1\lambda + \alpha_2\lambda^2 + (\beta_0 + \beta_1\lambda + \beta_2\lambda^2)\cos\left(\gamma_0 + \frac{\gamma_1}{\lambda} + \frac{\gamma_2}{\lambda^2 - \gamma_3}\right), \tag{5-5}$$

which contains enough terms to give a good fit to both the amplitude and the phase of the experimental data. The terms in α and β are needed to fit the transmission spectrum. The argument of the cosine gives the retardance as a function of wavelength to within $\pm 2n\pi$. The last term in the argument of the cosine is of the general form of a Sellmeier dispersion equation [89],[90], a relation typically used to represent the dispersion for CdS and CdSe and other infrared materials. γ_0 needs to be adjusted by $2n\pi$ using the birefringence at a specific wavelength and the known thickness of the sample in order to determine the absolute retardance and remove the 2π ambiguity mentioned above. Then, the birefringence spectrum $\Delta n(\lambda)$ is calculated from the retardance spectrum,

$$\Delta n(\lambda) = \frac{\lambda}{2\pi d}\delta(\lambda) = \frac{\lambda}{2\pi d}\left(\gamma_0 + \frac{\gamma_1}{\lambda} + \frac{\gamma_2}{\lambda^2 - \gamma_3}\right) \tag{5-6}$$

where d is the thickness of the sample.

Curve fitting was done by a commercial software package [94] which employed the Marquardt-Levenberg algorithm. Initial values for the free parameters were determined by obtaining close graphical matches to the data. The curve fit then converged rapidly. The result was independent of the starting values for the parameters, indicating that unique solutions were obtained.

3. Extrapolation of Dispersion Relations

This section describes the estimation of the ordinary and extraordinary refractive indices from 10.6 to 15 μm for CdS and to 16.5 μm for CdSe by a method which combines the birefringence measurements with previously published dispersion relations. The birefringence data is used to extrapolate the previous dispersion relations for the ordinary n_o and extraordinary n_e refractive indices to longer wavelengths.

Interpolation of refractive index data from experimental data has been performed by previous workers to obtain dispersion relations for CdS and CdSe from the visible to 10.6 μm [89],[90],[95],[96]. Dispersion relations for infrared materials are typically given in terms of the Sellmeier equation [89],[90]

$$n^2(\lambda) = A + \frac{B\lambda^2}{\lambda^2 - C} + \frac{D\lambda^2}{\lambda^2 - E}. \tag{5-7}$$

Two sets of Sellmeier constants A - E are required to describe uniaxial materials: one set for n_o and one for n_e. The dispersion relations for n_o and n_e were fitted to the birefringence values $\Delta n = n_e - n_o$ of Fig. 5-5 using the previously published values for the Sellmeier coefficients as starting points. Figure 5-7 shows the refractive indices resulting from the curve fit and from the previous dispersion relations [89]. The data for CdS extends only to 15 μm due to the proximity of its absorption

band. The agreement between the fitted refractive index data and the previous data is 0.04% or better over the 2.5 to 10.6 μm range. Table 5-3 contains the new coefficients. Table 5-2 contains tabulated values for the refractive indices.

Table 5-3: Coefficients for the Sellmeier equation extrapolated from previous dispersion relations and experimental birefringence.

	CdS		CdSe	
Coefficients	n_o	n_e	n_o	n_e
A	3.7255	3.6522	4.1318	4.0832
B	1.4491	1.5975	1.8584	2.0041
C	0.16339	0.14526	0.21999	0.20646
D	1.2612	1.4869	2.7673	3.9928
E	733.21	794.56	2962.98	3866.93

It should be emphasized that the refractive indicies reported here were not measured directly but are extrapolations from previous dispersion relations and the experimentally determined birefringence. The curve fit to the difference $\Delta n = n_e - n_o$ does not give a unique solution, since both ordinary and extraordinary indices could be higher or lower by the same amount and still give reasonable results for the difference $\Delta n(\lambda)$ in the curve fit. Thus, care should be taken in using the refractive index results presented here. In spite of these cautions, we believe these results to be useful in light of their excellent agreement with previous

results at shorter wavelengths and the current lack of data at longer wavelengths. The birefringence data is experimentally determined and does not suffer from this problem.

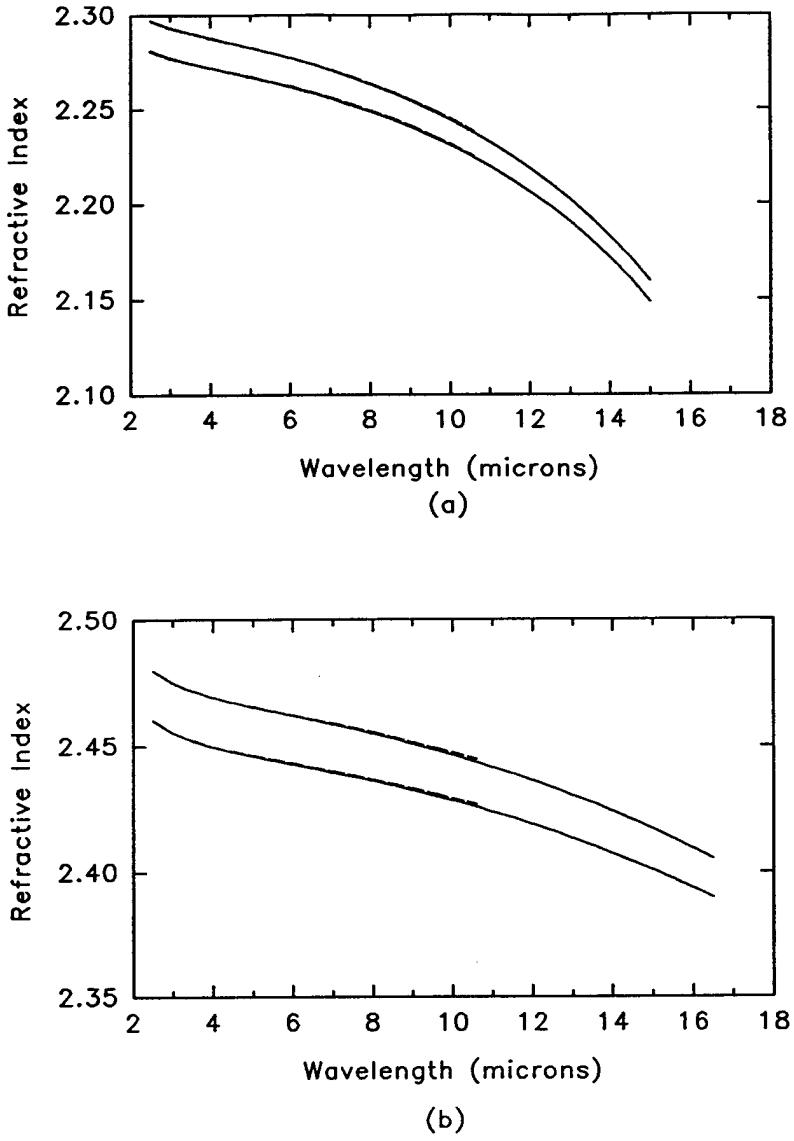

Figure 5-7: The refractive indices of (a) CdS and (b) CdSe. The solid lines show the extrapolation from previous relations using our birefringence data. The dashed lines show the indices calculated from previous dispersion relations to 10.6 μm, the long-wavelength limit of these relations. The extraordinary indices are on top.

4. Conclusion

The birefringence values reported here have been useful in analyzing the design of an achromatic retarder for infrared polarimetry applications [69]. An achromatic retarder can be constructed by placing the fast axes of a CdS and a CdSe plate perpendicular to each other and the transmission axis. By adjusting the thickness of the plates t_1 and t_2, the retardance of the system $\delta(\lambda) = \frac{2\pi}{\lambda}(\Delta n_1 t_1 - \Delta n_2 t_2)$ can be made relatively achromatic. Fig. 5-8 shows the retardance of such a device designed for a quarter-wave of retardance from 3 to 14 μm as measured on our spectropolarimeter [51].

The birefringence for CdS and CdSe has been reported in the wavelength range from 2.5 to 16.5 μm. This range represents a substantial increase in the valid wavelength range for these optical constants. This birefringence data was used to extrapolate previous dispersion relations for the ordinary and extraordinary indices of refraction.

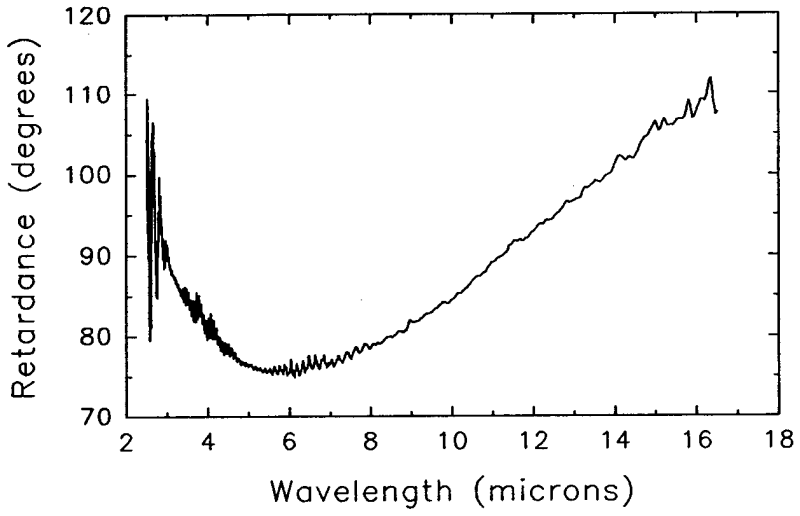

Figure 5-8: The retardance spectrum of the infrared achromatic retarder.

Chapter VI

Mueller Matrix Spectropolarimeter

The dual rotating retarder Mueller matrix polarimeter and its implementation in the infrared spectropolarimeter are presented in this Chapter. Derivation of the data reduction for the polarimeter is given assuming ideal polarization elements and proper alignment of the polarization elements. A discussion of some of the most important systematic errors possible in the dual rotating retarder polarimeter is given with examples of the effects of the systematic errors on some of the Mueller matrix elements. A derivation of an improved data reduction that removes or corrects some of the systematic errors is given. Using these data reduction algorithms and a calibration step, the systematic errors are calculated and removed from the experimental Mueller matrix. The calibration procedure, the calibration equations, and an example of how the data reduction improves spectropolarimetric Mueller matrix data are given in this Chapter.

Section B presents the data reduction equations for the dual rotating retarder polarimeter when all elements are assumed to be ideal. Section C shows the effect of the orientation and retardance errors on this data reduction. Section D gives the derivation of the data reduction equations that correct for these systematic errors

and describes how the errors are determined. Section E demonstrates the data reduction in an Fourier transform infrared spectropolarimeter. Section F discusses other systematic errors and how their effect is minimized in the spectropolarimeter.

A. Introduction

The dual rotating retarder polarimeter proposed by Azzam [10],[45],[72] yields a complete Mueller matrix through the Fourier analysis of a single detected signal. The data reduction algorithm for this polarimeter as originally presented assumes ideal polarization elements and no orientational errors. The data reduction algorithms may be generalized to remove systematic errors which result when these requirements on the polarization elements and their orientation are relaxed. We present here a technique to determine and remove systematic errors generated by large orientation errors of the polarization elements and large retardance errors in the quarter-wave retarders. We demonstrate how the accuracy of the Mueller matrix suffers from these errors and show how to remove the errors from the data set. Finally, we demonstrate the error correction technique on a system that is inherently subject to large retardance errors, a Fourier transform infrared spectropolarimeter, where the wavelength dependence of the retarders would otherwise produce unacceptable results.

Figure 6-1 shows the configuration of a dual rotating retarder polarimeter. It consists of a sample between a polarization state generator and polarization state analyzer each comprised of a stationary linear polarizer and rotating quarter-wave linear retarder. When the retarders are rotated in a five to one ratio, all sixteen elements of the sample Mueller matrix are encoded onto twelve harmonics of the detected intensity signal, which can then be Fourier analyzed to recover the Mueller matrix elements. If the polarization elements are misaligned, or the retarders do

not have exactly one-quarter wave of retardance, the Fourier amplitudes and phases change resulting in errors in the sample Mueller matrix. Even small orientational and retardance errors ($< 1°$) can lead to large errors in the measured Mueller matrix ($>$ 10% in some matrix elements). These errors become especially important when the retardance and alignment vary significantly from their nominal values such as in multi-wavelength or spectral instruments. Here we expand on previous work incorporating correction terms for large orientation and retardance errors into the dual rotating retarder data reduction algorithm. This procedure is useful for spectral and multi-wavelength systems where changing the retardances of the retardation elements or exchanging the retardation elements is impractical or impossible.

Goldstein and Chipman [59] developed data reduction equations to remove systematic errors in the measured Mueller matrix due to small errors in the initial orientations of the polarization elements ($< 0.3°$) and small retardance errors ($< 2°$). Hauge presented a similar analysis with imperfect retarders [46]. Hauge includes the diattenuation of the retarders but does not include orientational error of the second polarizer. In our application the former is less important than the latter [59]. We have extended the research by Goldstein to include large orientation errors of the retarders and the second polarizer and large retardance errors in the retarders. The data reduction equations we have developed correct for orientational errors up to $22.5°$ and retardance errors up to $\lambda/8$. The motivation was to establish data reduction equations for Mueller matrix measurements over a large spectral band ($3\,\mu m$ to $14\,\mu m$) in which the achromatic retarders in our infrared spectropolarimeter display relatively large deviations ($\pm 15°$) from one quarter wave of retardance.

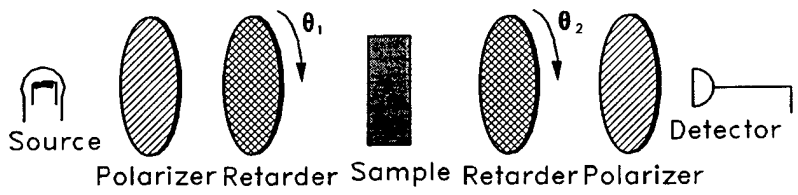

Figure 6-1: The dual rotating retarder polarimeter configuration.

B. Dual Rotating Retarder Mueller Matrix Polarimeter

Figure 6-1 shows the dual rotating retarder polarimeter proposed by Azzam. The polarizers remain stationary such that the transmission axes parallel to one another. The two retarders each have one quarter wave of retardance. The quarter wave retarders are rotated in a 5 to 1 ratio between radiometric measurements, which are made sequentially. The 5 to 1 rotation ratio of the two retarders is chosen so that all sixteen elements of the sample Mueller matrix are encoded onto twelve frequencies in the detected signal. The measurement cycle begins with the fast axes of the retarders parallel to the transmission axes of the polarizers. The detected signal is Fourier analyzed and the Mueller matrix elements are calculated from the Fourier amplitudes.

A set of N intensity measurements is required to determine the sample Mueller matrix. The n th measurement is described by the following Mueller matrix equation for the polarimeter,

$$\vec{S}_{out}(n) = \mathbf{M}_{sys}\vec{S}_{in} \tag{6-1}$$

$$= \mathbf{M}_{LP2}\mathbf{M}_{LR2}(n)\mathbf{M}_{sample}\mathbf{M}_{LR1}(n)\mathbf{M}_{LP1}\vec{S}_{in}$$

where M_{LP1} and M_{LP2} are the Mueller matrices of ideal polarizers with their transmission axes oriented along the horizontal $\hat{x}$ direction,

$$\mathbf{M}_{LP1} = \mathbf{M}_{LP2} = \frac{1}{2}\begin{pmatrix} 1 & 1 & 0 & 0 \\ 1 & 1 & 0 & 0 \\ 0 & 0 & 0 & 0 \\ 0 & 0 & 0 & 0 \end{pmatrix}. \tag{6-2}$$

$\mathbf{M}_{LR1}(n)$ and $\mathbf{M}_{LR2}(n)$ are the Mueller matrices of the quarter wave linear retarders in the polarization state generator and the polarization state analyzer,

$$\mathbf{M}_{LR1} = \begin{pmatrix} 1 & 0 & 0 & 0 \\ 0 & \cos^2 2n\Delta\theta & \sin 2n\Delta\theta\cos 2n\Delta\theta & -\sin 2n\Delta\theta \\ 0 & \cos 2n\Delta\theta\sin 2n\Delta\theta & \sin^2 2n\Delta\theta & \cos 2n\Delta\theta \\ 0 & \sin 2n\Delta\theta & -\cos 2n\Delta\theta & 0 \end{pmatrix} \tag{6-3}$$

and

$$\mathbf{M}_{LR2} = \begin{pmatrix} 1 & 0 & 0 & 0 \\ 0 & \cos^2 10n\Delta\theta & \sin 10n\Delta\theta\cos 10n\Delta\theta & -\sin 10n\Delta\theta \\ 0 & \cos 10n\Delta\theta\sin 10n\Delta\theta & \sin^2 10n\Delta\theta & \cos 10n\Delta\theta \\ 0 & \sin 10n\Delta\theta & -\cos 10n\Delta\theta & 0 \end{pmatrix}, \tag{6-4}$$

where $\theta_n = n\Delta\theta$. $\Delta\theta$ is given by $\Delta\theta = T/N$ where T is the total rotation of the first retarder in the measurement cycle (typically π or 2π) and N is the total number of measurements within one measurement cycle. For example if $T = \pi$ and $N = 30$, the first measurement is made with the first retarder oriented at $0°$ and the second retarder at $0°$, the second measurement is made with the first retarder oriented at $\Delta\theta = 6°$ and the second retarder at $5\Delta\theta = 30°$, and the nth measurement is made with the first retarder oriented at $n\Delta\theta$ and the second retarder at $5n\Delta\theta$. Finally, $\mathbf{M}_{sample}$ in Eq. 6-1 is the Mueller matrix of the sample under test,

$$\mathbf{M}_{sample} = \begin{pmatrix} m_{11} & m_{12} & m_{13} & m_{14} \\ m_{21} & m_{22} & m_{23} & m_{24} \\ m_{31} & m_{32} & m_{33} & m_{34} \\ m_{41} & m_{42} & m_{43} & m_{44} \end{pmatrix}. \tag{6-5}$$

The output intensity is given by the first element of the output Stokes vector, $s_{0,out}(n)$. The expression for the measured intensity I_n is expanded and rewritten to produce terms that correspond to the Fourier series expansion

$$I_n = \frac{a_0}{2} + \sum_{k=1}^{12} (a_k \cos 2k\theta_n + b_k \sin 2k\theta_n). \tag{6-6}$$

The Fourier coefficients a_k and b_k are functions of the sixteen elements of the sample Mueller matrix. These expressions are inverted to give the Mueller matrix elements in terms of the Fourier series coefficients. These relations for the Mueller matrix elements are given in Table 6-1.

The dual rotating retarder configuration has a number of advantages. First, the effect of any instrumental polarization preceding the polarizing optics or following the polarimeter is negated by the fixed position of the polarizers. Second, the Fourier transform on the data automatically performs a least squares fit to the overdetermined data set. Third, this configuration is largely immune to beam wander if measurements are made over a 2π cycle. In this case, modulation from beam wander produced by wedges in the rotating retarders is encoded principally on the first and fifth Fourier amplitudes. Since the polarimeter does not modulate these frequencies, the beam wander signal does not affect the accuracy of the measured Mueller matrix.

C. Computer Modelling

In this section, we present several plots that demonstrate how systematic errors seriously affect the accuracy of the dual rotating retarder polarimeter.

The errors that are included in the present development are shown in Figure 6-2. The two retarders have retardances δ_1 and δ_2. The transmission axis of the first polarizer defines the x-axis from which the orientations of the following ele-

ments are measured and thus has no error. The first and second retarders and second polarizer have orientation errors ϵ_3, ϵ_4, and ϵ_5 respectively. The orientation errors of the retarders ϵ_3 and ϵ_4 correspond to the initial orientations of the fast axes with respect to the coordinate system defined by the first polarizer. These misalignments remain constant throughout the measurement cycle. For example, for a misalignment of ϵ_3 of the first retarder, the orientation of the retarder for the n th measurement is $2n\Delta\theta - 2\epsilon_3$. The present development does not include the presence of retardance in the polarizers, diattenuation in the retarders, or diattenuation less than 1 in the polarizers.

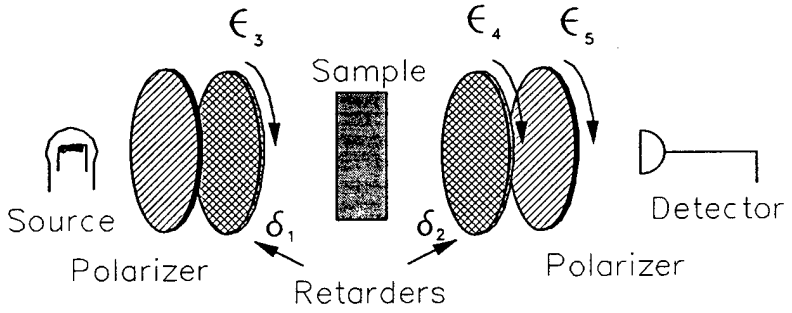

Figure 6-2: The dual rotating retarder polarimeter with retardance and orientation systematic errors.

All five systematic errors in the polarimeter may be present simultaneously, and the effect of the systematic errors may be different depending on the polarization properties of the sample. All possibilities cannot be presented here and we show only the effect of a few systematic errors on the identity matrix, i.e. the sample is completely non-polarizing. This does not give complete information on the effect of the systematic error on the calculated sample matrix when the sample is polarizing and care should be taken that wrong inferences are not drawn from what we

present here. However, an example matrix must be chosen in order to show the effect of the systematic errors. For purposes of the demonstration here, the effect of the systematic errors are seen as the deviations from the unit matrix.

Although all matrix elements show inaccuracies as a result of the systematic errors, the four elements in the middle sub-matrix show the largest. Of these four elements, the m_{22} and m_{33} elements are approximately of the same magnitude, and the m_{23} and m_{32} elements have the same magnitude. Thus only the m_{22} and m_{23} elements are shown here.

Three dimensional plots showing the effect of variations of two of the errors while the other three are held constant were generated from the simulation. Figure 6-3 shows the effects of varying the retardances of the two retarders δ_1 and δ_2 from 80° to 100° with $\epsilon_3 = \epsilon_4 = \epsilon_5 = 0°$. In this range, the value of the m_{22} element is linearly proportional to the value of the retardances. This situation could occur in a tunable laser polarimeter where any mis-orientations can be easily corrected, but the retardance in the retardance changes as the laser is detuned from the nominal $\lambda/4$ wavelength of the retarders. For $\delta_1 = \delta_2 = 80°$, the error in the m_{22} element is approximately 35%. The m_{23} element is unaffected by changes in the retardance and is not shown. Figure 6-4 shows the effect of a non-ideal second retarder on the sample Mueller matrix elements m_{22} and m_{23}. The orientation of the second retarder ϵ_4 varies from -10° to 10° and the retardance of the second retarder δ_2 from 80° to 100° with $\epsilon_3 = \epsilon_5 = 0°$ and $\delta_1 = 90°$. The situation could occur for systems in which the second retarder is imperfect and is difficult to align.

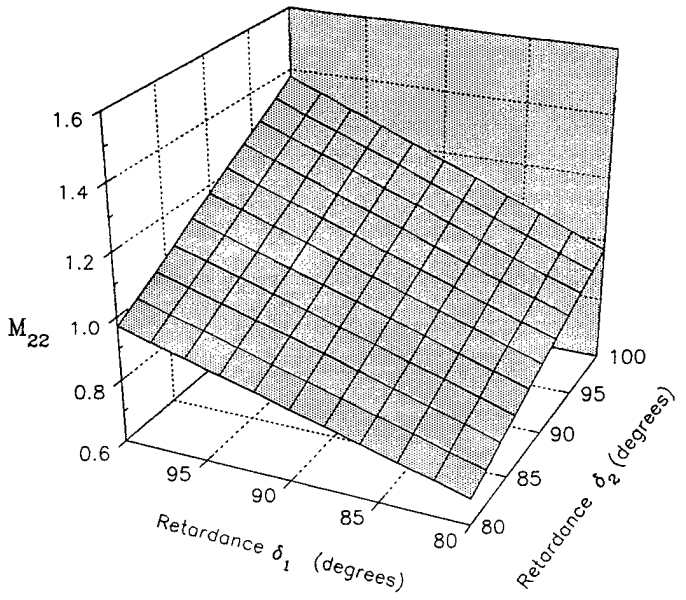

Figure 6-3: The uncorrected m_{22} element of a non-polarizing Mueller matrix as a function of the retardance of the two retarders.

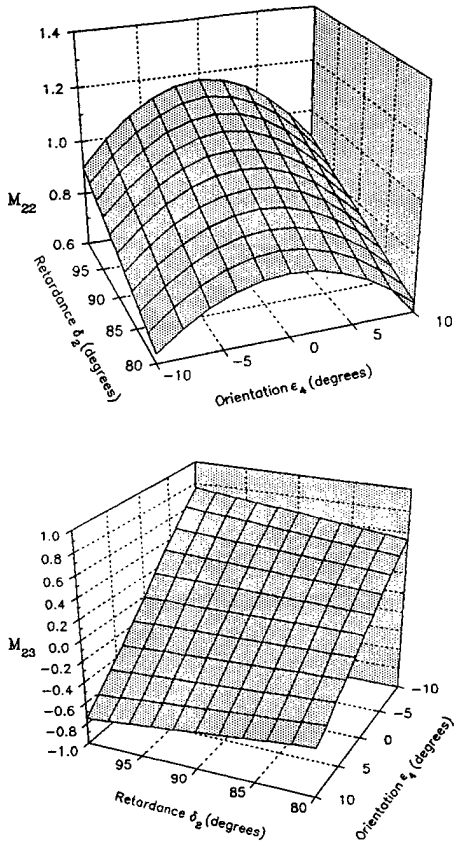

Figure 6-4: The uncorrected m_{22} and m_{23} elements of a non-polarizing Mueller matrix with a non-ideal second retarder in the polarimeter.

D. Removal of Systematic Errors

In this section, we present the data reduction equations which remove the five systematic errors of the previous section.

The system Mueller matrix equation for the dual rotating retarder polarimeter including the five systematic errors shown in Figure 6-2 is given by

$$\vec{S}_{out}(n) = \mathbf{M}_{sys}\vec{S}_{in} \tag{6-7}$$

$$= \mathbf{M}_{LP2}(\epsilon_5)\mathbf{M}_{LR2}(n, \delta_2, \epsilon_4)\mathbf{M}_{sample}\mathbf{M}_{LR1}(n, \delta_1, \epsilon_3)\mathbf{M}_{LP1}\vec{S}_{in},$$

where M_{LP2} is now misaligned by ϵ_5 from the $\hat{x}$ direction. The polarizer is rotated by an amount ϵ_5

$$\mathbf{M}_{LP2}(\epsilon_5) = \mathbf{R}(-\epsilon_5)\mathbf{M}_{LP2}\mathbf{R}(\epsilon_5), \tag{6-8}$$

where $\mathbf{R}(\epsilon)$ is the Mueller matrix used for a rotational change of basis perpendicular to the optical axis of the polarimeter [11]. $\mathbf{M}_{LR1}(n, \delta_1, \epsilon_3)$ and $\mathbf{M}_{LR2}(n, \delta_2, \epsilon_4)$ are the Mueller matrices of the quarter wave linear retarders with retardances δ_1 and δ_2 and misalignments ϵ_3 and ϵ_4,

$$\mathbf{M}_{LR1}(n, \delta_1, \epsilon_3) = \mathbf{R}(-\epsilon_3)\mathbf{M}_{LR1}(n, \delta_1)\mathbf{R}(\epsilon_3)$$

$$= \begin{pmatrix} 1 & 0 & 0 & 0 \\ 0 & C_4\sin^2(\delta_1/2)+\cos^2(\delta_1/2) & S_4\sin^2(\delta_1/2) & -S_2\sin\delta_1 \\ 0 & S_4\sin^2(\delta_1/2) & -C_4\sin^2(\delta_1/2)+\cos^2(\delta_1/2) & C_2\sin(\delta_1) \\ 0 & S_2\sin\delta_1 & -C_2\sin(\delta_1) & \cos(\delta_1) \end{pmatrix}, \tag{6-9}$$

where $C_2 = \cos(2\theta_n - 2\epsilon_3)$, $S_2 = \sin(2\theta_n - 2\epsilon_3)$, $C_4 = \cos(4\theta_n - 4\epsilon_3)$, and $S_4 = \sin(4\theta_n - 4\epsilon_3)$. Similarly for $\mathbf{M}_{LR2}$,

$$\mathbf{M}_{LR2}(n, \delta_2, \epsilon_4) = \mathbf{R}(-\epsilon_4)\mathbf{M}_{LR1}(n, \delta_2)\mathbf{R}(\epsilon_4)$$

$$= \begin{pmatrix} 1 & 0 & 0 & 0 \\ 0 & C_{20}\sin^2(\delta_2/2)+\cos^2(\delta_2/2) & S_{20}\sin^2(\delta_2/2) & -S_{10}\sin\delta_2 \\ 0 & S_{20}\sin^2(\delta_2/2) & -C_{20}\sin^2(\delta_2/2)+\cos^2(\delta_2/2) & C_{10}\sin(\delta_2) \\ 0 & S_{10}\sin\delta_2 & -C_{10}\sin(\delta_2) & \cos(\delta_2) \end{pmatrix}, \tag{6-10}$$

where $C_{10} = \cos(10\theta_n - 2\epsilon_4)$, $S_{10} = \sin(10\theta_n - 2\epsilon_4)$, $C_{20} = \cos(20\theta_n - 4\epsilon_4)$, and $S_{20} = \sin(20\theta_n - 4\epsilon_4)$. The intensity, given by the first element of the output Stokes vector in Eq. 6-7, is now a function of the five error terms, $\delta_1, \delta_2, \epsilon_3, \epsilon_4$, and ϵ_5. This is written in the form of the Fourier series of Eq. 6-6. The new coefficients in terms of the error terms and sample Mueller matrix elements are

$$a_0 = \frac{1}{2}m_{11} + \frac{1}{4}\beta_3 m_{12} + \frac{1}{4}\beta_4 \cos 2\epsilon_5 m_{21} + \frac{1}{8}\beta_3\beta_4 \cos 2\epsilon_5 m_{22}$$

$$+ \frac{1}{4}\beta_4 \sin 2\epsilon_5 m_{31} + \frac{1}{8}\beta_3\beta_4 \sin 2\epsilon_5 m_{32}$$

$$a_1 = \frac{1}{2}\sin\delta_1 \sin 2\epsilon_3 m_{14} + \frac{1}{4}\sin\delta_1\beta_4 \sin 2\epsilon_3 \cos 2\epsilon_5 m_{24}$$

$$+ \frac{1}{4}\beta_4 \sin\delta_1 \sin 2\epsilon_3 \sin 2\epsilon_5 m_{34}$$

$$a_2 = \frac{1}{4}\beta_1 \cos 4\epsilon_3 m_{12} + \frac{1}{4}\beta_1 \sin 4\epsilon_3 m_{13} + \frac{1}{8}\beta_1\beta_4 \cos 4\epsilon_3 \cos 2\epsilon_5 m_{22}$$

$$+ \frac{1}{8}\beta_1\beta_4 \sin 4\epsilon_3 \cos 2\epsilon_5 m_{23} + \frac{1}{8}\beta_1\beta_4 \cos 4\epsilon_3 \sin 2\epsilon_5 m_{32}$$

$$+ \frac{1}{8}\beta_1\beta_4 \sin 4\epsilon_3 \sin 2\epsilon_5 m_{33}$$

$$a_3 = -\frac{1}{8}\beta_1 \sin\delta_2 \sin\alpha_3 m_{42} - \frac{1}{8}\beta_1 \sin\delta_2 \cos\alpha_3 m_{43}$$

$$a_4 = -\frac{1}{4}\sin\delta_1 \sin\delta_2 \cos\alpha_1 m_{44}$$

$$a_5 = \frac{1}{2}\sin\delta_2 \sin\alpha_5 m_{41} + \frac{1}{4}\beta_3 \sin\delta_2 \sin\alpha_5 m_{42} \qquad (6\text{-}11)$$

$$a_6 = \frac{1}{4}\sin\delta_1 \sin\delta_2 \cos\alpha_2 m_{44}$$

$$a_7 = -\frac{1}{8}\beta_1 \sin\delta_2 \sin\alpha_4 m_{42} + \frac{1}{8}\beta_1 \sin\delta_2 \cos\alpha_4 m_{43}$$

$$a_8 = \frac{1}{16}\beta_1\beta_2 \cos\alpha_9 (m_{22} + m_{33}) + \frac{1}{16}\beta_1\beta_2 \sin\alpha_9 (m_{32} - m_{23})$$

$$a_9 = \frac{1}{8}\beta_2 \sin\delta_1 \sin\alpha_6 m_{24} + \frac{1}{8}\beta_2 \sin\delta_1 \cos\alpha_6 m_{34}$$

$$a_{10} = \frac{1}{4}\beta_2 \cos\alpha_{11} m_{21} + \frac{1}{8}\beta_2\beta_3 \cos\alpha_{11} m_{22} + \frac{1}{4}\beta_2 \sin\alpha_{11} m_{31} + \frac{1}{8}\beta_2\beta_3 \sin\alpha_{11} m_{32}$$

$$a_{11} = -\frac{1}{8}\beta_2 \sin\delta_1 \sin\alpha_7 m_{24} - \frac{1}{8}\beta_2 \sin\delta_1 \cos\alpha_7 m_{34}$$

$$a_{12} = \frac{1}{16}\beta_1\beta_2 \cos\alpha_{10}(m_{22} - m_{33}) + \frac{1}{16}\beta_1\beta_2 \sin\alpha_{10}(m_{23} + m_{32})$$

$$b_0 = 0$$

$$b_1 = \frac{1}{2}\sin\delta_1 \cos 2\epsilon_3 m_{14} + \frac{1}{4}\beta_4 \sin\delta_1 \cos 2\epsilon_3 \cos 2\epsilon_5 m_{24}$$

$$+ \frac{1}{4}\beta_4 \sin\delta_1 \cos 2\epsilon_3 \sin 2\epsilon_5 m_{34}$$

$$b_2 = -\frac{1}{4}\beta_1 \sin 4\epsilon_3 m_{12} + \frac{1}{4}\beta_1 \cos 4\epsilon_3 m_{13} + \frac{1}{8}\beta_1\beta_4 \cos 4\epsilon_3 \cos 2\epsilon_5 m_{23}$$

$$-\frac{1}{4}\beta_1\beta_4 \sin 4\epsilon_3 \cos 2\epsilon_5 m_{22} + \frac{1}{8}\beta_1\beta_4 \cos 4\epsilon_3 \sin 2\epsilon_5 m_{33}$$

$$-\frac{1}{8}\beta_1\beta_4 \sin 4\epsilon_3 \sin 2\epsilon_5 m_{32}$$

$$b_3 = -\frac{1}{8}\beta_1 \sin\delta_2 \cos\alpha_3 m_{42} + \frac{1}{8}\beta_1 \sin\delta_2 \sin\alpha_3 m_{43}$$

$$b_4 = \frac{1}{4}\sin\delta_1 \sin\delta_2 \sin\alpha_1 m_{44}$$

$$b_5 = -\frac{1}{2}\sin\delta_2 \cos\alpha_5 m_{41} - \frac{1}{4}\beta_3 \sin\delta_2 \cos\alpha_5 m_{42} \qquad \text{(6-12)}$$

$$b_6 = -\frac{1}{4}\sin\delta_1 \sin\delta_2 \sin\alpha_2 m_{44}$$

$$b_7 = -\frac{1}{8}\beta_1 \sin\delta_2 \cos\alpha_4 m_{42} - \frac{1}{8}\beta_1 \sin\delta_2 \sin\alpha_4 m_{43}$$

$$b_8 = -\frac{1}{16}\beta_1\beta_2 \sin\alpha_9 (m_{22} + m_{33}) - \frac{1}{16}\beta_1\beta_2 \cos\alpha_9 (m_{23} - m_{32})$$

$$b_9 = -\frac{1}{8}\beta_2 \sin\delta_1 \cos\alpha_6 m_{24} + \frac{1}{8}\beta_2 \sin\delta_1 \sin\alpha_6 m_{34}$$

$$b_{10} = -\frac{1}{4}\beta_2 \sin\alpha_{11} m_{21} - \frac{1}{8}\beta_2\beta_3 \sin\alpha_{11} m_{22} + \frac{1}{4}\beta_2 \cos\alpha_{11} m_{31} + \frac{1}{8}\beta_2\beta_3 \cos\alpha_{11} m_{32}$$

$$b_{11} = \frac{1}{8}\beta_2 \sin\delta_1 \cos\alpha_7 m_{24} - \frac{1}{8}\beta_2 \sin\delta_1 \sin\alpha_7 m_{34}$$

$$b_{12} = -\frac{1}{16}\beta_1\beta_2 \sin\alpha_{10} (m_{22} - m_{33}) + \frac{1}{16}\beta_1\beta_2 \cos\alpha_{10} (m_{32} + m_{23})$$

There are a number of repeated terms in the errors and the substitutions in α and β have been made to simplify these equations. These substitutions are given in Table 6-2. For a measurement period $T = \pi$, the subscripts k on the Fourier coefficients a_k and b_k correspond to the k th harmonic. For $T = 2\pi$, the k th subscript corresponds to the $2k$ th harmonic.

These expressions are inverted to give the corrected sample Mueller matrix elements which are given by

$$m_{44} = \frac{4}{\sin\delta_1 \sin\delta_2}\left(-\frac{a_4}{\cos\alpha_1} + \frac{a_6}{\cos\alpha_2}\right)$$

$$m_{43} = 8 \cdot \frac{-a_3 \cos\alpha_3 + b_3 \sin\alpha_3 + a_7 \cos\alpha_4 - b_7 \sin\alpha_4}{\beta_1 \sin\delta_2}$$

$$m_{42} = -8 \cdot \frac{a_3 \sin\alpha_3 + b_3 \cos\alpha_3 + a_7 \sin\alpha_4 + b_7 \cos\alpha_4}{\beta_1 \sin\delta_2}$$

$$m_{41} = \frac{-\beta_3 m_{42}}{2} - \frac{4b_5}{\cos\alpha_5 \sin\delta_2}$$

$$m_{24} = 8 \cdot \frac{a_9 \sin\alpha_6 - b_9 \cos\alpha_6 - a_{11} \sin\alpha_7 + b_{11} \cos\alpha_7}{\beta_2 \sin\delta_1}$$

$$m_{34} = 8 \cdot \frac{a_9 \cos\alpha_6 + b_9 \sin\alpha_6 - a_{11} \cos\alpha_7 - b_{11} \sin\alpha_7}{\beta_2 \sin\delta_1}$$

$$m_{14} = \frac{-\beta_4 \cos 2\epsilon_5 m_{24}}{2} + \frac{4b_1}{\cos 2\epsilon_3 \sin\delta_1} - \frac{\beta_4 \sin 2\epsilon_5 m_{34}}{2}$$

$$m_{22} = 16 \cdot \frac{a_8 \cos\alpha_9 + a_{12} \cos\alpha_{10} - b_8 \sin\alpha_9 - b_{12} \sin\alpha_{10}}{\beta_1 \beta_2}$$

$$m_{33} = 16 \cdot \frac{a_8 \cos\alpha_9 - a_{12} \cos\alpha_{10} - b_8 \sin\alpha_9 + b_{12} \sin\alpha_{10}}{\beta_1 \beta_2} \qquad (6\text{-}13)$$

$$m_{23} = 16 \cdot \frac{-a_8 \sin\alpha_9 + a_{12} \sin\alpha_{10} - b_8 \cos\alpha_9 + b_{12} \cos\alpha_{10}}{\beta_1 \beta_2}$$

$$m_{32} = 16 \cdot \frac{a_8 \sin\alpha_9 + a_{12} \sin\alpha_{10} + b_8 \cos\alpha_9 + b_{12} \cos\alpha_{10}}{\beta_1 \beta_2}$$

$$m_{12} = \frac{16a_2 \cos 4\epsilon_3 - 16b_2 \sin 4\epsilon_3 - \beta_1\beta_4 \cos 2\epsilon_5 m_{22} - \beta_1\beta_4 \sin 2\epsilon_5 m_{32}}{2\beta_1}$$

$$m_{13} = \frac{16a_2 \sin 4\epsilon_3 + 16b_2 \cos 4\epsilon_3 - \beta_1\beta_4 \cos 2\epsilon_5 m_{23} - \beta_1\beta_4 \sin 2\epsilon_5 m_{33}}{2\beta_1}$$

$$m_{21} = \frac{16a_{10} \cos\alpha_{11} - 16b_{10} \sin\alpha_{11} - \beta_2\beta_3 m_{22}}{2\beta_2}$$

$$m_{31} = \frac{-(\beta_2\beta_3 m_{32} - 16b_{10} \cos\alpha_{11} - 16a_{10} \sin\alpha_{11})}{2\beta_2}$$

$$m_{11} = 4a_0 - \frac{1}{2}\beta_3 m_{12} - \frac{1}{2}\beta_4 \cos 2\epsilon_5 m_{21} - \frac{1}{4}\beta_3\beta_4 \cos 2\epsilon_5 m_{22}$$

$$- \frac{1}{2}\beta_4 \sin 2\epsilon_5 m_{31} - \frac{1}{4}\beta_3\beta_4 \sin 2\epsilon_5 m_{32}$$

Note that some of the Mueller matrix elements are written in terms of others so that the elements m_{44}, m_{43}, m_{42}, m_{41}, m_{34}, m_{24}, m_{14}, m_{22}, m_{23}, m_{32}, and m_{33} are calculated first, then m_{12}, m_{13}, m_{21}, and m_{31}, and finally m_{11}.

These relations reduce to the equations given in Table 6-1 when the orientational errors go to zero ($\epsilon_3 = \epsilon_4 = \epsilon_5 \rightarrow 0$) and the retardance values go to 90° ($\delta_1 = \delta_2 \rightarrow 90°$). There are no singularities as the orientational errors go to zero or the retardance values go to 90°.

In practice it may be difficult to determine the systematic errors δ_1, δ_2, ϵ_3, ϵ_4, and ϵ_5. If the sample is known, however, the errors can be determined experimentally. Air is non-polarizing and its Mueller matrix, the identity matrix, is known to high accuracy. Accordingly, to determine the systematic errors in the dual rotating retarder polarimeter, the sample is removed and data is collected as described above. With $m_{11} = m_{22} = m_{33} = m_{44} = 1$ and all other elements of the sample matrix zero, the Fourier coefficients become functions of the five systematic errors only. The coefficients are given in Table 6-3. These relations are inverted to give the errors in terms of the experimentally determined Fourier coefficients. The orientational errors and retardance values are given by

$$\epsilon_3 = \frac{1}{4}\tan^{-1}\left(\frac{b_8}{a_8}\right) - \frac{1}{4}\tan^{-1}\left(\frac{b_{10}}{a_{10}}\right)$$

$$\epsilon_4 = \frac{1}{2}\tan^{-1}\left(\frac{b_2}{a_2}\right) - \frac{1}{2}\tan^{-1}\left(\frac{b_6}{a_6}\right) + \frac{1}{4}\tan^{-1}\left(\frac{b_8}{a_8}\right) - \frac{1}{4}\tan^{-1}\left(\frac{b_{10}}{a_{10}}\right)$$

$$\epsilon_5 = \frac{1}{2}\tan^{-1}\left(\frac{b_2}{a_2}\right) + \frac{1}{2}\tan^{-1}\left(\frac{b_8}{a_8}\right) - \frac{1}{2}\tan^{-1}\left(\frac{b_{10}}{a_{10}}\right) \qquad (6\text{-}14)$$

$$\delta_1 = \cos^{-1}\left(\frac{a_{10}\cos\alpha_9 - a_8\cos\alpha_{11}}{a_{10}\cos\alpha_9 + a_8\cos\alpha_{11}}\right)$$

$$\delta_2 = \cos^{-1}\left(\frac{a_2\cos\alpha_9 - a_8\cos(4\epsilon_3 - 2\epsilon_5)}{a_2\cos\alpha_9 + a_8\cos(4\epsilon_3 - 2\epsilon_5)}\right)$$

These values are calculated from the set of intensity measurements made with nothing in the sample compartment. Note that these expressions are in the form of ratios and are therefore independent of the incident intensity as they should be. These calculated errors are then substituted into Eqs. 6-13 to give the corrected Mueller matrix for an arbitrary sample.

The procedure for calibrating and making accurate measurements is as follows.

1. A set of measurements is made with no sample present in the sample compartment. Standard Fourier techniques are used to recover the Fourier coefficients. These coefficients are used to calculate the errors using Eqs. 6-14.
2. The orientations are minimized and another calibration sequence determines the errors again.
3. A set of measurements is made with the sample present. The Fourier coefficients are found. The Mueller matrix elements of the sample are calculated using the errors and the new Fourier coefficients using Eqs. 6-13.

These data reductions equations correct the errors exactly when no other error sources are present. However, if noise sources are present, the system is more efficient with a corresponding increase in signal-to-noise when the errors are minimized, hence the minimization process in step 2 above. In addition, the equations become singular if the retardance go to π or a multiple of 2π or for certain combinations of orientation errors (such as $\alpha_1 = 2\epsilon_4 - 2\epsilon_3 - 2\epsilon_5 = \pi/2$). Therefore as a general rule, we recommend that this data reduction be used only when the orientation errors are less than 22.5° and the retardances are within $\lambda/8$ of the nominal $\lambda/4$.

E. Removal of Systematic Error from an IR Spectropolarimeter

These data reduction equations are essential in broad band instruments where achromatic retarders are not precisely one quarter wave across the spectrum of interest. Our work in infrared spectropolarimetry [51],[72],[74] prompted the development of these equations. The spectropolarimeter is a Fourier transform spectrometer with the dual rotating retarder polarimeter inserted in the sample compartment. The retardance of the achromatic retarders [69] used in the spectropolarimeter varies by $\pm 15°$ over the 3 to 14 μm range of their design (cf. Fig. 6-5). Although this achromatic response is exceptional over such a large wavelength range, the deviation from one quarter wave would introduce unacceptable inaccuracies without proper compensation (Fig. 6-3). In addition, the calibration of the orientation of the polarization elements is difficult in the infrared spectrometer. This section describes our calibration efforts on the FTIR spectropolarimeter utilizing the data reduction for the error correction of the five systematic errors.

The calibration proceeded as described in Section D. A set of measurements were made with no sample in the sample compartment. The orientation errors and retardance values were calculated at each wavelength from the wavelength dependent Fourier series coefficients. The orientation errors were minimized, another set of calibration measurements were made, and the residual errors were calculated. Figures 6-5 and 6-6 show the retardance of the two retarders and the orientations of the polarization elements calculated from the Fourier coefficients in the calibration using Eqs. 6-14. The variation of the orientation for the second retarder is due to a slight misalignment between the two plates of the retarder [51]. The error spectra were then substituted into the equations to produce the corrected identity Mueller matrix.

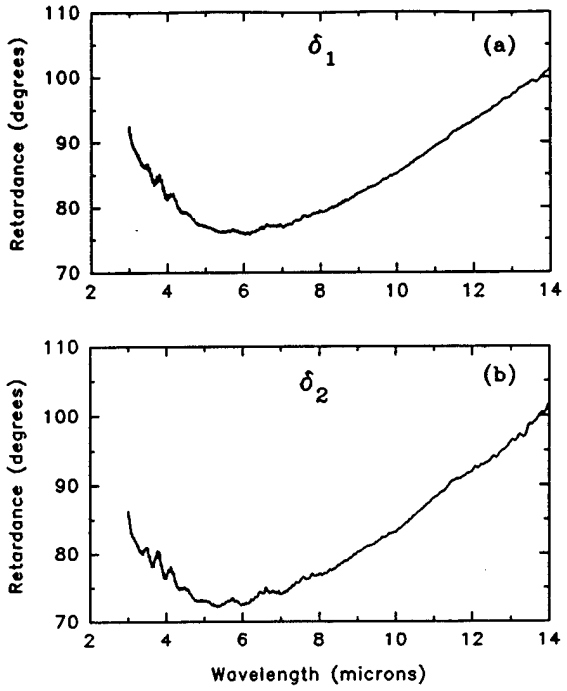

Figure 6-5: The calibrated retardance of the two retarders.

Figure 6-7 shows the calculated Mueller matrix before any correction was done, i.e. using the equations of Table 6-1. Each of the plots shows a spectrum of the Mueller matrix element at its proper position in the Mueller matrix. The wavelength range is 3 to 14 microns, and the matrix has been normalized to the (1,1) element. The expected Mueller matrix spectrum for a non-polarizing sample is the identity matrix. The effect of the wavelength dependence of the retardance is readily apparent in those elements whose behavior is similar to the retardance spectra in Figure 6-6. In elements m_{31}, m_{32}, and m_{23}, the effect of the variation of the fast axis of the one retarder is evident. The amount of error in these Mueller matrix elements due to the misalignment of the fast axis at 5, 7, and 10 μm is as high as 25%. In Figure 6-8 the misalignment of the two plates of the achromatic retarder has been corrected and the oscillation due to this misalignment has been eliminated.

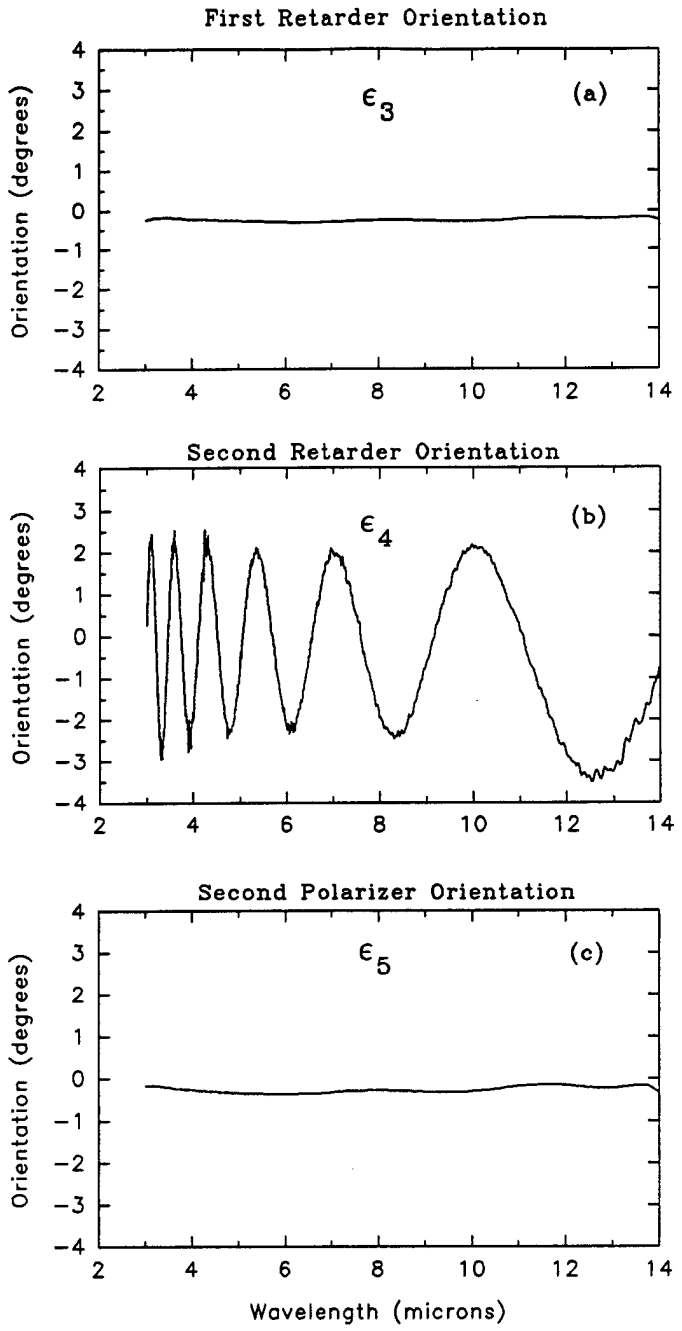

Figure 6-6: The calibrated orientation errors of the polarization elements.

Other residual orientational errors of the elements of the polarimeter have also been corrected. The variation in the retardance of the two retarders has not been corrected. Errors as high as 50% are present in some Mueller matrix elements at certain wavelengths due solely to the wavelength dependence of the retardance. In Figure 6-9 all retardance and orientational errors have been corrected and the measured Mueller matrix agrees with the expected Mueller matrix for a non-polarizing sample. The residual error is less than 4% and is the result of other noise sources in the system. These other noise sources are discussed in the next section.

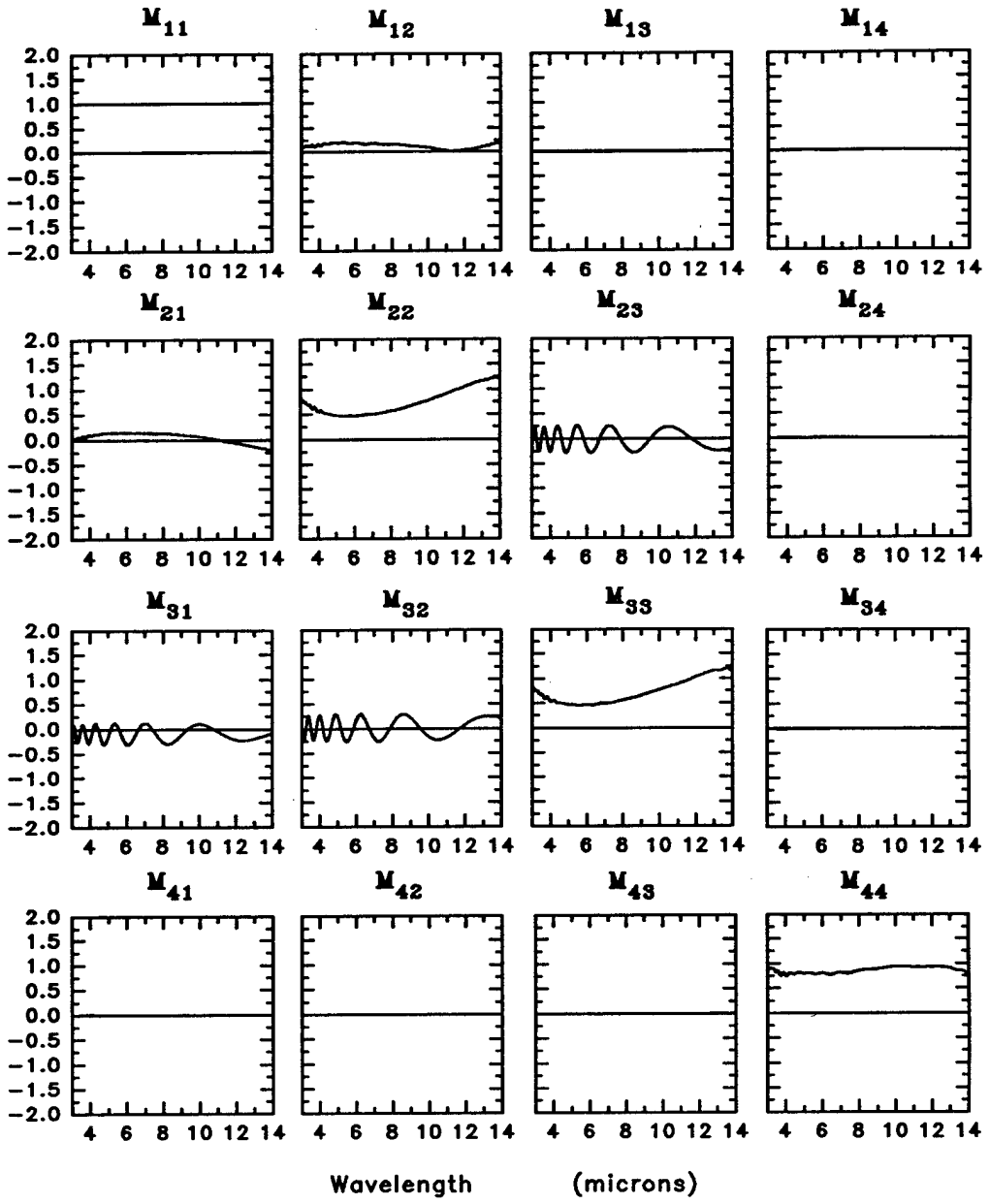

Figure 6-7: The uncorrected Mueller matrix spectrum.

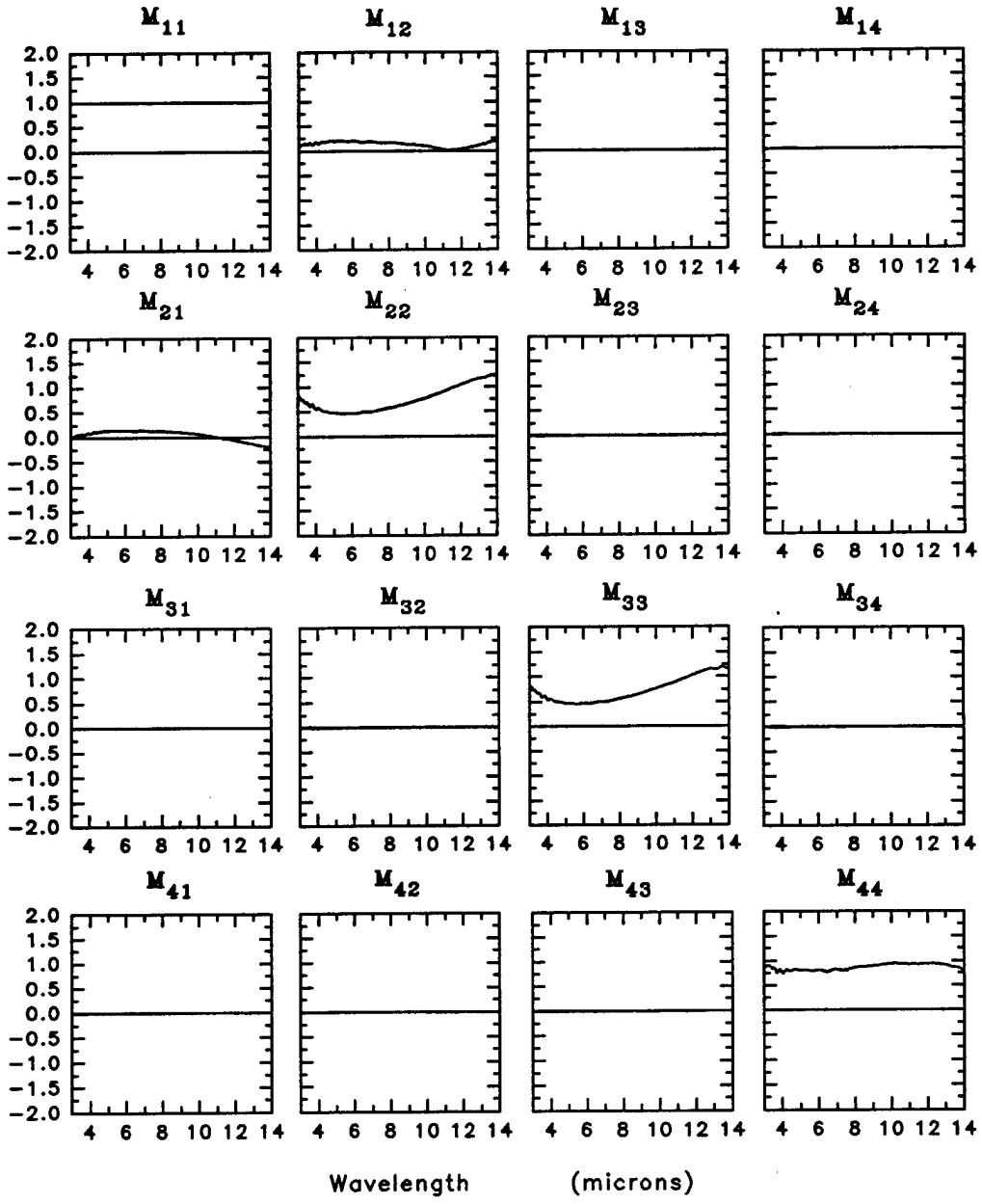

Figure 6-8: The Mueller matrix spectrum corrected for orientation errors but not for the wavelength dependence of the retardance.

As a final note, we describe another application where these data reduction equations are applicable and useful. A laser polarimeter system can be designed to be highly accurate at a particular design wavelength [10]. However without some means of error correction, new retarders would have to be obtained if a different wavelength is to be examined. The data reduction equations provide a means to measure and correct these errors without replacing the retarders. Of course, the wavelength could not be changed so that the retarders have zero or a half-wave of net retardance, but the corrections presented here would allow the same retarders to be used in a much broader wavelength band.

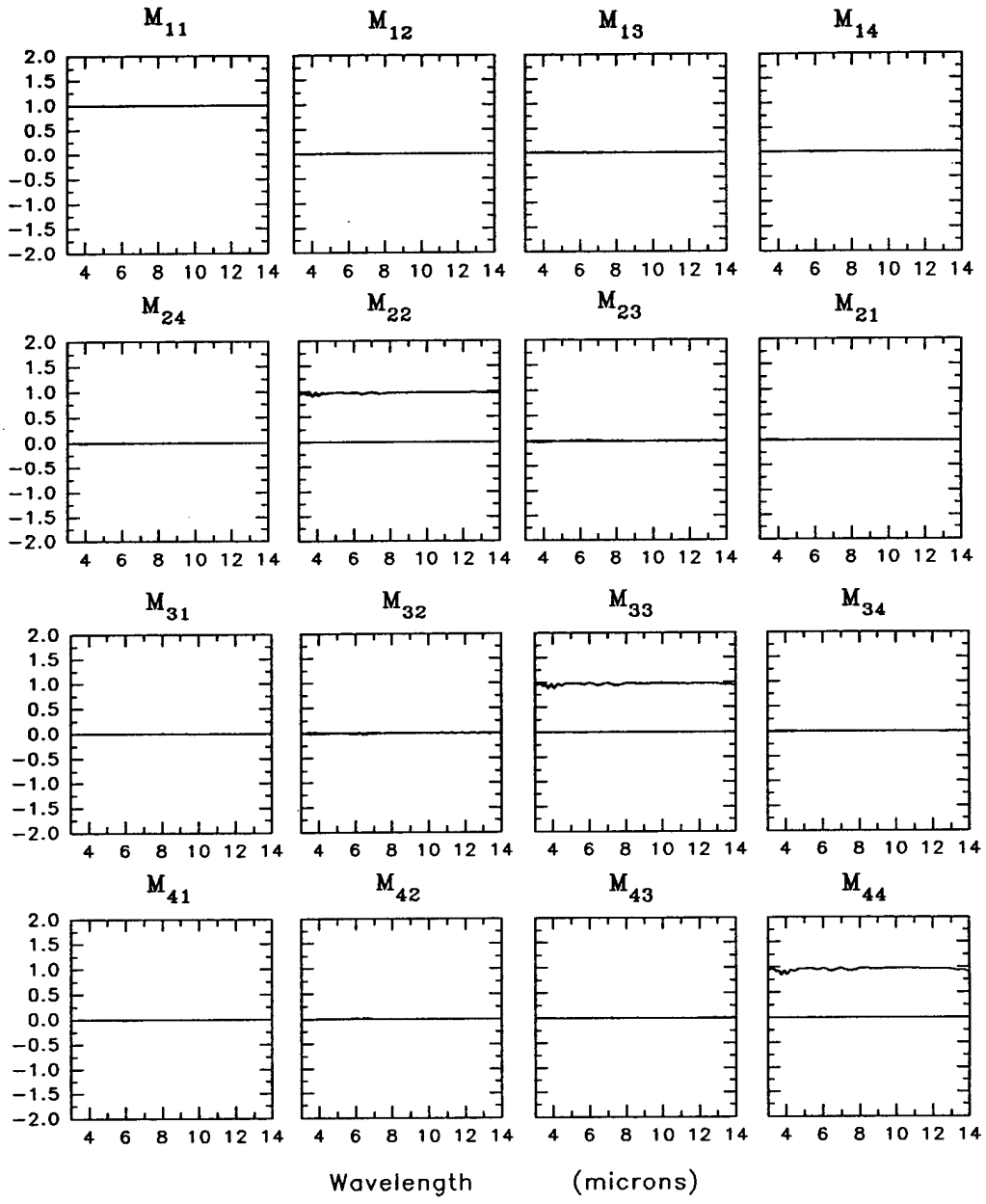

Figure 6-9: The corrected Mueller matrix spectrum.

F. Other Systematic Errors

The residual systematic error in the Mueller matrix of Figure 6-9 is as high as 4% in some parts of the spectrum. This section discusses the likely sources of this error.

The residual error in the Mueller matrix spectrum is seen as a deviation of the diagonal elements from the ideal value of one. This deviation is wavelength dependent and is largest around 4 μm. The off diagonal elements, chiefly the m_{23} and m_{32} elements, display deviations from zero in this same part of the spectrum.

It is likely that there are two main contributors to this residual systematic error. One of the sources of additional error is the non-ideal diattenuation of the polarizers. Figure 6-10 shows the diattenuation and retardance spectra of the wire grid polarizers measured with the rotating sample spectropolarimeter. The diattenuation falls off at shorter wavelengths as would be expected for a wavelength close to the size of the wire grid spacings. This non-ideal diattenuation results in light leaking through the first polarizer in the wrong polarization state. This appears as a partially polarized component of the light in the polarimeter and decreases the modulation of the light as the retarders rotate. This in turn appears as depolarization in the Mueller matrix and all elements of the Mueller matrix take on slightly smaller values at the shorter wavelengths. Since the polarizer allows light to leak through in the orthogonal polarization state, there can be some phase difference between the light in the proper polarization state and the leaked light. This phase difference is simply the retardance shown in Figure 6-10. At longer wavelengths, the retardance becomes a meaningless quantity since the amount of leaked light goes to zero. The data at longer wavelengths has been omitted for this reason.

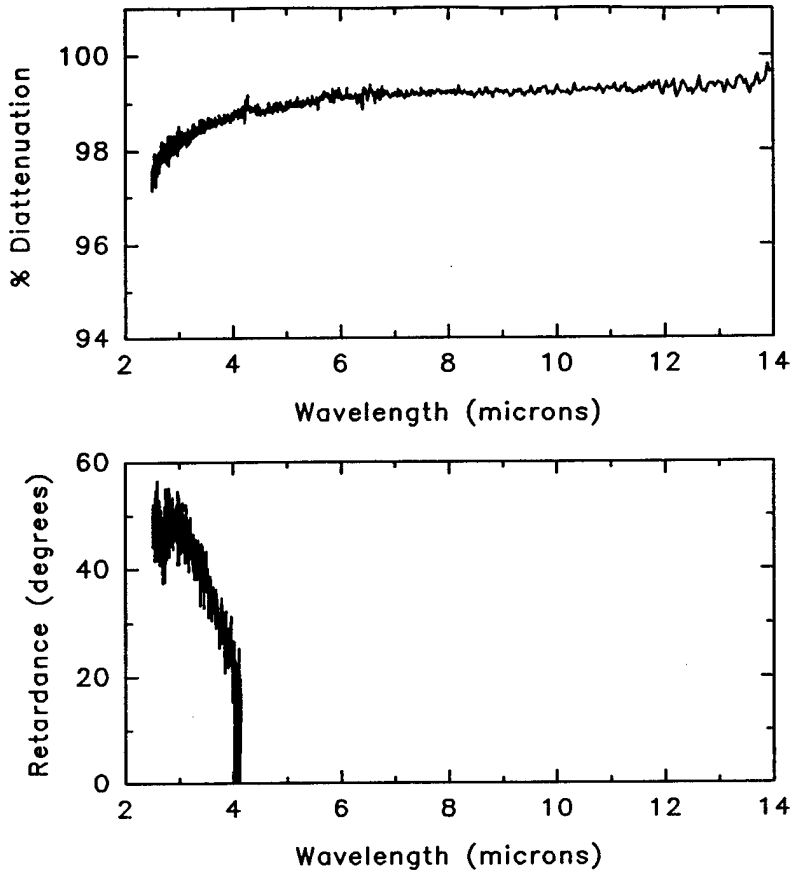

Figure 6-10: Linear diattenuation and retardance spectra of the wire grid polarizer.

The second largest contributor to the systematic error results from the anti-reflection coating of the achromatic retarder. There are significant interference effects from the coatings between 2.5 and 3 μm that prevent Mueller matrix measurements in this part of the spectrum. There are residual effects that can be seen in the retardance spectra (Fig. 6-5) around 4 μm. These effects cause the deviation in the elements of the Mueller matrix that is apparent in Figure 6-9. This exacerbates the problem from the polarizers at these shorter wavelengths and the overall accuracy of the Mueller matrix spectrum is reduced for these wavelengths.

Other possible sources of systematic error that are not removed in the data reduction equations derived above are beam wander produced by the rotating retarders, angle of incidence effects on the retarders, and instrument drift. The error due to beam wander is believed to be minimal since the measurements are made over a rotation of 360° for the first polarizer. This measurement sequence minimizes the effect of the beam wander as discussed in Chapter III. Retardance can vary with angle of incidence for retarders that utilize birefringent materials [97]. This is not believed to be a problem for the achromatic retarders used in the spectropolarimeter. Since the fast axes of the two birefringent plates in the retarder are perpendicular, the change in retardance for a given angle of incidence in the first plate is offset by an opposite change in the second. Further study of the angle of incidence dependence is probably warranted, however.

The reduction or removal of these additional sources of error through a new data reduction algorithm is proposed in Chapter VIII.

G. Conclusion

The dual rotating retarder Mueller matrix polarimeter has been reviewed, and the effect of five systematic errors on its accuracy has been demonstrated. All systematic errors discussed here are associated with the polarization elements used in the polarimeter. These errors are: orientational error in three of the four polarization elements, and retardance error in the quarter wave retarders. The equations presented allow large orientational and retardance errors. There are no singularities as the orientation errors go to zero or the retardances of the retarders go to $\lambda/4$. These equations were developed to facilitate data reduction in a 3 - 14 μm infrared spectropolarimeter which suffers from large retardance error in the

quarter wave retarders. The data reduction equations and error removal procedures presented here have been successful in substantially reducing the systematic errors in an infrared spectropolarimeter.

Table 6-1: Sample Mueller matrix elements in terms of Fourier coefficients when no errors are assumed in the polarimeter.

$$m_{11} = 4a_0 - 4a_2 + 4a_8 - 4a_{10} + 4a_{12}$$

$$m_{12} = 8a_2 - 8a_8 - 8a_{12}$$

$$m_{13} = 8b_2 + 8b_8 - 8b_{12}$$

$$m_{14} = 4b_1 + 4b_9 - 4b_{11}$$

$$m_{21} = -8a_8 + 8a_{10} - 8a_{12}$$

$$m_{22} = 16a_8 + 16a_{12}$$

$$m_{23} = 16b_8 + 16b_{12}$$

$$m_{24} = -8b_9 + 8b_{11}$$

$$m_{31} = -8b_8 + 8b_{10} - 8b_{12}$$

$$m_{32} = 16b_8 + 16b_{12}$$

$$m_{33} = 16a_8 - 16a_{12}$$

$$m_{34} = 8a_9 - 8a_{11}$$

$$m_{41} = 4b_3 - 4b_5 + 4b_7$$

$$m_{42} = -8a_3 - 8b_7$$

$$m_{43} = -8a_3 + 8a_7$$

$$m_{44} = 4a_6 - 4a_4$$

Table 6-2: Substitutions to simplify the error correction equations.

$\alpha_1 = 2\epsilon_4 - 2\epsilon_3 - 2\epsilon_5$	$\alpha_7 = 2\epsilon_5 - 4\epsilon_4 - 2\epsilon_3$
$\alpha_2 = 2\epsilon_4 + 2\epsilon_3 - 2\epsilon_5$	$\alpha_8 = -2\epsilon_5 + 4\epsilon_4 - 2\epsilon_3 = -\alpha_6$
$\alpha_3 = 2\epsilon_4 - 4\epsilon_3 - 2\epsilon_5$	$\alpha_9 = 4\epsilon_4 - 4\epsilon_3 - 2\epsilon_5$
$\alpha_4 = 2\epsilon_4 + 4\epsilon_3 - 2\epsilon_5$	$\alpha_{10} = 4\epsilon_4 + 4\epsilon_3 - 2\epsilon_5$
$\alpha_5 = 2\epsilon_5 - 2\epsilon_4$	$\alpha_{11} = 4\epsilon_4 - 2\epsilon_5$
$\alpha_6 = 2\epsilon_5 - 4\epsilon_4 + 2\epsilon_3$	
$\beta_1 = 1 - \cos\delta_1$	$\beta_3 = 1 + \cos\delta_1$
$\beta_2 = 1 - \cos\delta_2$	$\beta_4 = 1 + \cos\delta_2$

Table 6-3: Fourier coefficients when sample matrix is the identity matrix (all other coefficients are zero).

$a_0 = \frac{1}{2} + \frac{1}{8}\beta_3\beta_4\cos 2\epsilon_5$	$b_2 = -\frac{1}{8}\beta_1\beta_4\sin(4\epsilon_3 - 2\epsilon_5)$
$a_2 = \frac{1}{8}\beta_1\beta_4\cos(4\epsilon_3 - 2\epsilon_5)$	$b_4 = \frac{1}{4}\sin\delta_1\sin\delta_2\sin\alpha_1$
$a_4 = -\frac{1}{4}\sin\delta_1\sin\delta_2\cos\alpha_1$	$b_6 = -\frac{1}{4}\sin\delta_1\sin\delta_2\sin\alpha_2$
$a_6 = \frac{1}{4}\sin\delta_1\sin\delta_2\cos\alpha_2$	$b_8 = -\frac{1}{8}\beta_1\beta_2\sin\alpha_9$
$a_8 = \frac{1}{8}\beta_1\beta_2\cos\alpha_9$	$b_{10} = -\frac{1}{8}\beta_2\beta_3\sin\alpha_{11}$
$a_{10} = \frac{1}{8}\beta_2\beta_3\cos\alpha_{11}$	$b_{12} = 0$
$a_{12} = 0$	

Chapter VII

Electro-optic Coefficient Spectrum of Cadmium Telluride

This Chapter describes a measurement of the electro-optic coefficient spectrum of a cadmium telluride electro-optic modulator taken with the infrared Mueller matrix spectropolarimeter. The electro-optic effect produces a voltage dependent retardance in electro-optic crystals and is used in electro-optic devices for modulation of light. Mueller matrix spectra were measured as a function of applied voltage for the device. From the Mueller matrix spectra, the retardance as a function of voltage and wavelength was calculated. This data was used in turn to calculate the electro-optic coefficient spectrum of cadmium telluride.

The first section describes the material parameters of cadmium telluride and the configuration of cadmium telluride as a transverse electro-optic modulator. The second section describes the Mueller matrix for an ideal retarder and how the retardance is calculated from the matrix. This section also discusses the calculation of the electro-optic coefficient from the retardance. Section C describes the initial test results. Section D describes the measurements of the Mueller matrices as a function

of voltage. Mueller matrix spectra are given at several voltages and the derived retardance and electro-optic coefficient spectra are given. Section E describes some of the experimental errors relevant to these measurements.

A. Properties of Cadmium Telluride

This section gives the refractive index at several wavelengths and describes the electro-optic properties of cadmium telluride. A brief description of the electro-optic effect relevant to cadmium telluride and its application as a transverse electro-optic modulator is given in this section.

Cadmium telluride (CdTe) is a cubic crystal with $\bar{4}3m$ symmetry. Refractive index data from various sources is given Table 7-1. Note that there is substantial disparity in the data for some wavelengths.

Table 7-1: Refractive index data for CdTe.

Wavelength $\lambda(\mu m)$	Index of Refraction n		
3.39		2.696[a]	
6	2.682[b]		
7	2.680		
8	2.677		
9	2.675		
10	2.672		
10.6	2.670	2.674[a]	2.60[d]
11	2.667		
12	2.664	2.57[c]	
13	2.662	2.57	
14	2.660		

Notes: *a*. Reference [98]
b. Reference [99]
c. Reference [100]
d. Reference [19]

Cadmium telluride is an electro-optic crystal. The linear electro-optic effect is the change in the ordinary and extraordinary refractive indices that is caused by and is proportional to an electric field applied across the crystal. The relationship between the refractive indices and the applied field is given by the electro-optic tensor. For crystals with $\bar{4}3m$ symmetry, the fundamental characterization of the electro-optic properties of the crystal may be reduced to a single element of the electro-optic tensor, the r_{41} element. For a transverse modulator, the electric field is applied perpendicular to the direction of light propagation through the crystal. Figure 7-1 shows the configuration for a transverse mode modulator. The retardance as a function of wavelength $\delta(\lambda)$ for a $\bar{4}3m$ crystal in terms of the applied voltage V is

$$\delta(\lambda, V) = \frac{2\pi n^3(\lambda) r_{41}(\lambda) V L}{\lambda d}, \tag{7-1}$$

where $n(\lambda)$ is the refractive index, $r_{41}(\lambda)$ is the electro-optic coefficient, L is the length of the crystal along the direction of propagation, and d is the electrode separation. The voltage necessary to achieve a half wave of retardance $\delta = \pi$ for a given wavelength is

$$V_{\lambda/2} = \frac{d\lambda}{2n^3(\lambda) r_{41}(\lambda) L}, \tag{7-2}$$

and for a quarter wave of retardance

$$V_{\lambda/4} = \frac{d\lambda}{4n^3(\lambda) r_{41}(\lambda) L}. \tag{7-3}$$

Values for $n^3 r_{41}$ and r_{41} have been measured previously and are tabulated in Table 7-2. The data in the table is at a wavelength of 10.6 μm unless otherwise noted. The quantity $n^3 r_{41}$ is sufficient to characterize the electro-optic characteris-

tics of the modulator and is often reported when the refractive index is not accurately known. Due to the large disparity in the reported refractive index data, the electro-optic coefficient will reported here in the form $n^3 r_{41}$. Differences in impurities in the crystal, growth processes, and measurement accuracy could be responsible for the large discrepancies in the reported data.

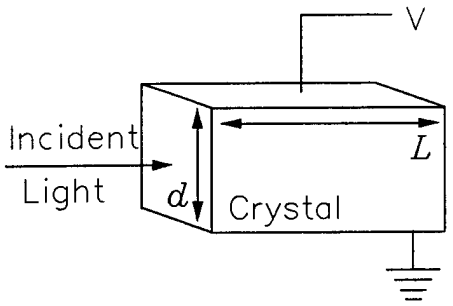

Figure 7-1 Transverse electro-optic modulator.

Table 7-2: Electro-optic coefficient data for CdTe.

Source	r_{41} ($\times 10^{-12}$ m/V) (λ μm)	$n^3 r_{41}$ ($\times 10^{-10}$ m/V)
Yariv [19]	6.8 (λ = 3.39)	
	6.8	1.20
Goldstein [10]	5.9	1.03
II-VI[a]	5.7	1.00
Herrit and Reedy [101]	5.5	1.05

Note: *a*. II-VI, Inc. specifications for this device.

B. Calculating the Electro-optic Coefficient from Mueller Matrix Data

This section describes the measurement procedure and the calculation of the electro-optic coefficient from the Mueller matrix data. The Mueller matrix model that is assumed for the electro-optic modulator and how the retardance is calculated using this model are also described.

Over most parts of the mid-infrared it can be assumed that the cadmium telluride modulator acts as a nearly ideal linear retarder. The modulator is represented by the Mueller matrix for an ideal linear retarder from which the retardance is calculated. The Mueller matrix for an ideal linear retarder of retardance δ is

$$M_r(\delta,\theta)=\tau\begin{pmatrix} 1 & 0 & 0 & 0 \\ 0 & C_4\sin^2(\delta/2)+\cos^2(\delta/2) & S_4\sin^2(\delta/2) & -S_2\sin\delta \\ 0 & S_4\sin^2(\delta/2) & -C_4\sin^2(\delta/2)+\cos^2(\delta/2) & C_2\sin(\delta) \\ 0 & S_2\sin\delta & -C_2\sin(\delta) & \cos(\delta) \end{pmatrix}, \quad (7\text{-}4)$$

where

$$C_2=\cos 2\theta \qquad S_2=\sin 2\theta$$

$$C_4=\cos 4\theta \qquad S_4=\sin 4\theta,$$

and τ is the transmission. The orientation θ is the angle between the fast axis of the modulator and the coordinate system of the polarimeter defined by the first polarizer. Note that the three by three sub-matrix in the lower right corner of the Mueller matrix forms an orthogonal matrix. If the Mueller matrix is properly normalized and there is no depolarization, the square root of the sum of the squares of the elements of the rows of this sub-matrix should equal one. This will be exploited shortly to examine possible depolarization by the modulator.

The retardance δ can be calculated from one, some, or all of the non-zero Mueller matrix elements. For example, the retardance can be calculated from the m_{44} element

$$\delta = \arccos m_{44}, \tag{7-5}$$

or from the m_{24}, m_{34}, m_{42}, and m_{43} elements

$$\delta = \arcsin\sqrt{\frac{1}{2}(m_{24}^2 + m_{34}^2 + m_{42}^2 + m_{43}^2)}. \tag{7-6}$$

Other combinations of elements may also be used. The measured Mueller matrix should be properly normalized for accurate results when calculating δ from these elements. If the Mueller matrix is not normalized, i.e. the determinant of the nine element sub-matrix is not one, the retardance should be calculated from ratios of the elements

$$\delta = \arctan\left(\frac{\sin\delta}{\cos\delta}\right) = \arctan\sqrt{\frac{(m_{34} - m_{43})^2 + (m_{42} - m_{24})^2}{2m_{44}}} \tag{7-7}$$

The following steps are carried out for measurement of the electro-optic coefficient of the CdTe modulator: 1) the Mueller matrix is measured with a voltage applied to the modulator, 2) the retardance is calculated from the Mueller matrix, and 3) the electro-optic coefficient is calculated from δ, λ, n, V, L, and d.

The linear relationship between the retardance and the applied voltage can be exploited by making measurements at several voltages and performing a linear regression. The electro-optic coefficient is found from the slope m of the linear regression

$$n^3 r_{41} = \frac{\lambda d}{2\pi L} m \tag{7-8}$$

The linear regression is performed on the data as a function of voltage at each wavelength. The correlation coefficient of the linear regression provides a measure of the goodness of fit of the regression to the data. A correlation coefficient of 1 indicates complete correlation.

C. Initial Test Results

The crystal used in these experiments is 5mm by 5mm by 50mm long. The crystal is oriented so that the light is incident on the square face of the crystal defined by the (110) plane. The electrodes are applied to the $(\bar{1}\,1\,1)$ planes, and the (001) planes define the third direction of the crystal. The slow axis is parallel to the applied electric field. The II-VI, Inc. operation and service manual for the modulator gives a half wave voltage at 10.6 μm of 5300V. This corresponds to a value for $n^3 r_{41}$ of 1.00×10^{-10} m/V assuming an index of refraction of 2.6.

The CdTe modulator was placed into the spectropolarimeter and 2650V applied to the crystal. This voltage was specified by the manufacturer to be the quarter-wave voltage of the modulator at 10.6 μm. The fast axis of the crystal was oriented at approximately $-45°$ to the x-axis defined by the first polarizer. The maximum angle for rays incident on the modulator was about 9°. Figure 7-2 shows the measured Mueller matrix spectrum of the modulator. Each of the Mueller matrix elements has been normalized to the (1,1) element and the (1,1) element is replaced by the transmission spectrum.

Several interesting observations can be made about these initial results. First, the values of the Mueller matrix elements in the first row and first column except for m_{11} are very nearly zero. This indicates that the diattenuation of the modulator is very small. The spectrum is noisier in the low transmission band between 3 and 6 μm. A small amount of diattenuation near the limits of measurement accuracy

may be present. Second, the remaining elements behave as a linear retarder oriented at approximately $-45°$. At approximately 11.6 μm the m_{22} and m_{44} elements change sign. This implies that the modulator acts as a quarter wave retarder for this wavelength and voltage since these Mueller matrix elements for an ideal retarder go to zero for a quarter-wave of retardance. The retardance should be a half wave at half of this wavelength. At approximately 5.8 μm, the magnitudes of the m_{22} m_{44} elements reach a maximum and the m_{42}, m_{43}, m_{24}, and m_{34} elements go through zero as is expected for a half-wave of retardance. This data indicates that the quarter-wave voltage for this modulator is 2650V for 11.6 μm, not 10.6 μm as specified by the manufacturer.

A calculation of the electro-optic coefficient at 10.6 μm from this Mueller matrix using Eq. 7-1 yields a value of $n^3 r_{41}$ of 1.125×10^{-10} m/V.

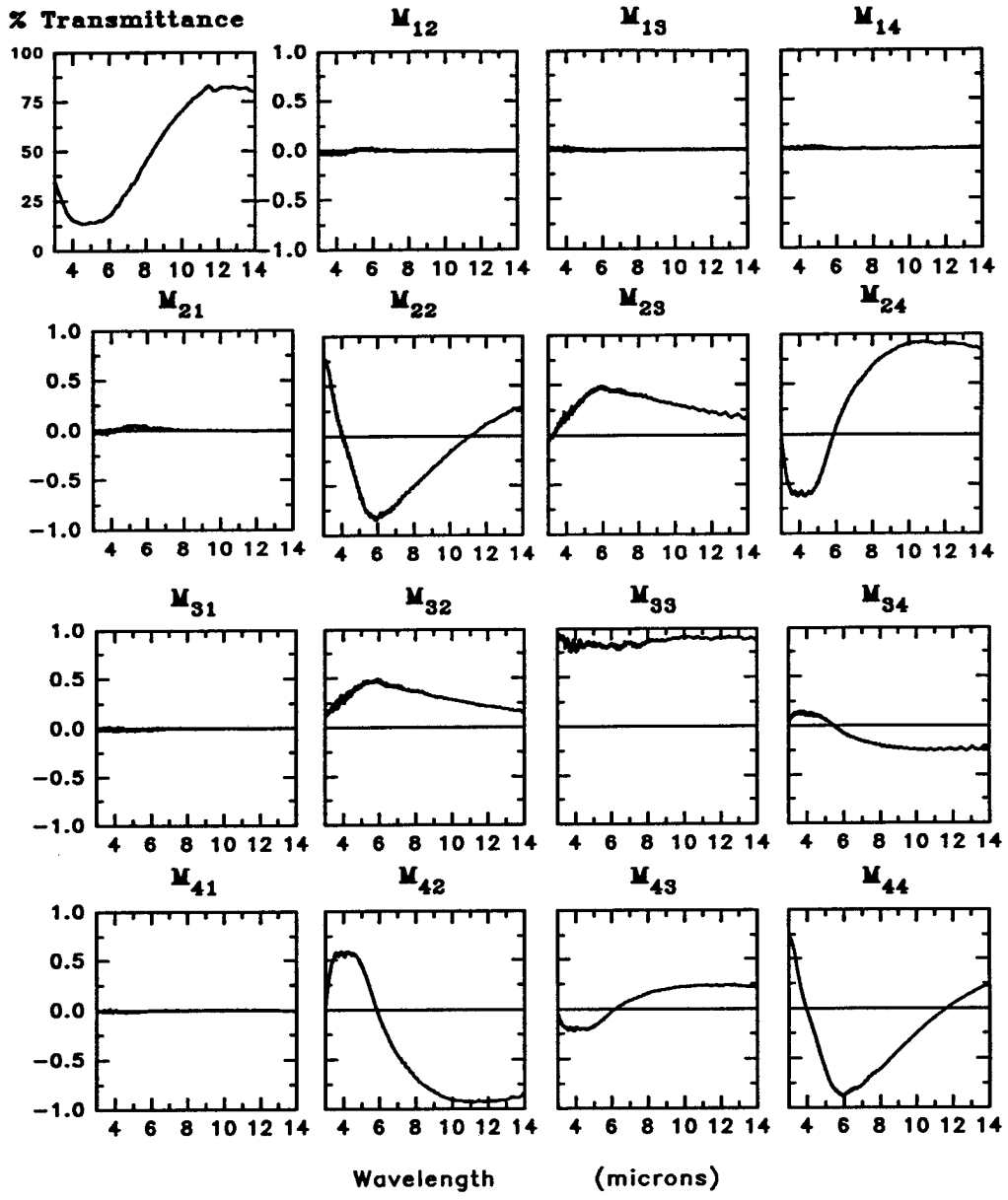

Figure 7-2 Mueller matrix of initial test of the CdTe modulator.

D. Measurements and Calculation of $n^3 r_{41}$

The initial results described in the previous section demonstrate the validity of the measurement technique. A set of ten measurements was made on the crystal and the $n^3 r_{41}$ values were found as a function of wavelength.

Mueller matrix spectra were acquired for applied voltages every 300V ranging from zero to 2700V. The voltage was applied to the crystal with a Fluke high voltage power supply. The power supply was calibrated and found to be accurate within 1% of the expected voltage. Figure 7-3 shows the Mueller matrix spectrum for the modulator with no applied voltage. Figures 7-4 through 7-9 show the Mueller matrix spectra for applied voltages of 300, 900, 1200, 1800, 2100, and 2700 volts. The Mueller matrix has been normalized by the m_{11} and this element replaced by the transmission spectrum.

The Mueller matrix elements exhibit more noise at the shorter wavelengths. This noise results from two factors: first, the calibration Mueller matrix is noisier and less accurate at shorter wavelength due to non-ideal diattenuation in the polarizers and non-ideal behavior of the retarder anti-reflection coatings as described in Chapter VI. Second, the transmission of the modulator is reduced at shorter wavelengths resulting in less light and a lower signal-to noise ratio. Since the fourth row and fourth column of the Mueller matrix are less noisy than the rest of the Mueller matrix, these elements were used to calculate the retardance by Eq. 7-7.

Retardance spectra were calculated from the Mueller matrix spectra for each of the applied voltages. Figure 7-10 shows the resulting retardance spectra. The plots range from applied voltages of 300 volts on the bottom to 2700 volts on top. A linear regression was performed on the retardance as a function of voltage at each wavelength over the spectrum shown. The retardance values calculated with zero

Table 7-3: Values of $n^3 r_{41}$, correlation coefficient, and intercept from linear regression.

Wavelength (μm)	$n^3 r_{41}$ ($\times 10^{-10}$ m/V)	Correlation Coefficient	Intercept b (degrees)
3	1.10	1.000	1.1
3.39	1.09	1.000	2.2
4	1.10	0.997	2.5
5	1.07	0.996	3.9
6	1.04	0.999	5.1
7	1.06	0.999	2.8
8	1.08	1.000	0.7
9	1.09	1.000	0.0
10	1.09	1.000	0.0
10.6	1.09	1.000	0.0
11	1.09	1.000	0.0
12	1.09	1.000	0.1
13	1.09	1.000	0.2
14	1.09	1.000	0.4

applied voltage were not included in the linear regression. The $n^3 r_{41}$ spectrum is shown in Figure 7-11. An example of the linear regression for a wavelength of 10.6 μm is shown in Figure 7-12. The correlation coefficient of the regression as a function of wavelength is shown in Figure 7-13. The intercept b calculated from the regression and the retardance with no applied voltage are shown together in Figure 7-14. Values for $n^3 r_{41}$, the correlation coefficient, and the intercept are tabulated for several wavelengths in Table 7-3.

The value of $n^3 r_{41}$ at 10.6 μm is 1.09×10^{-10} m/V. This is within 6% of the value measured by Goldstein on this same crystal [10] and in the middle of the range of values previously published. The value of r_{41} at 3.39 μm is 5.5×10^{-12} m/V if an index of 2.696 from reference [97] is assumed. This value differs from the

value given by Yariv [19] by almost 20%. However, due to the large discrepancy in previously reported refractive indices, the quantity $n^3 r_{41}$ is believed to be more accurate than r_{41} and is emphasized here.

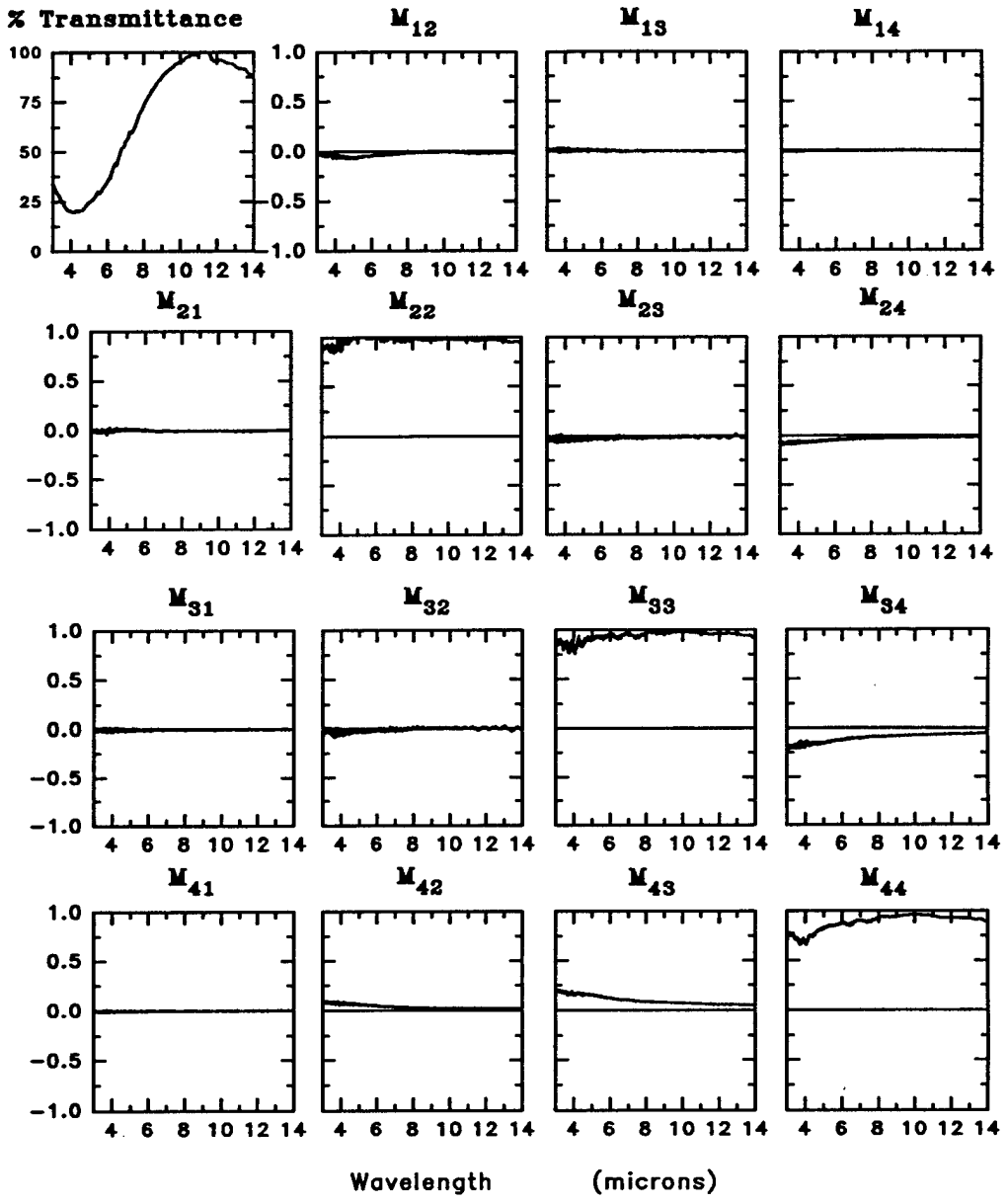

Figure 7-3 Mueller matrix of CdTe modulator with no applied voltage.

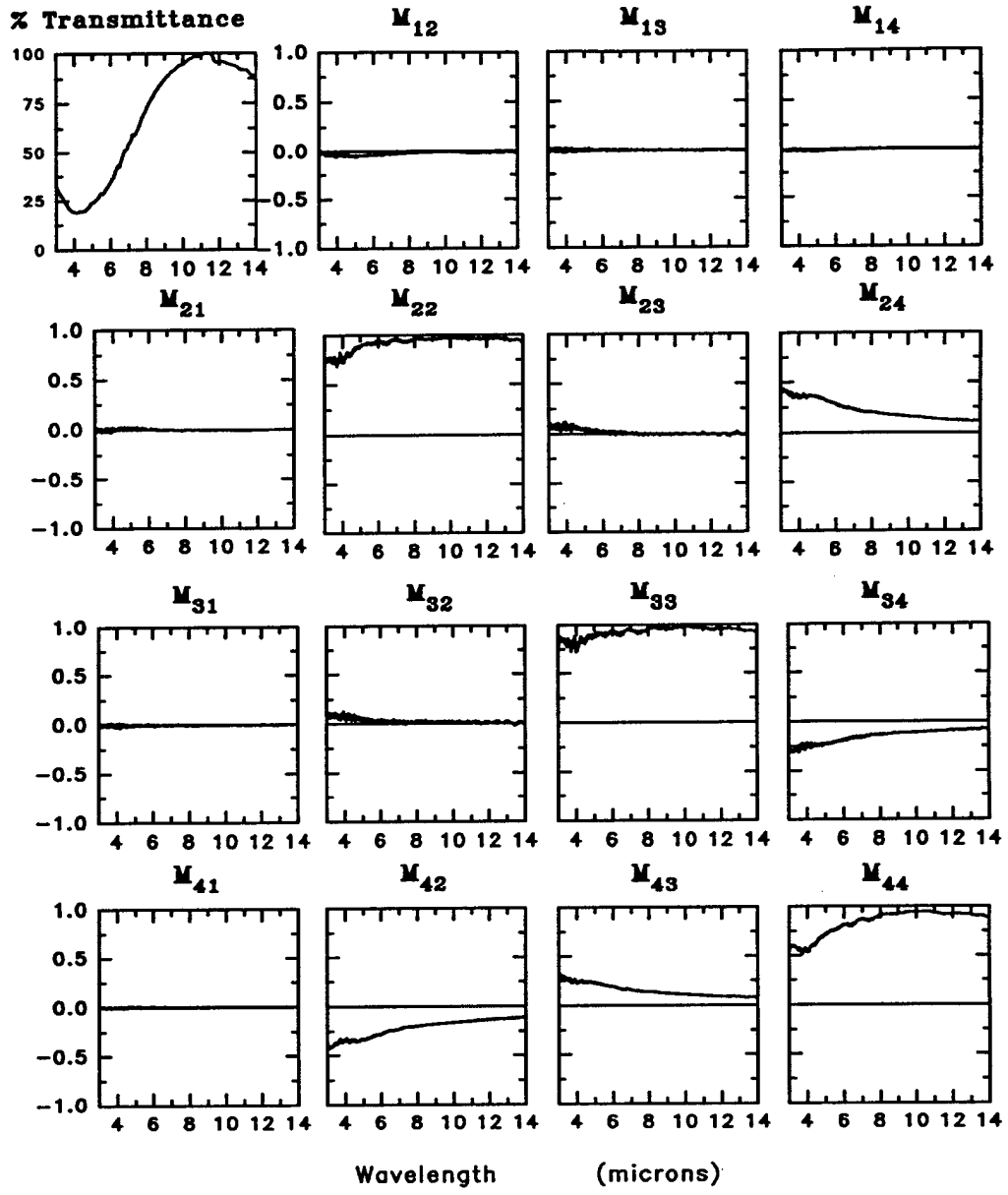

Figure 7-4 Mueller matrix of CdTe modulator with an applied voltage of 300 volts.

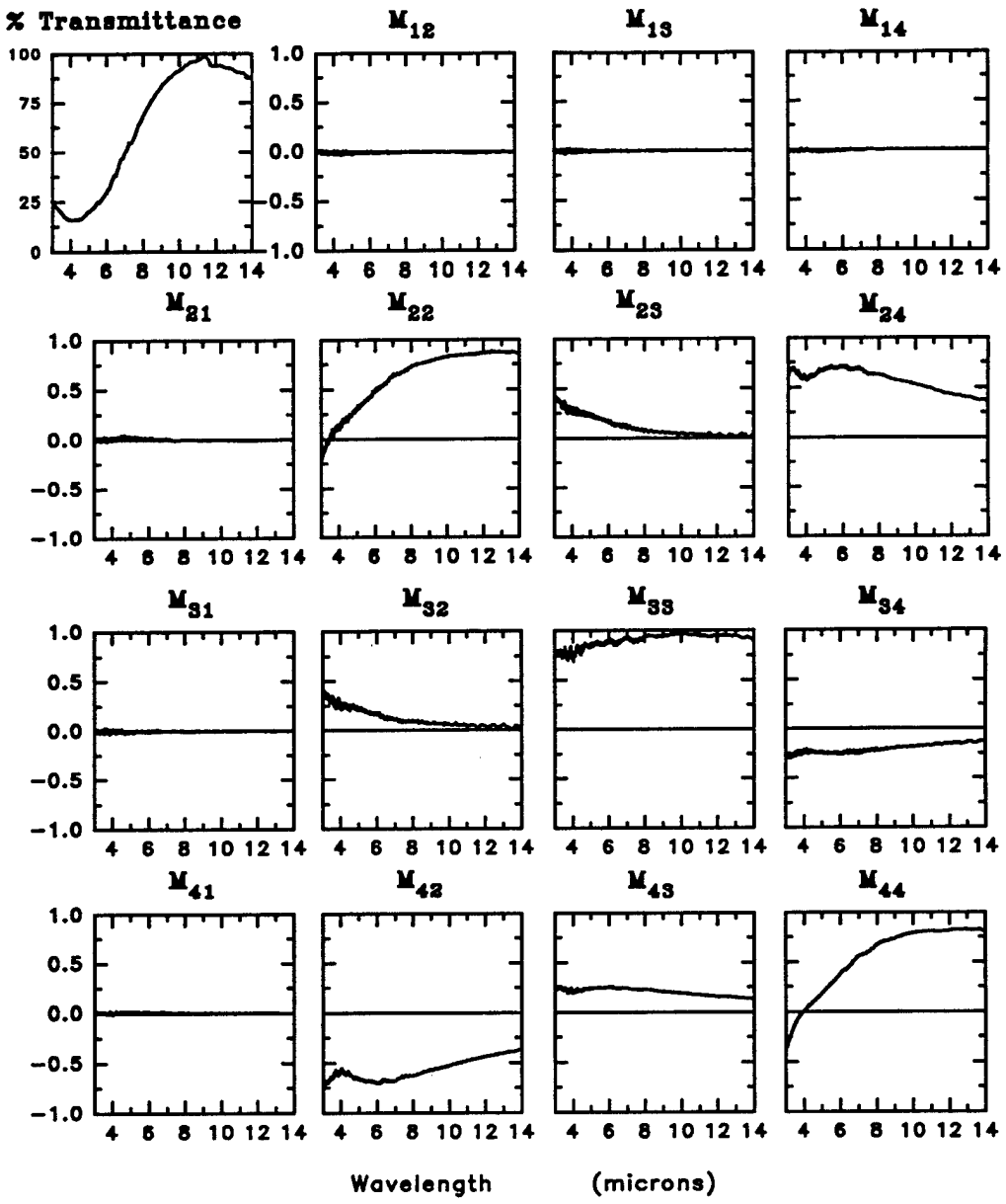

Figure 7-5 Mueller matrix of CdTe modulator with an applied voltage of 900 volts.

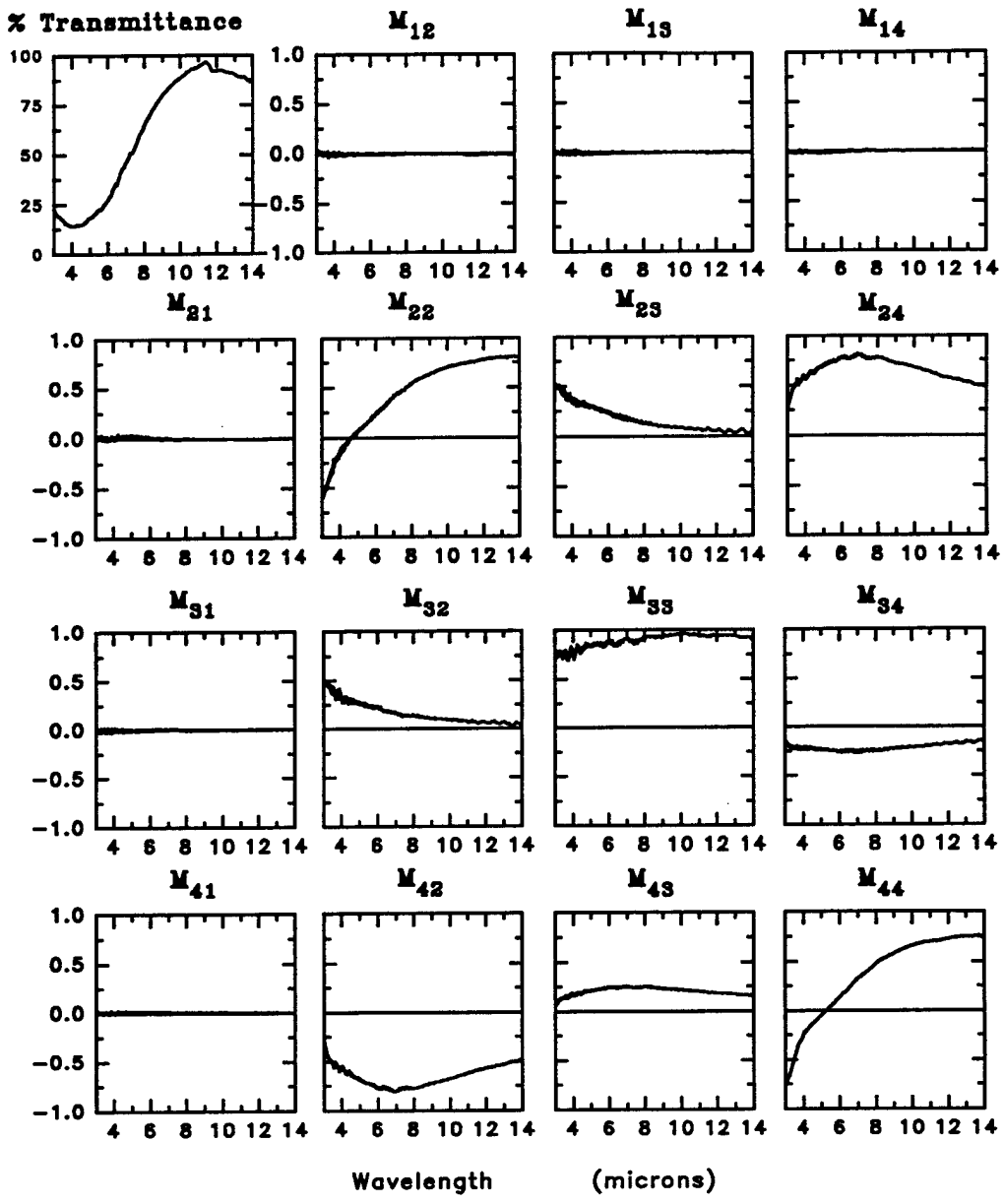

Figure 7-6 Mueller matrix of CdTe modulator with an applied voltage of 1200 volts.

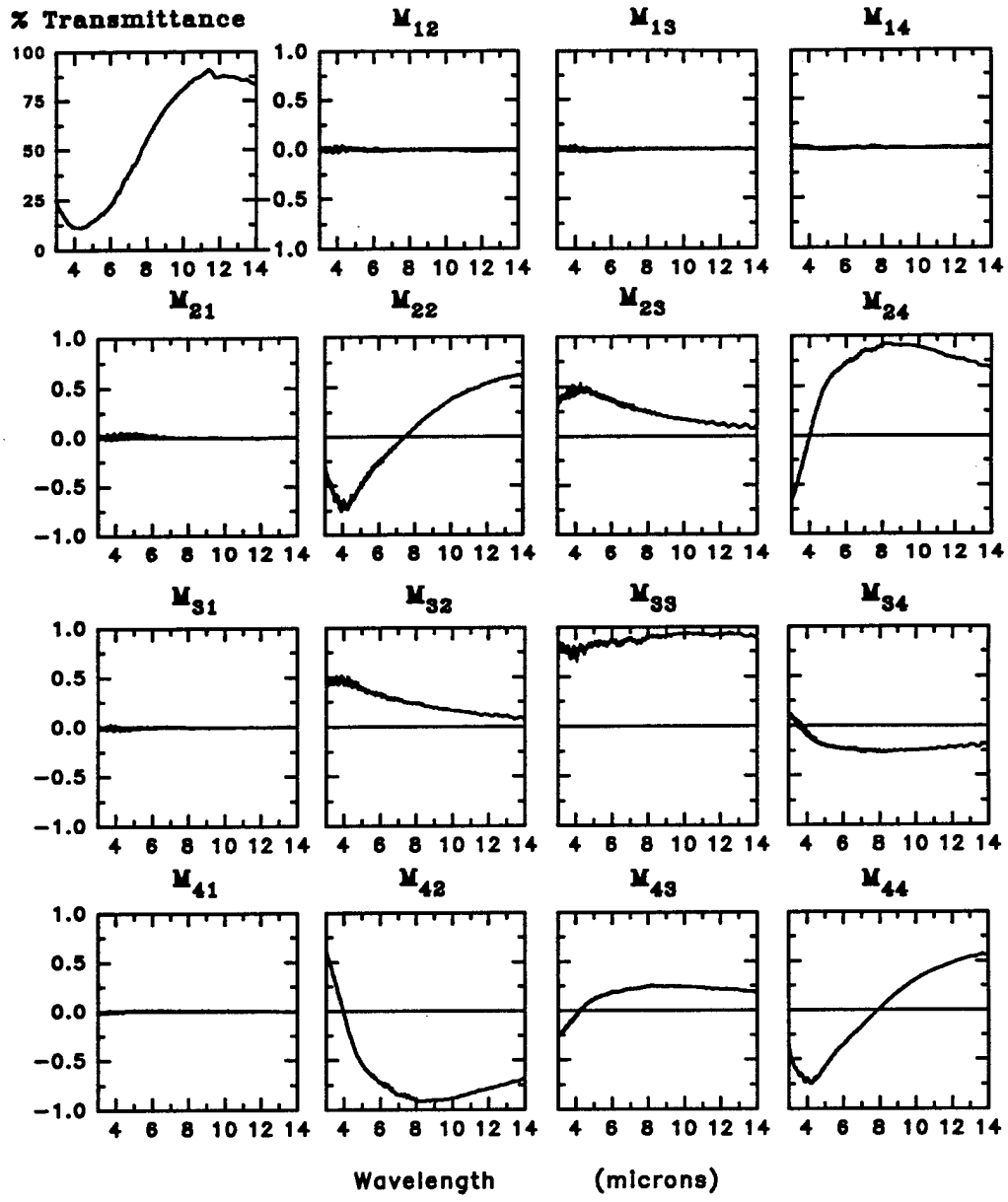

Figure 7-7 Mueller matrix of CdTe modulator with an applied voltage of 1800 volts.

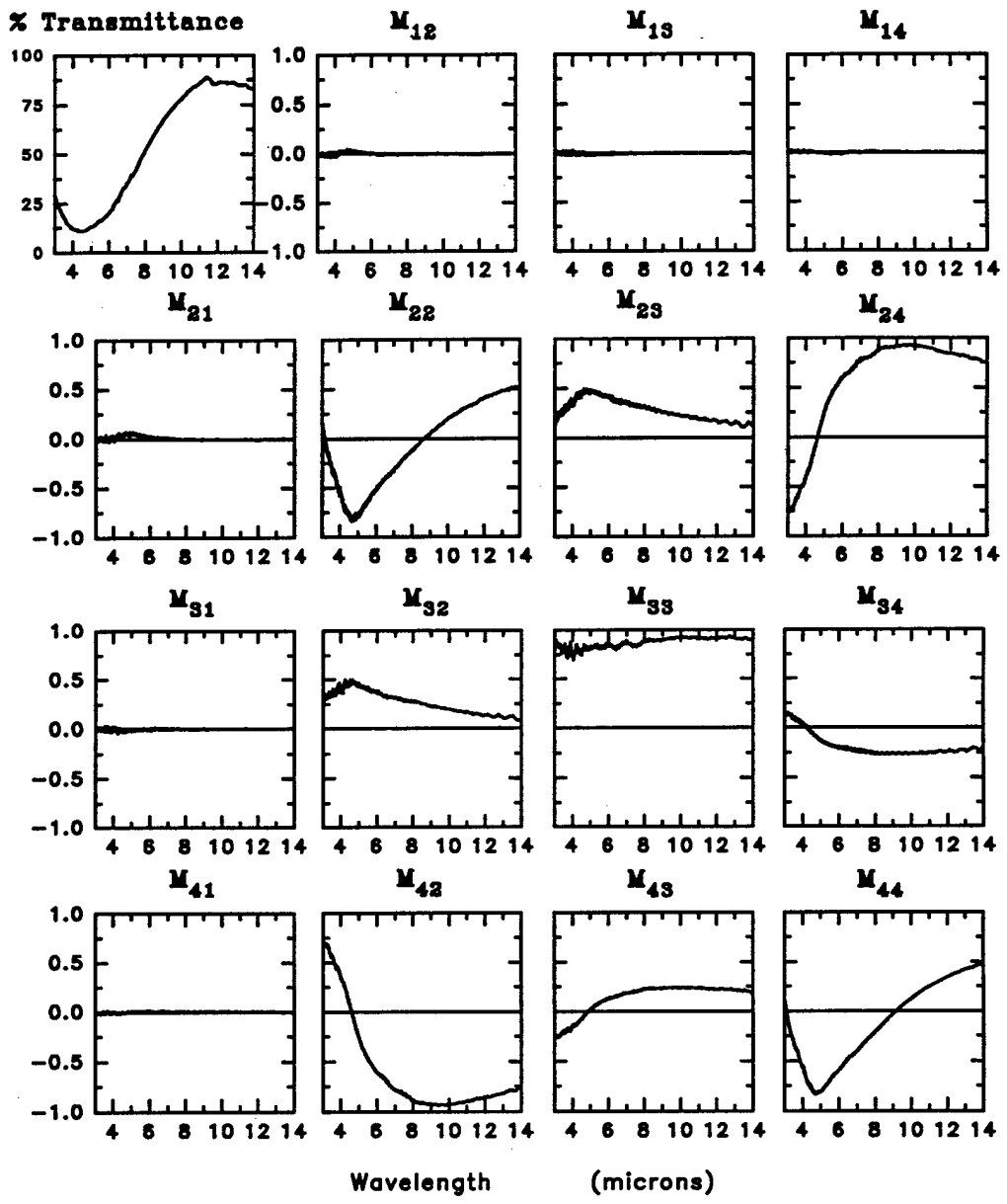

Figure 7-8 Mueller matrix of CdTe modulator with an applied voltage of 2100 volts.

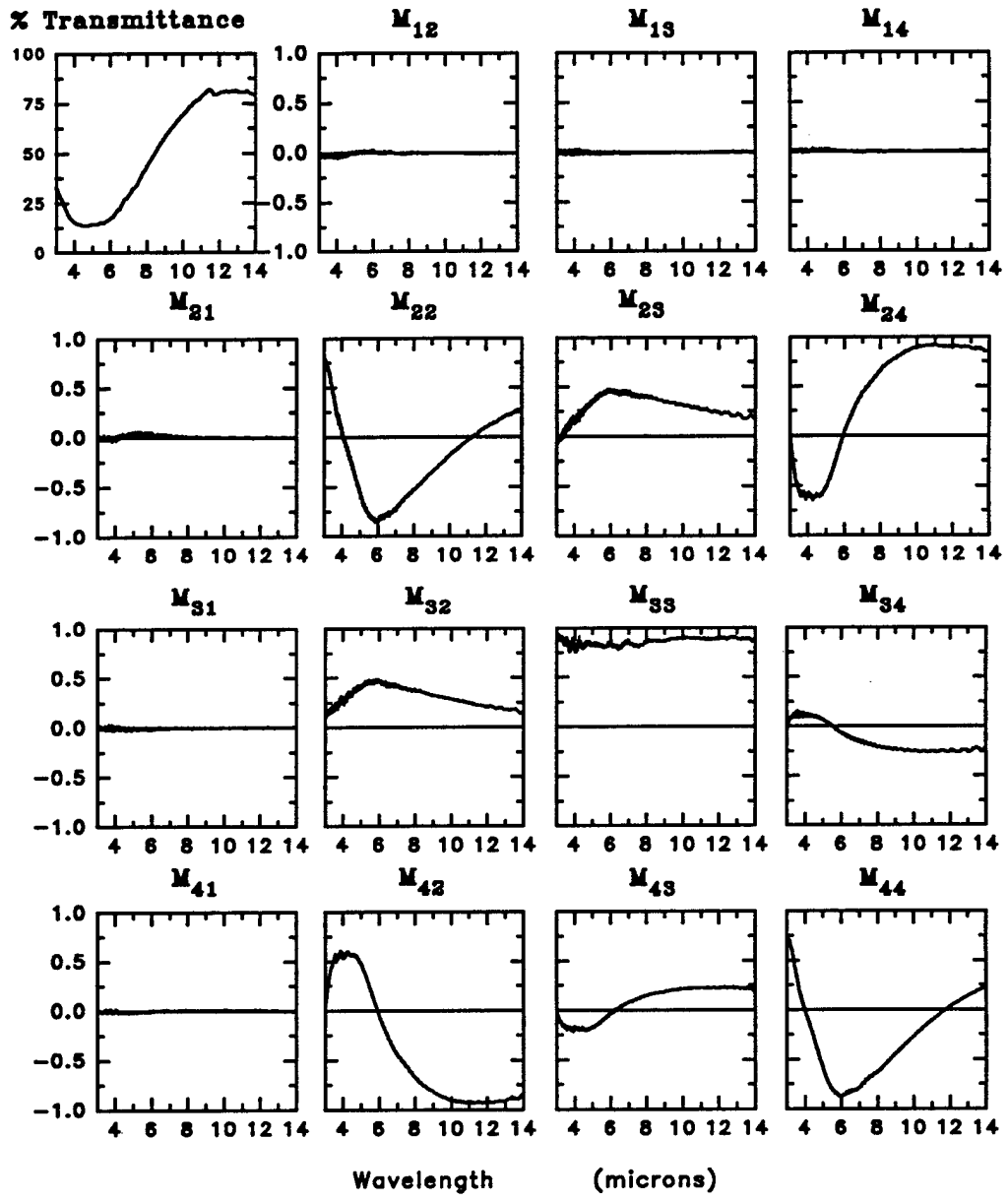

Figure 7-9 Mueller matrix of CdTe modulator with an applied voltage of 2700 volts.

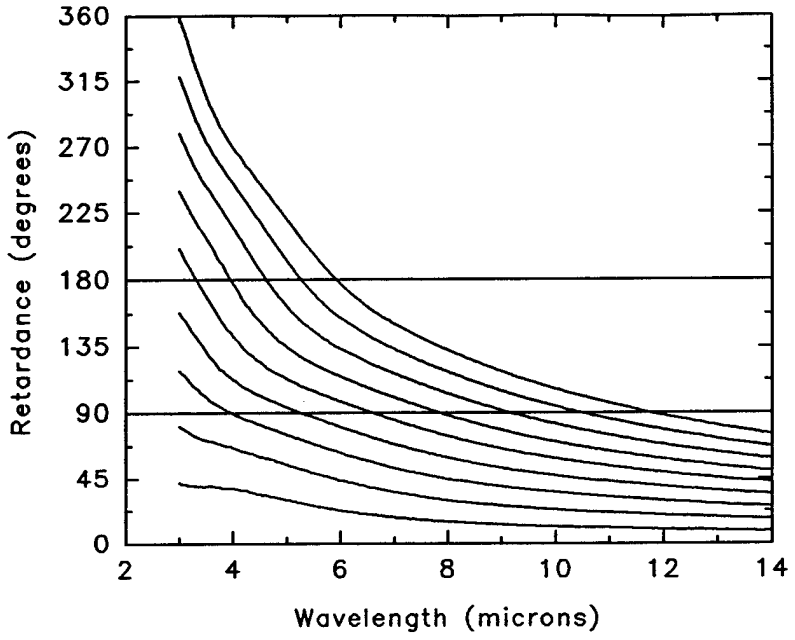

Figure 7-10 Retardance as a function of wavelength and voltage.

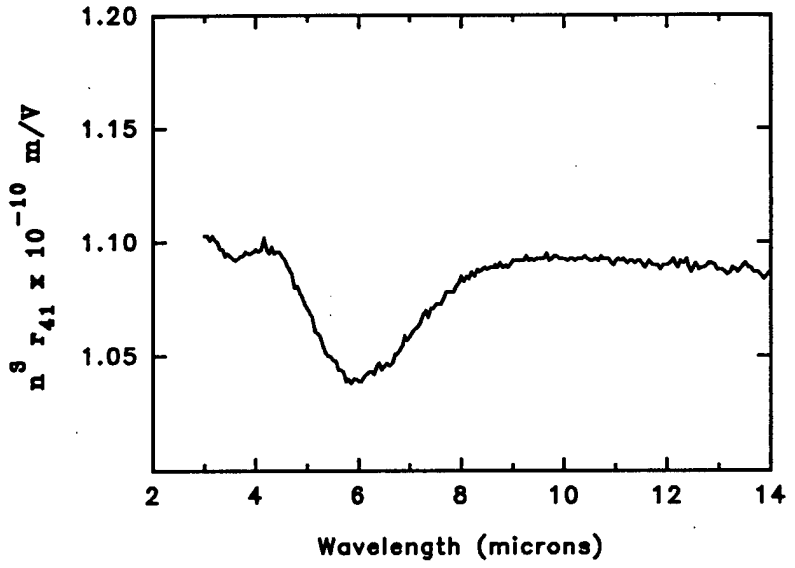

Figure 7-11 Spectrum of $n^3 r_{41}$ calculated from retardance.

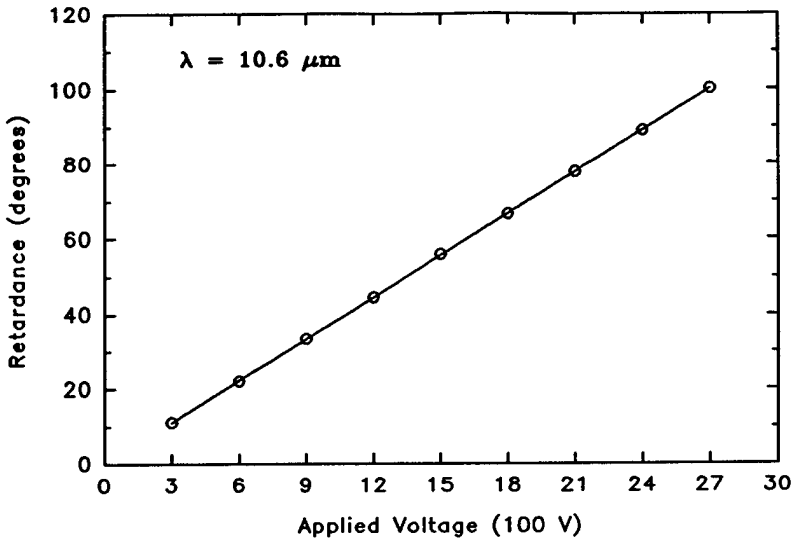

Figure 7-12 Linear regression of retardance as a function of voltage at 10.6 μm.

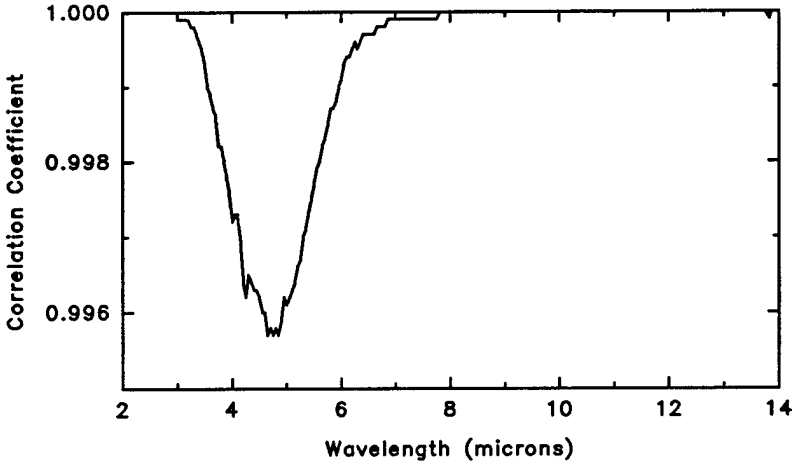

Figure 7-13 Correlation coefficient spectrum of linear regression.

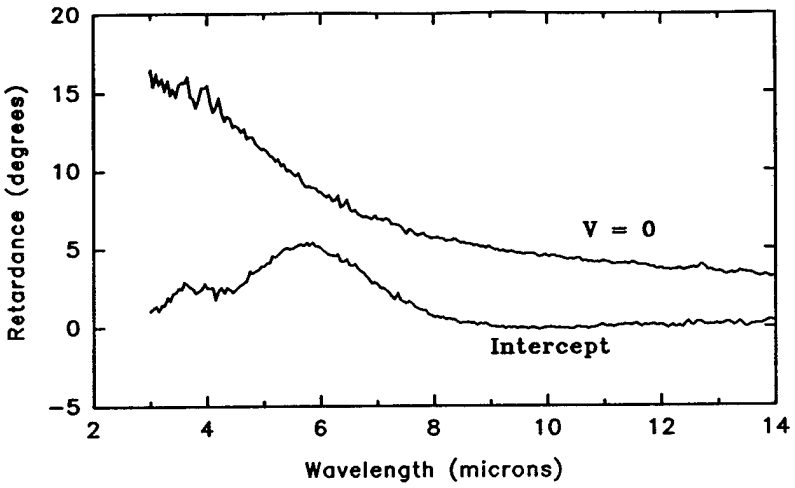

Figure 7-14 Retardance for zero applied voltage and intercept of regression.

E. Discussion of Results

This section discusses the calculation of the quantity $n^3 r_{41}$ and describes possible sources for error. Several additional measurements and other features of the data are presented.

The correlation coefficients of the linear regression given in Table 7-3 and plotted in Figure 7-13 are not an absolute value of the uncertainty in these measurements but provide an indication of the quality of the data and the reliability of the Mueller matrices. The remarkably high correlation indicates that the linear relationship of the retardance and the voltage holds very well. The calculation of the quantity $n^3 r_{41}$ from the slope (Eq. 7-8) exploits the linear relationship between the retardance and voltage. The linear regression returns the proper value for the slope, and hence $n^3 r_{41}$, even if the absolute value of retardance has a slight bias.

Ideally the CdTe electro-optic modulator should exhibit no retardance with no applied voltage. However, the m_{24}, m_{34}, m_{42}, and m_{43} elements are not zero

which indicates that there is some residual retardance present. This is thought to be due to stresses induced in the crystal during the fabrication process [102]. The residual retardance is plotted in Figure 7-14. Linear regressions were performed both including the no applied voltage retardance spectrum and excluding it. Since the correlation for the linear regression was reduced when this retardance was included, the data shown in Figures 7-11 through 7-13 do not include the residual retardance. The y -intercept spectrum shown in Figure 7-14 shows that the linear regression produces an intercept very near zero as it should according to Eq. 7-1 except in and near the absorption band.

The matrix calculated in Chapter VI from the calibration spectra gives an indication of the accuracy of the Mueller matrix elements for different parts of the spectrum. The discussion of sources for error in Section F of Chapter VI applies here as well. The systematic errors are more prominent at shorter wavelengths, and the accuracy of the Mueller matrices for the modulator are less accurate at these shorter wavelengths.

Comparison of the m_{12} and m_{21} elements in Figures 7-3 through 7-10 show that the values of these elements in the absorption band changes as a function of voltage. A non-zero value of the m_{12} element implies horizontal and vertical diattenuation for horizontally or vertically incident polarized light. A non-zero value of the m_{21} element increases the degree of polarization for incident unpolarized light. At zero voltage, the m_{12} element is slightly negative and the m_{21} element is approximately zero. As the voltage increases, the magnitude of the m_{12} element decreases while the m_{21} element becomes slightly positive. There is no change for the linear diattenuation along the $\pm 45°$ axis or circular diattenuation. Since the

magnitudes of these elements are very near the limits of accuracy of the spectropolarimeter, nothing conclusive can be stated here except that this effect should be studied further, perhaps at higher voltages.

The orientation of the fast axis of the retarder as a function of voltage at a wavelength of 10.6 μm is shown in Figure 7-15. The orientation of the residual retardance with no applied voltage is approximately 10°. The m_{24} and m_{42} elements change sign when voltage is applied (cf. Figs. 7-3 and 7-4) and the orientation of the fast axis of retardance changes sign when voltage is applied. The orientation approaches about -40° as the residual birefringence is overcome by the electro-optically induced retardance. The behavior shown in this Figure is typical of the orientation of the fast axis at other wavelengths.

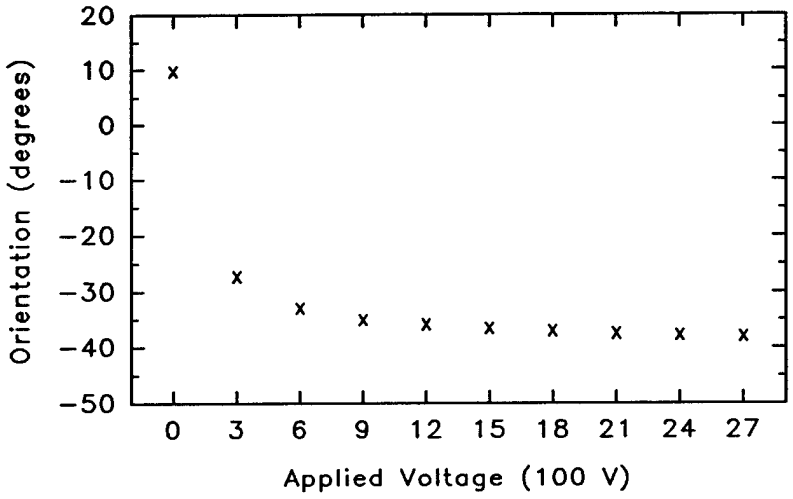

Figure 7-15 Orientation of fast axis as a function of voltage at 10.6 μm.

Figures 7-16 and 7-17 show the measured Mueller matrices for voltages of 1200 and 1800 volts applied with opposite polarity. Comparison of these figures with Figures 7-6 and 7-7 and Eq. 7-4 show that the effect of reversing the polarity is

to change the sign of the retardance. In addition, the magnitudes of the m_{23}, m_{32}, m_{34}, and m_{43} elements are slightly less in the reversed polarity measurements. This is most likely due to a change in orientation of the fast axis of about 4° for the two cases. The possible diattenuation apparent in the m_{12} and m_{21} elements is not affected.

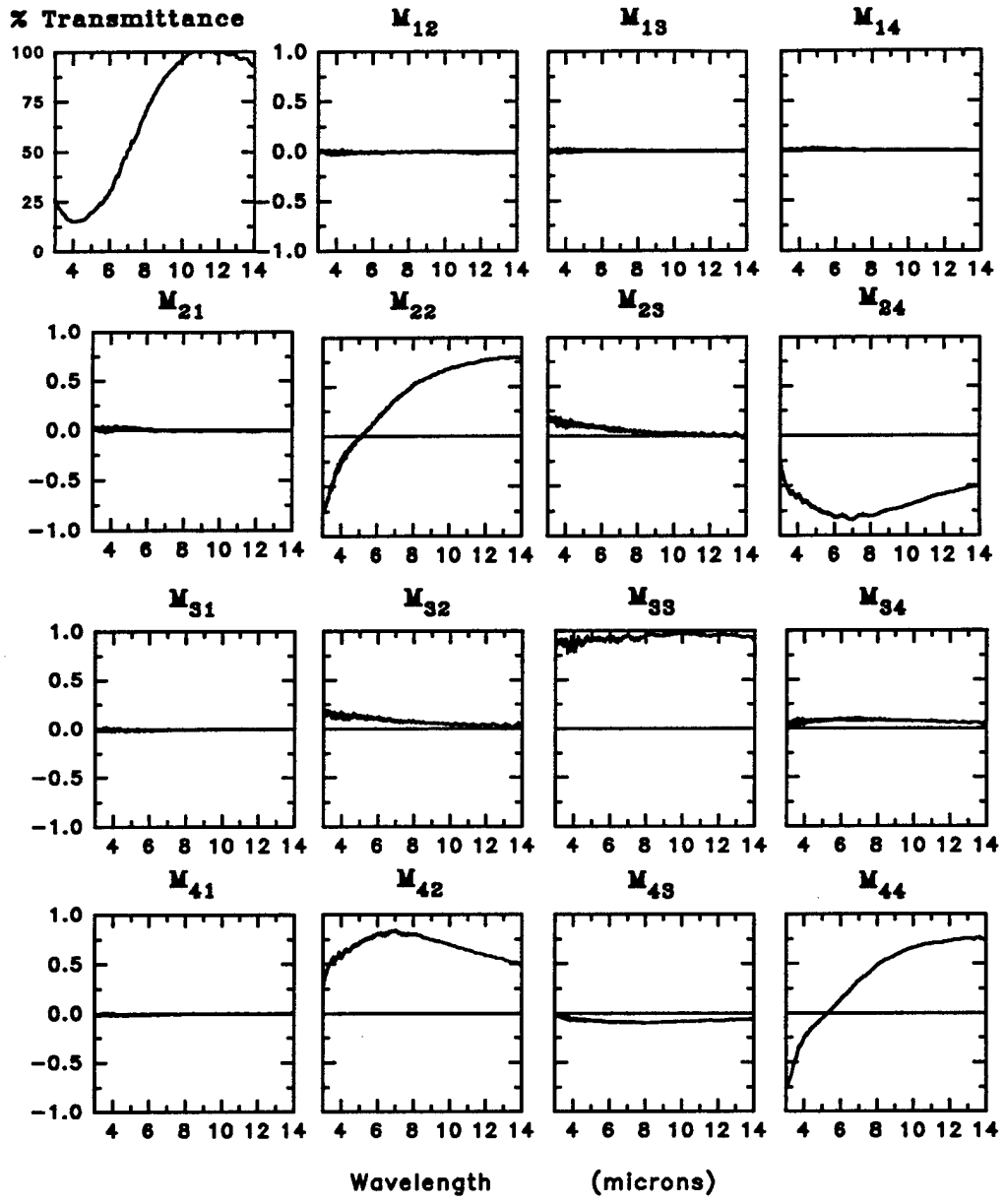

Figure 7-16 Mueller matrix of CdTe modulator with an applied voltage of negative 1200 volts.

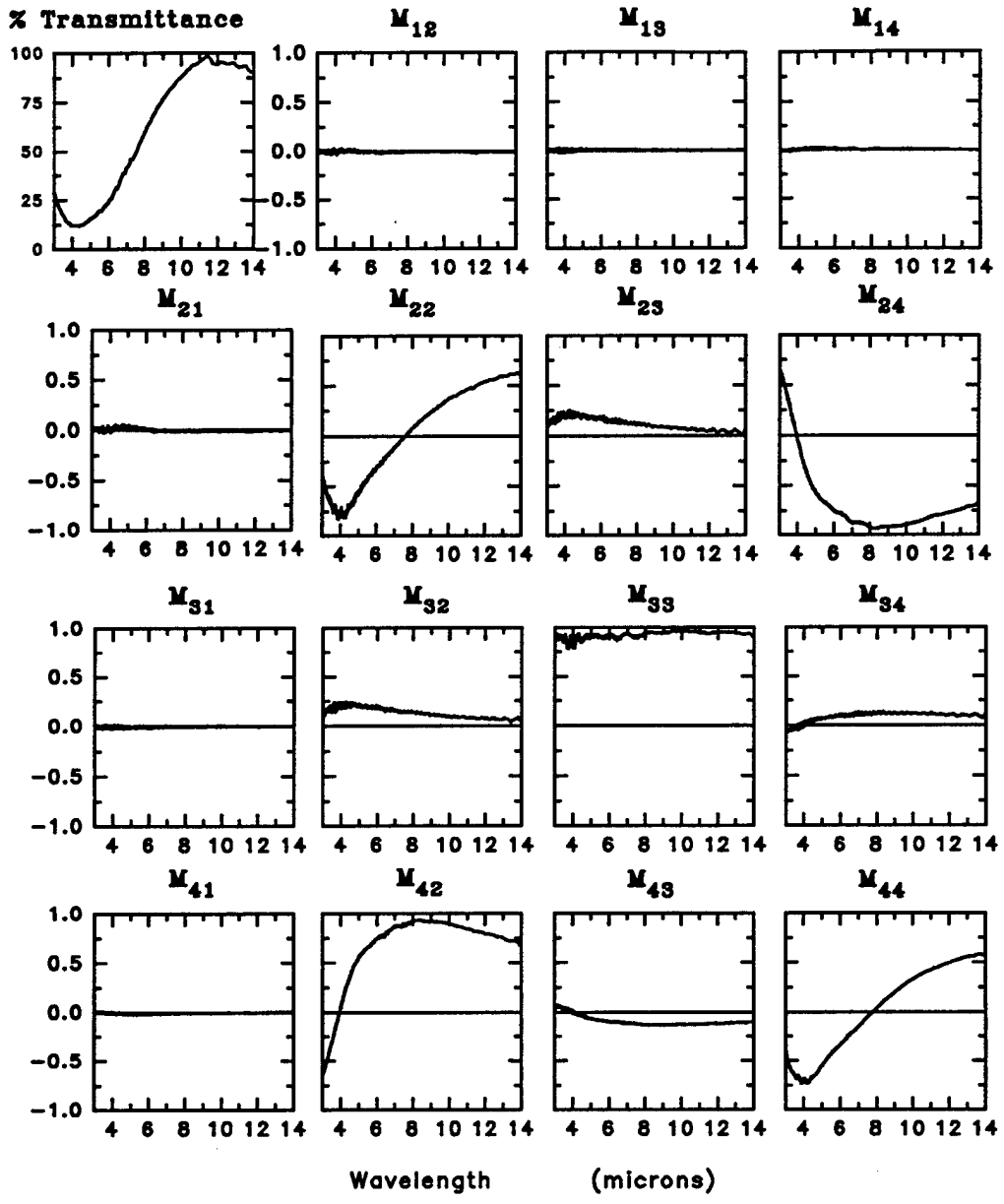

Figure 7-17 Mueller matrix of CdTe modulator with an applied voltage of negative 1800 volts.

The transmission spectra shown in the m_{11} position in the Mueller matrix spectra appear to vary with applied voltage. This change in transmission is not, however, due to the applied voltage but rather due to instrumental drift. The measurements were acquired over many hours and the instrumental response drifted over this time period due to liquid nitrogen boiling off in the detector and changes in temperature in the instrument. This drift affected only the transmission measurements and not the measurement of the Mueller matrix. The drift was negligible over the period required to acquire a single Mueller matrix spectrum. Since each Mueller matrix spectrum was normalized by the m_{11} element, the calculation of the retardance was not affected by the long term drift.

Recall the relationship for the rows of the 3×3 sub-matrix in the lower right corner of the Mueller matrix. The magnitude of a row in this sub-matrix is the square root of the sum of the squares of the elements of the row. The first row of this sub-matrix transforms the incident Stokes vector into horizontally and vertically polarized states, the second row transforms the incident Stokes vector into states polarized along the $\pm 45°$ axis, and the third row into circularly polarized states. The magnitude of each row in this sub-matrix should equal one if the Mueller matrix is properly normalized and there is no depolarization. The magnitude of the row is related to the degree of polarization of the transmitted polarization state.

Figure 7-18 shows these quantities as a function of wavelength and voltage. The top three plots show these values for three voltages overlaid for each of the rows. The bottom nine plots show the magnitudes of the rows for the three voltages separately for clarity. The interesting behavior occurs in the absorption band around $4\,\mu$m. The magnitude of the second row shows only minor change in the absorption band indicating relatively small amounts of depolarization along the

$\pm 45°$. The slow axis of the modulator and the applied field are aligned approximately along this axis. However, there is significant change in the magnitude of rows 1 and 3. This indicates that the degree of polarization is less than one for circular states and for linear states transmitted along the x-y axes. One possible explanation for this is areas of anisotropy on a microscopic scale where the local electric field is reduced or whose orientation changes [103]. The resulting depolarization would be a minimum for polarization states aligned with the electric field.

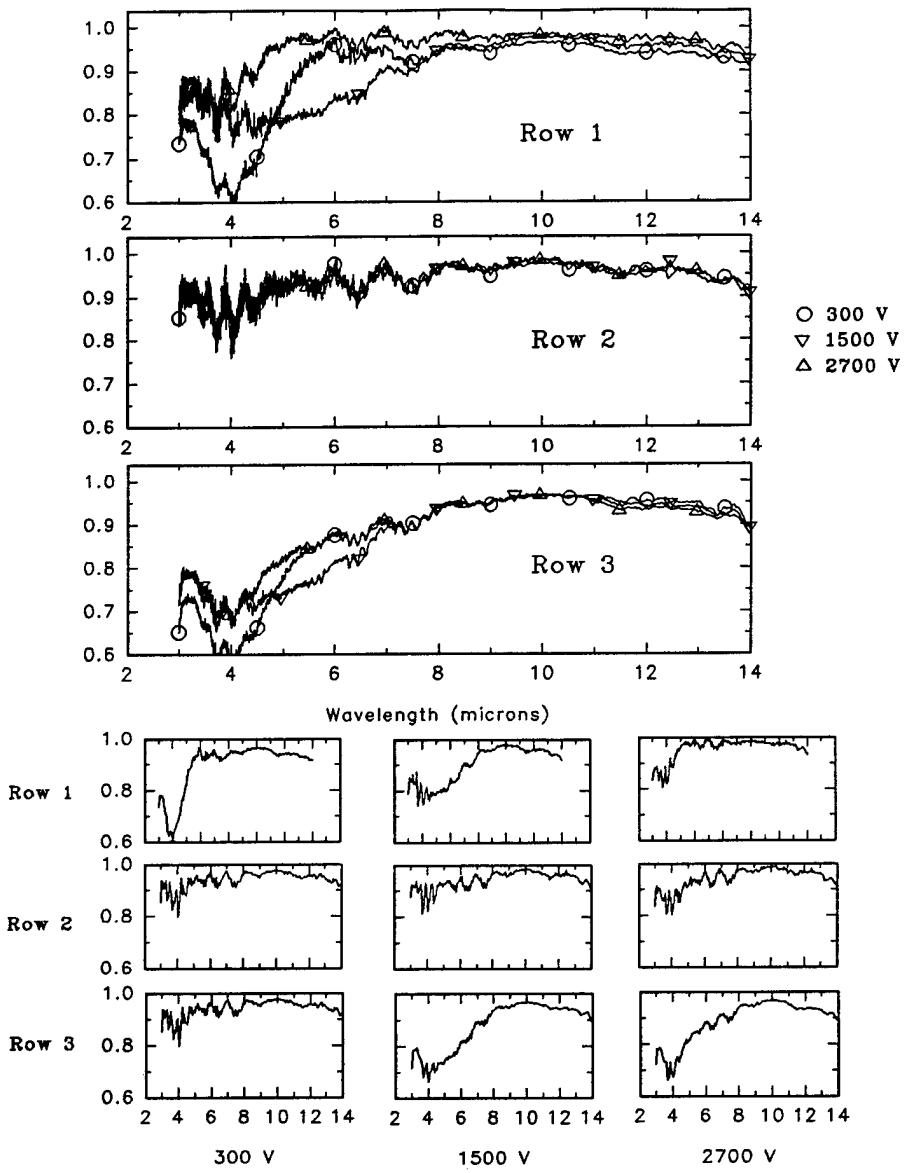

Figure 7-18 Magnitudes of rows of sub-matrix as a function of wavelength and voltage.

Chapter VIII

Directions for Data Reduction Improvement

The first part of this Chapter describes a data reduction formalism that expresses the measurement process as a polarimetric measurement matrix. Through the polarimetric measurement matrix, the data reduction is reduced to a sequence of matrix manipulations. The second part of this Chapter describes the calibration procedure in which the polarimetric measurement matrix is determined experimentally. With this calibration step, polarimetric systematic errors are compensated in data reduction.

The data reduction equations described in Chapter VI corrected and eliminated five of the systematic errors in the dual rotating retarder Mueller matrix polarimeter. These data reduction equations reduced the error in the Mueller matrices measured in the infrared spectropolarimeter due to these errors from over 50% to less than 5%. The residual error, as discussed in Chapter VI, is due to other systematic errors such as non-ideal diattenuation in the polarizers, anti-reflection coating effects in the retarders, instrumental polarization, angle of incidence effects in the retarders, and other sources.

Reducing the remaining error requires correction or elimination of these other systematic errors. The data reduction equations with orientation and retardance errors are already complex and including additional systematic error sources is impractical at best. It is likely that some of the systematic errors present are difficult or impossible to identify. This Chapter describes an algorithm and calibration procedure for a data reduction which takes many systematic errors into account.

The notation for the elements of the Mueller matrix is changed slightly from previous Chapters. In this Chapter, the row and column indices for the Mueller matrix elements range from 0 to 3 rather than from 1 to 4 as previously.

A. Polarimetric Data Reduction Matrix

A generalized polarimetric data reduction formalism developed by Chipman [76] is used in describing the polarization state analyzer in Section 1. Two examples presented in Section 2 are used to illustrate the data reduction for the polarization state analyzer. The data reduction formalism is generalized for Mueller matrix polarimeters in the Section 3 followed by an example in Section 4 of the data reduction for a polarimeter that measures nine elements of the Mueller matrix.

1. Polarimetric Data Reduction Matrix for Polarization State Analyzers

This section introduces the generalized polarimeter data reduction formalism and describes the polarimetric data reduction matrix for polarization state analyzers.

Figure 8-1 shows the block diagram of the polarization state analyzer. The Stokes vector incident on the detector is

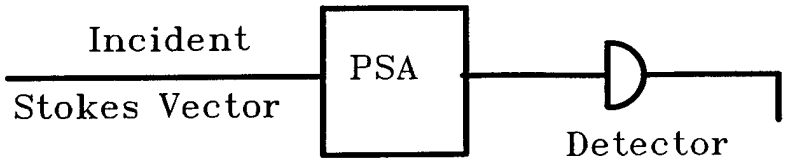

Figure 8-1 Polarization state analyzer and Stokes polarimeter.

$$\vec{S}' = \mathrm{A}\vec{S}_{inc} \tag{8-1}$$

where $\vec{S}_{inc} = (s_0, s_1, s_2, s_3)^T$ is the Stokes vector incident on the polarization state analyzer and A is the Mueller matrix that describes both the elements of the polarization state analyzer and instrumental polarization between the polarization state analyzer and the detector. An analyzer vector $\vec{A} = (a_0, a_1, a_2, a_3)^T$ analogous to the Stokes vector can be constructed by the vector product

$$\begin{pmatrix} a_0 \\ a_1 \\ a_2 \\ a_3 \end{pmatrix} = \vec{A} = \vec{D}\mathrm{A} = (d_0 \quad d_1 \quad d_2 \quad d_3)\begin{pmatrix} a_{00} & a_{01} & a_{02} & a_{03} \\ a_{10} & a_{11} & a_{12} & a_{13} \\ a_{20} & a_{21} & a_{22} & a_{23} \\ a_{30} & a_{31} & a_{32} & a_{33} \end{pmatrix}$$
$$= \begin{pmatrix} d_0a_{00} + d_0a_{10} + d_0a_{20} + d_0a_{30} \\ d_1a_{01} + d_1a_{11} + d_1a_{21} + d_1a_{31} \\ d_2a_{02} + d_2a_{12} + d_2a_{22} + d_2a_{32} \\ d_3a_{03} + d_3a_{13} + d_3a_{23} + d_3a_{33} \end{pmatrix} \tag{8-2}$$

where $\vec{D} = (d_0, d_1, d_2, d_3)$ is a vector that represents the polarization sensitivity of the detector. The effects of instrumental polarization and polarization sensitivity of the detector are included in the polarization state analyzer vector $\vec{A}$. The output at the detector i is proportional to the incident intensity and is found by the dot product

$$i = \vec{A} \cdot \vec{S}_{inc} = a_0 s_0 + a_1 s_1 + a_2 s_2 + a_3 s_3 . \tag{8-3}$$

The incident Stokes vector $\vec{S}_{inc}$ is determined by making a series of measurements i_q, changing the elements of the polarization state analyzer for each measurement. The intensity for the q'th measurement is

$$i_q = \vec{A}_q \cdot \vec{S}_{inc} . \tag{8-4}$$

where $\vec{A}_q$ is the analyzer vector for the q'th measurement. The expression for Q measurements is conveniently expressed

$$\begin{pmatrix} i_0 \\ i_1 \\ . \\ . \\ . \\ i_{Q-1} \end{pmatrix} = \begin{pmatrix} a_{0,0} & a_{0,1} & a_{0,2} & a_{0,3} \\ a_{1,0} & a_{1,1} & a_{1,2} & a_{1,3} \\ . & & & \\ . & & & \\ . & & & \\ a_{Q-1,0} & a_{Q-1,1} & a_{Q-1,2} & a_{Q-1,3} \end{pmatrix} \begin{pmatrix} s_0 \\ s_1 \\ s_2 \\ s_3 \end{pmatrix} \tag{8-5}$$

where $a_{q,j}$ is the j th ($j = 0, 1, 2, 3$) element of $\vec{A}_q$ for the q'th measurement. This is rewritten

$$\vec{I} = \mathbf{W} \vec{S}_{inc} \tag{8-6}$$

where $\mathbf{W}$ is the polarimetric measurement matrix

$$\mathbf{W} = \begin{pmatrix} a_{0,0} & a_{0,1} & a_{0,2} & a_{0,3} \\ a_{1,0} & a_{1,1} & a_{1,2} & a_{1,3} \\ . & & & \\ . & & & \\ . & & & \\ a_{Q-1,0} & a_{Q-1,1} & a_{Q-1,2} & a_{Q-1,3} \end{pmatrix} . \tag{8-7}$$

If the polarimetric measurement matrix is known, the calculated Stokes vector $\vec{R}$ can be found from the inverse of the polarimetric measurement matrix and the measured intensities by the polarimetric data reduction equation

$$\vec{R} = \mathbf{W}^{-1}\vec{I} = \mathbf{U}\vec{I}, \tag{8-8}$$

where $\mathbf{U}$ is the polarimetric data reduction matrix.

The polarimetric measurement matrix $\mathbf{W}$ must be non-singular in order to calculate the polarimetric data reduction matrix $\mathbf{U}$. If four of the Q measurements are linearly independent, the four columns of $\mathbf{W}$ are linearly independent and $\mathbf{W}$ is of rank four. Physically, this means the polarimeter measures all four elements of the incident Stokes vector.

If $Q = 4$ linearly independent measurements are made to determine the complete Stokes vector, the calculated Stokes vector $\vec{R}$ is uniquely determined. With more than four measurements, $\vec{R}$ is overdetermined and the polarimetric measurement matrix $\mathbf{W}$ is not square. The solution of Eq. 8-8 takes the form

$$\vec{R} = (\mathbf{W}^T\mathbf{W})^{-1}\mathbf{W}^T\vec{I} = \mathbf{U}\vec{I}. \tag{8-9}$$

In general, the calculated Stokes vector $\vec{R}$ is not equal to the actual Stokes vector $\vec{S}$ because of noise in the measurements. Eq. 8-9 represents the least squares solution for $\vec{R}$ and minimizes the effects of noise in the measurement [104].

2. Examples for Polarization State Analyzers

To illustrate the data reduction technique for the polarization state analyzer data reduction, two typical configurations will be examined; the rotating polarizer polarimeter, and the rotating retarder polarimeter. The polarimetric data reduction equation and polarimetric data reduction matrix used to calculate the unknown incident Stokes vector is derived.

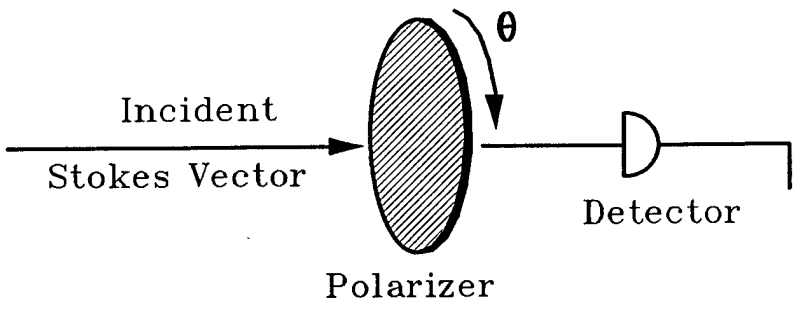

Figure 8-2 Rotating polarizer polarization analyzer.

The rotating polarizer polarimeter configuration is shown in Figure 8-2. The Mueller calculus equation describing the q'th measurement is

$$\vec{S}_q' = \mathbf{M}_p(\theta_q)\vec{S}_{inc},$$

or

$$\begin{pmatrix} s'_0 \\ s'_1 \\ s'_2 \\ s'_3 \end{pmatrix}_q = \frac{1}{2}\begin{pmatrix} 1 & \cos 2\theta_q & \sin 2\theta_q & 0 \\ \cos 2\theta_q & \cos^2 2\theta_q & \cos 2\theta_q \sin 2\theta_q & 0 \\ \sin 2\theta_q & \cos 2\theta_q \sin 2\theta_q & \sin^2 2\theta_q & 0 \\ 0 & 0 & 0 & 0 \end{pmatrix}\begin{pmatrix} s_0 \\ s_1 \\ s_2 \\ s_3 \end{pmatrix}, \tag{8-10}$$

where S_{inc} is the incident Stokes vector to be determined and $\vec{S}'$ is the Stokes vector incident on the detector. $\mathbf{M}_p(\theta_q)$ describes the transformation of the incident Stokes vector by a polarizer at angle θ_q.

If the detector is polarization insensitive, the detection vector is $\vec{D} = (1,0,0,0)$ and the analyzer vector $\vec{A}_q$ is given by the top row of the matrix $\mathbf{M}_p(\theta_q)$

$$\vec{A}_q = \frac{1}{2}(1, \cos 2\theta_q, \sin 2\theta_q, 0). \tag{8-11}$$

Consider the polarizer rotated to four orientations, $\theta_q = 0°, 45°, 90°, \text{and } 135°$, for example. The polarimetric data reduction matrix $\mathbf{W}$ is

$$\mathbf{W} = \frac{1}{2}\begin{pmatrix} 1 & 1 & 0 & 0 \\ 1 & 0 & 1 & 0 \\ 1 & -1 & 0 & 0 \\ 1 & 0 & -1 & 0 \end{pmatrix}, \tag{8-12}$$

and the measurements at the four orientations of θ_q are written

$$\vec{I} = \begin{pmatrix} i_0 \\ i_1 \\ i_2 \\ i_3 \end{pmatrix} = \frac{1}{2}\begin{pmatrix} 1 & 1 & 0 & 0 \\ 1 & 0 & 1 & 0 \\ 1 & -1 & 0 & 0 \\ 1 & 0 & -1 & 0 \end{pmatrix}\begin{pmatrix} s_0 \\ s_1 \\ s_2 \\ s_3 \end{pmatrix} = \mathbf{W}\vec{S}_{inc}, \tag{8-13}$$

where $\vec{I}$ is the vector of the intensities at the four orientations.

This rotating polarizer polarimeter cannot measure the circular component s_3 of $\vec{S}_{inc}$. This insensitivity to circularly polarized light is represented by the zeros in the fourth column of $\mathbf{W}$. $\mathbf{W}$ is of rank 3 and is singular. In order to calculate a reduced (3-element) Stokes vector, the fourth column is dropped from $\mathbf{W}$ to form a new polarimetric measurement matrix $\mathbf{W}'$ that is non-singular and invertible. $\mathbf{W}'$ is used in Eq. 8-9 and the calculated reduced Stokes vector $\vec{R}$ is

$$\vec{R} = (\mathbf{W}'^{T}\mathbf{W}')^{-1}\mathbf{W}'^{T}\vec{I} = \mathbf{U}\vec{I} = \begin{pmatrix} 1/2 & 1/2 & 1/2 & 1/2 \\ 1 & 0 & -1 & 0 \\ 0 & 1 & 0 & -1 \end{pmatrix}\begin{pmatrix} i_0 \\ i_1 \\ i_2 \\ i_3 \end{pmatrix} \tag{8-14}$$

or

$$\vec{R} = \begin{pmatrix} [i_0 + i_1 + i_2 + i_3]/2 \\ i_0 - i_2 \\ i_1 - i_3 \end{pmatrix}. \tag{8-15}$$

With this particular choice of orientations for the polarizer, the action of the polarimetric measurement matrix U is easily related to the Stokes vector. The first element of $\vec{R}$ is the average of the four intensity measurements. The second element is the difference of the intensities of the horizontally and vertically polarized light and the third element is the difference of the light polarized at $45°$ and $135°$.

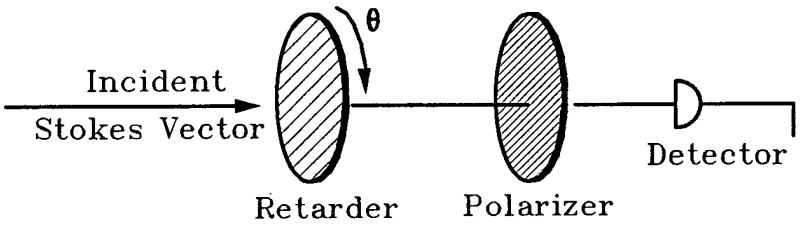

Figure 8-3 Rotating retarder Stokes polarimeter.

The configuration for the second example of a polarization state analyzer is the rotating $\lambda/4$ retarder, fixed polarizer configuration as shown in Figure 8-3. It is a complete polarization state analyzer, i.e. all four elements of the incident Stokes vector are determined. The Mueller calculus equation for the linear retarder at angle θ_q is

$$\vec{S}' = \mathbf{M}_p \mathbf{M}_r(\theta_q)\vec{S}_{inc}$$

or

$$\begin{pmatrix} s'_0 \\ s'_1 \\ s'_2 \\ s'_3 \end{pmatrix} = \frac{1}{2}\begin{pmatrix} 1 & 1 & 0 & 0 \\ 1 & 1 & 0 & 0 \\ 0 & 0 & 0 & 0 \\ 0 & 0 & 0 & 0 \end{pmatrix}\begin{pmatrix} 1 & 0 & 0 & 0 \\ 0 & \cos^2 2\theta_q & \cos 2\theta_q \sin 2\theta_q & -\sin 2\theta_q \\ 0 & \cos 2\theta_q \sin 2\theta_q & \sin^2 2\theta_q & \cos 2\theta_q \\ 0 & \sin 2\theta_q & -\cos 2\theta_q & 0 \end{pmatrix}\begin{pmatrix} s_0 \\ s_1 \\ s_2 \\ s_3 \end{pmatrix} \quad (8\text{-}16)$$

$$= \frac{1}{2}\begin{pmatrix} 1 & \cos^2 2\theta_q & \cos 2\theta_q \sin 2\theta_q & -\sin 2\theta_q \\ 1 & \cos^2 2\theta_q & \cos 2\theta_q \sin 2\theta_q & -\sin 2\theta_q \\ 0 & 0 & 0 & 0 \\ 0 & 0 & 0 & 0 \end{pmatrix}\begin{pmatrix} s_0 \\ s_1 \\ s_2 \\ s_3 \end{pmatrix}.$$

If $Q = 8$ and a measurement is made every $22.5°$ from $0°$ to $157.5°$, the polarimetric measurement equation is

$$\vec{I} = \begin{pmatrix} i_0 \\ i_1 \\ i_2 \\ i_3 \\ i_4 \\ i_5 \\ i_6 \\ i_7 \end{pmatrix} = \begin{pmatrix} 1 & 1 & 0 & 0 \\ 1 & 0.5 & 0.5 & -1/\sqrt{2} \\ 1 & 0 & 0 & -1 \\ 1 & 0.5 & -0.5 & -1/\sqrt{2} \\ 1 & 1 & 0 & 0 \\ 1 & 0.5 & 0.5 & 1/\sqrt{2} \\ 1 & 0 & 0 & 1 \\ 1 & 0.5 & -0.5 & 1/\sqrt{2} \end{pmatrix} \begin{pmatrix} s_0 \\ s_1 \\ s_2 \\ s_3 \end{pmatrix} = \mathbf{W}\vec{S} \tag{8-17}$$

and the calculated Stokes vector $\vec{R}$ is

$$\vec{R} = \begin{pmatrix} r_0 \\ r_1 \\ r_2 \\ r_3 \end{pmatrix} = (\mathbf{W}^T\mathbf{W})^{-1}\mathbf{W}^T\vec{I} = \mathbf{U}\vec{I}, \tag{8-18}$$

The polarimetric data reduction matrix U is

$$\mathbf{U} = (\mathbf{W}^T\mathbf{W})^{-1}\mathbf{W}^T$$

$$= \begin{pmatrix} -0.25 & 0.25 & 0.75 & 0.25 & -0.25 & 0.25 & 0.75 & 0.25 \\ 1 & 0 & -1 & 0 & 1 & 0 & -1 & 0 \\ 0 & 1 & 0 & -1 & 0 & 1 & 0 & -1 \\ 0 & -\sqrt{2}/4 & -0.5 & -\sqrt{2}/4 & 0 & \sqrt{2}/4 & 0.5 & \sqrt{2}/4 \end{pmatrix}. \tag{8-19}$$

All four Stokes vector elements are detected with this polarimeter, i.e. the polarimeter is complete.

Note that the four Stokes vector elements can be found from many other linear combinations of the measured intensities. For example, the Stokes vector can be found from the following set of equations:

$$\begin{aligned} r_0 &= \frac{1}{2}(i_2 + i_6) \\ r_1 &= 2(i_1 + i_7 - r_0) \\ r_2 &= 2(i_1 - i_3) \\ r_3 &= i_6 - i_2 \end{aligned} \tag{8-20}$$

These equations do not use all eight measurements, however. The data reduction equation using the polarimetric measurement matrix (Eq. 8-19) uses all of the data and automatically gives the least squares fit to the data when the measurement is overdetermined [101].

The Stokes vector can also be found using the Fourier techniques introduced in Chapter III for this particular measurement sequence. The rotation of the retarder through equal increments encodes the incident Stokes vector onto the harmonics of the detected signal. This can be seen by examining the modulation of the values in the rows of the polarimetric data reduction matrix U. The first row, which determines the first element r_0 of the calculated Stokes vector, contains a dc term and a second harmonic. The second and third rows determine r_1 and r_2 and exhibit even and odd second harmonics respectively. The fourth row shows the first harmonic behavior of r_3 for this measurement sequence.

3. Polarimetric Data Reduction Matrix for Mueller Matrix Polarimeters

The formalism developed for the polarization state analyzer is now generalized for a Mueller matrix polarimeter that contains both polarization state analyzer and generator.

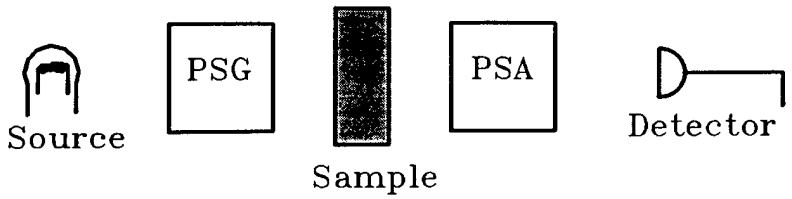

Figure 8-4 Block diagram of general polarimeter.

Consider the Mueller matrix polarimeter shown in Figure 8-4. It consists of a source, a polarization state generator, a sample, a polarization state analyzer, and a detector. The Mueller matrix equation describing the polarimeter is

$$\vec{S}' = \mathbf{A}\,\mathbf{M}_{sample}\,\mathbf{G}\,\vec{S}_{inc}, \tag{8-21}$$

where $\vec{S}_{inc}$ is the Stokes vector of the light incident on the polarization state generator, $\mathbf{G}$ is the Mueller matrix for the polarization state generator, $\mathbf{M}_{sample}$ is the Mueller matrix for the sample, and $\mathbf{A}$ is the Mueller matrix for the polarization state analyzer. The Stokes vector $\vec{S}$ incident on the sample is

$$\vec{S} = \mathbf{G}\,\vec{S}_{inc}. \tag{8-22}$$

The polarization of the source and the instrumental polarization before the sample are included in $\vec{S}$. The analyzer vector $\vec{A}$ is formed from the vector product of the detector vector $\vec{D}$, representing the polarization sensitivity of the detector, and the Mueller matrix for the analyzing optics

$$\vec{A} = \vec{D}\,\mathbf{A}. \tag{8-23}$$

The effects of instrumental polarization and polarization sensitivity of the detector are included in the polarization state analyzer vector $\vec{A}$. The output at the detector i is proportional to the incident intensity and is found by the dot product

$$i = \vec{A} \cdot M_{sample}\vec{S}_{inc}. \tag{8-24}$$

Eq. 8-24 can be rewritten

$$i = \sum_{j,k=0}^{3} a_j m_{j,k} s_k \tag{8-25}$$

or

$$i = \sum_{j,k=0}^{3} w_{j,k} m_{j,k} \tag{8-26}$$

where $w_{j,k} = a_j s_k$ are the elements of a sixteen element polarimetric measurement matrix. A polarimetric measurement vector $\vec{W} = (w_{00}, w_{01}, w_{02}, w_{03}, w_{10}, w_{11}, w_{12}, w_{13}, w_{20}, \ldots, w_{33},)$ is formed from the polarimetric measurement matrix by taking the first four elements of the vector from the top row of the matrix, the second four elements from the second row of the matrix, and so on. The indices of $\vec{W}$ are chosen to clearly show the dependence of each element $w_{j,k}$ on the elements of the analyzer and generator vectors a_j and s_k. In a similar fashion, the Mueller matrix is written as a sixteen element column vector $\vec{M} = (m_{00}, \ m_{01}, \ m_{02}, \ m_{03}, \ m_{10}, \ m_{11}, \ \ldots, \ m_{33})^T$, where again the indices are written to clearly show the origin of the vector element from the matrix element. The intensity is the dot product

$$i = \vec{W} \cdot \vec{M}. \tag{8-27}$$

A Mueller matrix is determined by making a series of Q measurements i_q with various configurations of the polarization state analyzer and generator. For the q'th measurement, $q = 0, 1, \ldots, Q-1$, the polarization state analyzer $\vec{A}_q = (a_{q,0}, a_{q,1}, a_{q,2}, a_{q,3})$ and generator $\vec{S}_q = (s_{q,0}, s_{q,1}, s_{q,2}, s_{q,3})^T$ form the polarimetric measurement vector $\vec{W}_q$. The intensity is

$$i_q = \vec{W}_q \cdot \vec{M}, \tag{8-28}$$

where the element $w_{q,jk} = a_{q,j} s_{q,k}$ of $\mathbf{W}$ is given by the j'th element of $\vec{A}_q$ and the k'th element of $\vec{S}_q$ for the q'th measurement. The relationship between the set of measured intensities, the sample Mueller matrix, and the polarizing and analyzing optics for Q measurements is then

$$\vec{I} = \mathbf{W}\vec{M}$$

or

$$\begin{pmatrix} i_0 \\ i_1 \\ \cdot \\ \cdot \\ \cdot \\ i_{Q-1} \end{pmatrix} = \begin{pmatrix} w_{0,00} & w_{0,01} & \cdot & \cdot & \cdot & w_{0,33} \\ w_{1,00} & w_{1,01} & \cdot & \cdot & \cdot & w_{1,33} \\ \cdot & & & & & \\ \cdot & & & & & \\ \cdot & & & & & \\ w_{Q-1,00} & w_{Q-1,01} & \cdot & \cdot & \cdot & w_{Q-1,33} \end{pmatrix} \begin{pmatrix} m_{00} \\ m_{01} \\ \cdot \\ \cdot \\ \cdot \\ m_{33} \end{pmatrix}, \tag{8-29}$$

where $\vec{W}_q$ forms the q'th row of the $Q \times 16$ polarimetric measurement matrix $\mathbf{W}$.

The index following the comma for the elements in $\mathbf{W}$ and the index of the Mueller vector take on values as described above, i.e. the second index ranges from 0 to 3 for each value of the first index. If $\mathbf{W}$ contains sixteen linearly independent columns, all sixteen elements of the sample Mueller vector are determined and the polarimeter is complete. In general, $Q > 16$ and the Mueller vector is calculated from the intensity vector $\vec{I}$ and $\mathbf{U}$

$$\vec{M} = [\mathbf{W}^T \mathbf{W}]^{-1} \mathbf{W}^T \vec{I} = \mathbf{U}\vec{I}. \tag{8-30}$$

The sample Mueller matrix is found by rewriting the Mueller vector in matrix form.

The polarimetric measurement matrix $\mathbf{W}$ and consequently $\mathbf{U}$ depend on the exact configuration of the polarization state generator and analyzer and how these

elements are varied over the measurement sequence. One convenient sequence of measurements is made with N positions each of the polarization state generator and analyzer. The generated and analyzed states are not necessarily the same. The sequence of measurements proceeds as follows: the polarization state generator and analyzer are moved to the initial setting. The analyzer is kept fixed while intensity measurements are made at all N settings of the polarization state generator. The analyzer is set to the next state and the generated polarization states are repeated. This is repeated until both polarization state generator and analyzer are each stepped through N positions for a total of $Q = N^2$ measurements. Appendix B describes this iterative measurement sequence for a complete Mueller matrix polarimeter for $N = 8$. The specific configurations and orientations of the elements of the polarization state analyzer and generator and an algorithm to calculate the polarimetric measurement matrix are given.

The analyzed states and generated states do not have to be the same and in general they are not. The generated and detected polarization states $\vec{S} = \mathbf{G}\,\vec{S}_{inc}$ and $\vec{A}$ should be well known. If Mueller matrices for the polarization elements are accurately known and the polarization of the source $\vec{S}_{inc}$ and the polarization sensitivity of the detector $\vec{D}$ are either well known or negligible, the quantities $\vec{S}$ and $\vec{A}$ can be calculated directly.

4. Partial Mueller Matrix Polarimeter Example

To illustrate how a Mueller matrix is found, a polarimeter that measures nine of the sixteen elements of the Mueller matrix will be examined. In this example, the Mueller matrix elements that provide information on the circular polarization properties of the sample, i.e. the fourth row and fourth column of the Mueller matrix, are not determined. Since only linear polarizers are used in this polarimeter, the fourth

row and fourth column of the matrices for the polarization state analyzer and generator are zero. If zeros of the analyzer and generator were included in the polarimetric measurement matrix W, it would be singular and an inverse could not be calculated. To make W non-singular, these elements have been omitted. The terms reduced Stokes vector and reduced Mueller matrix refer to a three element Stokes vector and a nine element Mueller matrix that contain no information on the circular polarization.

Figure 8-5 Dual rotating polarizer polarimeter.

The system, shown in Figure 8-5, consists of two polarizers, one on either side of the sample. The two polarizers are oriented at angles θ_1 and θ_2. The Mueller matrix equation (using reduced Stokes vectors and Mueller matrices) describing a sample between two linear polarizers is

$$\vec{S}' = \mathrm{M}_p(\theta_2)\mathrm{M}_s\mathrm{M}_p(\theta_1)\vec{S}_{inc}$$

or

$$\vec{S}' = \frac{1}{4}\begin{pmatrix} 1 & \cos 2\theta_2 & \sin 2\theta_2 \\ \cos 2\theta_2 & \cos^2 2\theta_2 & \cos 2\theta_2 \sin 2\theta_2 \\ \sin 2\theta_2 & \cos 2\theta_2 \sin 2\theta_2 & \sin^2 2\theta_2 \end{pmatrix} \tag{8-31}$$

$$\times \begin{pmatrix} m_{00} & m_{01} & m_{02} \\ m_{10} & m_{11} & m_{12} \\ m_{20} & m_{21} & m_{22} \end{pmatrix} \begin{pmatrix} 1 & \cos 2\theta_1 & \sin 2\theta_1 \\ \cos 2\theta_1 & \cos^2 2\theta_1 & \cos 2\theta_1 \sin 2\theta_1 \\ \sin 2\theta_1 & \cos 2\theta_1 \sin 2\theta_1 & \sin^2 2\theta_1 \end{pmatrix} \vec{S}_{inc}.$$

It is assumed that the source is unpolarized and there is no polarization sensitivity of the detector.

The iterative measurement sequence described at the end of the last section is used with $N = 4$. A total of $Q = N^2 = 16$ measurements are made with the first polarizer at angles $\theta_1 = 0°, 45°, 90°, 135°$ for each orientation of the second polarizer at angles $\theta_2 = 0°, 45°, 90°, 135°$. The polarimetric measurement matrix W is calculated given the known polarization state generator and analyzer

$$\mathbf{W} = \frac{1}{4}\begin{pmatrix} 1 & 1 & 0 & 1 & 1 & 0 & 0 & 0 & 0 \\ 1 & 0 & 1 & 1 & 0 & 1 & 0 & 0 & 0 \\ 1 & -1 & 0 & 1 & -1 & 0 & 0 & 0 & 0 \\ 1 & 0 & -1 & 1 & 0 & -1 & 0 & 0 & 0 \\ 1 & 1 & 0 & 0 & 0 & 0 & 1 & 1 & 0 \\ 1 & 0 & 1 & 0 & 0 & 0 & 1 & 0 & 1 \\ 1 & -1 & 0 & 0 & 0 & 0 & 1 & -1 & 0 \\ 1 & 0 & -1 & 0 & 0 & 0 & 1 & 0 & -1 \\ 1 & 1 & 0 & -1 & -1 & 0 & 0 & 0 & 0 \\ 1 & 0 & 1 & -1 & 0 & -1 & 0 & 0 & 0 \\ 1 & -1 & 0 & -1 & 1 & 0 & 0 & 0 & 0 \\ 1 & 0 & -1 & -1 & 0 & 1 & 0 & 0 & 0 \\ 1 & 1 & 0 & 0 & 0 & 0 & -1 & -1 & 0 \\ 1 & 0 & 1 & 0 & 0 & 0 & -1 & 0 & -1 \\ 1 & -1 & 0 & 0 & 0 & 0 & -1 & 1 & 0 \\ 1 & 0 & -1 & 0 & 0 & 0 & -1 & 0 & 1 \end{pmatrix} \tag{8-32}$$

and the polarimetric data reduction matrix U is

$$\mathbf{U} = \begin{pmatrix} 1 & 1 & 1 & 1 & 1 & 1 & 1 & 1 & 1 & 1 & 1 & 1 & 1 & 1 & 1 & 1 \\ 2 & 0 & -2 & 0 & 2 & 0 & -2 & 0 & 2 & 0 & -2 & 0 & 2 & 0 & -2 & 0 \\ 0 & 2 & 0 & -2 & 0 & 2 & 0 & -2 & 0 & 2 & 0 & -2 & 0 & 2 & 0 & -2 \\ 2 & 2 & 2 & 2 & 0 & 0 & 0 & 0 & -2 & -2 & -2 & -2 & 0 & 0 & 0 & 0 \\ 4 & 0 & -4 & 0 & 0 & 0 & 0 & 0 & -4 & 0 & 4 & 0 & 0 & 0 & 0 & 0 \\ 0 & 4 & 0 & -4 & 0 & 0 & 0 & 0 & 0 & -4 & 0 & 4 & 0 & 0 & 0 & 0 \\ 0 & 0 & 0 & 0 & 2 & 2 & 2 & 2 & 0 & 0 & 0 & 0 & -2 & -2 & -2 & -2 \\ 0 & 0 & 0 & 0 & 4 & 0 & -4 & 0 & 0 & 0 & 0 & 0 & -4 & 0 & 4 & 0 \\ 0 & 0 & 0 & 0 & 0 & 4 & 0 & -4 & 0 & 0 & 0 & 0 & 0 & -4 & 0 & 4 \end{pmatrix} \tag{8-33}$$

The polarimetric data reduction matrix operates on a set of sixteen measurements producing the estimate of the sample Mueller matrix.

B. Calibration of the Polarimetric Measurement Matrix

The polarimetric data reduction formalism described in the previous section requires the polarimetric measurement matrix W to be known before it is used to calculate the sample Mueller matrix from the measured intensities. This requires accurate knowledge of the polarization properties of the polarization elements in the polarimeter and of any instrumental polarization present. If the polarization elements are not ideal or if there is non-negligible instrumental polarization, the Stokes vector incident on the sample $\vec{S}$ and the analyzing vector $\vec{A}$ must be determined in order to calculate the polarimetric measurement matrix. This section describes the calibration procedure through which these quantities and consequently the polarimetric measurement matrix are found.

Consider the general Mueller matrix polarimeter shown in Figure 8-4. The Mueller matrices of the polarization elements in the polarization state analyzer and generator are known approximately but exhibit unknown behavior associated with some systematic error. For example, polarizers may have diattenuation less than one and have some retardance or linear retarders may have a retardance that is different from the expected value or have some diattenuation. In addition, there may be unknown instrumental polarization resulting from a polarized source, polarizing elements such as mirrors or beamsplitters, or polarization sensitivity of the detector. These effects are reflected in the values of the elements of the polarimetric measurement matrix.

An outline of the calibration procedure to remove the effects of these systematic errors is as follows: first, a set of Q intensity calibration measurements is made with nothing in the sample compartment. The polarization state generator and analyzer are varied exactly as when measuring an arbitrary Mueller matrix. Next, the elements of the polarization generator vector $\vec{S}_q$ and polarization analyzer vector $\vec{A}_q$ are found by a minimization algorithm. Finally, the polarimetric measurement matrix $\mathbf{W}$ is reconstructed using the elements of $\vec{S}_q$ and $\vec{A}_q$. The polarimetric measurement matrix is now calibrated and accurately represents the measurement process. This procedure is now examined in detail.

Eq. 8-29 describes the Q intensity measurements made with the polarization state generator and analyzer

$$\vec{I} = \mathbf{W}\vec{M}$$

or

$$\begin{pmatrix} i_0 \\ i_1 \\ \cdot \\ \cdot \\ \cdot \\ i_{Q-1} \end{pmatrix} = \begin{pmatrix} w_{0,00} & w_{0,01} & \cdot & \cdot & \cdot & w_{0,33} \\ w_{1,00} & w_{1,01} & \cdot & \cdot & \cdot & w_{1,33} \\ \cdot & & & & & \\ \cdot & & & & & \\ \cdot & & & & & \\ w_{Q-1,00} & w_{Q-1,01} & \cdot & \cdot & \cdot & w_{Q-1,33} \end{pmatrix} \begin{pmatrix} m_{00} \\ m_{01} \\ \cdot \\ \cdot \\ \cdot \\ m_{33} \end{pmatrix}. \qquad (8\text{-}34)$$

where the elements of the polarimetric measurement matrix $w_{j,k} = a_j s_k$ are approximately known. A series of Q measurements is now made with a non-polarizing sample (air) in the sample compartment. The Mueller vector in Eq. 8-34 is replaced by the Mueller vector corresponding to the identity Mueller matrix $M_I = (1,0,0,0,0,1,0,0,0,0,1,0,0,0,0,1)^T$. Since twelve elements of the identity matrix

are zero, twelve columns of the polarimetric measurement matrix $\mathbf{W}$ cannot be determined with the identity matrix as a calibration matrix. All elements of $\mathbf{W}$ can be recovered if the elements of the analyzer and generator vectors can be found.

The calibration is carried out by varying the elements of the polarization state generator and analyzer for the measurement sequence. For each setting of the generator and analyzer, an intensity i_q is measured. The intensity for the q'th measurement is

$$\begin{aligned} i_q &= w_{q,00} + w_{q,11} + w_{q,22} + w_{q,33} \\ &= a_{q,0}s_{q,0} + a_{q,1}s_{q,1} + a_{q,2}s_{q,2} + a_{q,3}s_{q,3}. \end{aligned} \tag{8-35}$$

A total of Q measurements are made.

Eq. 8-35 is non-linear in the elements of $\vec{A}$ and $\vec{S}$ and the values of the elements of the polarization state generator and analyzer must be found through minimization of the function

$$\begin{aligned} \chi^2 &= \sum_{q=0}^{Q-1} (i'_q - i_q)^2 \\ &= \sum_{q=0}^{Q-1} [i'_q - (a_{q,0}s_{q,0} + a_{q,1}s_{q,1} + a_{q,2}s_{q,2} + a_{q,3}s_{q,3})]^2, \end{aligned} \tag{8-36}$$

where i'_q represents the measured value of the intensity for the q'th position of the generator and analyzer and i_q represents the estimate of the intensity using the values of the elements $\vec{S}_q$ and $\vec{A}_q$. The approximately known Mueller matrices for the polarization state generator and polarization state analyzer are used as an initial guess for the elements of $\vec{S}_q$ and $\vec{A}_q$. A suitable minimization algorithm [101],[105] is used to successively improve the estimate of $\vec{S}_q$ and $\vec{A}_q$.

The equation for the q'th intensity measurement (Eq. 8-35) contains four unknowns for the polarization state generator and four for the polarization state analyzer. For an arbitrary set of Q measurements there will be Q equations in $8Q$ unknowns. For the iterative measurement sequence proposed in Section A.3, the number of measurements is $Q = N^2$ for N iterations each for the polarization state generator and analyzer. Since there must be at least as many equations as unknowns, $N^2 \geq 8N$ or $N \geq 8$ and $N^2 = Q = 64$ is the minimum number of measurements required for calibration for the iterative measurement sequence.

The vectors $\vec{A}_q$ and $\vec{S}_q$ are determined except to within a rotation of the whole polarimeter. Each generating and analyzing vector can be rotated by an equal amount and still produce a minimum for χ^2 in Eq. 8-36. By setting the second element of the first generated Stokes vector $s_{0,2}$ equal to zero during minimization, the major axis of the polarization ellipse of this Stokes vector defines the x-axis of the coordinate system. In order to prevent the magnitudes of the analyzed and generated vectors from becoming too different in the minimization process, an additional constraint can be introduced by setting the first elements of the generated and analyzed vectors equal to each other, $s_{0,0} = a_{0,0}$.

With χ^2 minimized, the elements of $\vec{S}_q$ and $\vec{A}_q$ are used to calculate the polarimetric measurement matrix $\mathbf{W}$. $\mathbf{W}$ is now calibrated and includes the effects of non-ideal polarization elements and instrumental polarization. The data reduction matrix $\mathbf{U} = (\mathbf{W}^T \mathbf{W})^{-1} \mathbf{W}^T$ also includes these effects and can now be used to find the Mueller matrix for an arbitrary sample through the polarimetric data reduction equation Eq. 8-30.

This calibration procedure will correct for many but not all systematic errors. The measurement sequence must produce a polarimetric measurement matrix $\mathbf{W}$ that is of rank 16, i.e. the sixteen columns of $\mathbf{W}$ must be linearly independent. If the non-ideal properties of the polarization elements vary too greatly, this requirement may be violated and $\mathbf{W}$ could become singular. This could occur, for example, in the spectropolarimeter at wavelengths where the retardance of a linear retarder becomes a multiple of 2π. Details on one possible configuration and measurement sequence are given in Appendix B.

The systematic errors corrected in the polarimetric measurement matrix must be repeatable from one measurement sequence to the next. For example, a repeatable orientation error can be corrected, but a random error in positioning a rotation stage cannot.

It should be noted that a similar calibration procedure has been used successfully [106] in an instrument for measuring the Mueller matrices of scattered light. The calibration was carried out by a procedure very similar to the one described here with two exceptions - the light source was assumed to be completely polarized and the polarization elements were assumed to be non-depolarizing. With these assumptions, the relationship between the elements of the Stokes vector for completely polarized light provides additional constraints that allow the reduction of the minimum number of measurements for the calibration to 36. By using 64 measurements in the calibration procedure as described here, these assumptions can be relaxed and any partial polarization of the source and depolarization of the polarization elements are included in the polarimetric data reduction matrix $\mathbf{W}$.

Chapter IX

Summary and Directions for Future Research

A. Summary

The purpose of this work was to develop the infrared spectropolarimeter and use it to measure spectra of polarization properties of several infrared samples. This development has encompassed several different aspects including development of the instrument and its components, development of the appropriate algorithms suitable for application to a spectral instrument, and implementation of the algorithms in software.

A review of the nomenclature and mathematics of polarization was given along with a brief history of previous research in spectral measurements of polarization properties. This was followed by an in-depth discussion of polarization metrology techniques with special attention to the Fourier analysis of periodic polarization signals. The advantages of this technique in general and for spectral instruments in particular were discussed. Systematic error and noise considerations for spectropolarimetry and their solutions were described.

The rotating sample and dual rotating retarder polarimeters and their implementation in the FTIR spectropolarimeter were presented. Data reduction algorithms were derived with consideration for pertinent systematic errors. Example measurements were given for both polarimeter configurations.

The novel and new parts of this work include the following: 1) the development of the rotating sample polarimeter and its implementation in the FTIR spectrometer, 2) the infrared achromatic retarder used in the dual rotating retarder spectropolarimeter, 3) the use of the dual rotating retarder polarimeter in a FTIR spectrometer, and 4) the data reduction algorithm for five systematic errors in the dual rotating retarder polarimeter.

The following measurements were made: 1) linear diattenuation and linear retardance spectra of two infrared retarders, 2) linear diattenuation and linear retardance spectra of two infrared wire grid polarizers, 3) linear diattenuation and linear retardance measurements of bulk cadmium sulfide and cadmium selenide resulting in birefringence spectra and dispersion relations for these materials at longer wavelengths than previously given, 4) transmission, linear diattenuation, and linear retardance measurements of three bulk liquid crystal materials, and 5) Mueller matrix spectra as a function of voltage and the resulting electro-optic coefficient spectrum of a cadmium telluride electro-optic modulator.

B. Directions for Future Research

The infrared spectropolarimeter has the potential to provide a tremendous amount of information for infrared devices and materials. The spectropolarimeter's capability for calibration of infrared polarization elements has been demonstrated in this dissertation. As these calibration spectra are used to improve polarization elements, the accuracy of the spectropolarimeter and other infrared polarimeters

should increase. The wealth of information available from materials measurements such as electro-optic crystals has also been demonstrated. This section describes research directions that should be pursued in the near term to take advantage of the spectropolarimeter's capabilities and to maximize the information obtained from spectropolarimetric measurements.

1. Experimental Considerations

Chapter VI discussed some of the sources of residual error in the Mueller matrix measurements for the infrared spectropolarimeter. Chapter VIII outlined a new data reduction algorithm that should improve the accuracy of Mueller matrix measurements by removing the effects of many systematic errors. With the improved data reduction and the self-calibration described in Chapter VIII, the residual errors should be reduced to well below the one percent level. The major task that needs to be completed before this data reduction can be implemented in the spectropolarimeter is to find a suitable minimization algorithm for the self-calibration. It should be noted that this data reduction algorithm is not specific to the spectropolarimeter, but can be applied to single wavelength polarimeters, spectropolarimeters in other parts of the optical spectrum, and imaging polarimeters.

As the accuracy of the Mueller matrix measurements in the spectropolarimeter increases, other systematic errors of smaller magnitude will become important. One important additional source of systematic error that cannot be removed in the self-calibration is the drift in the response of the instrument over the measurement sequence. The best solution to removing the effects of drift on the results is to reduce it and this is best done by decreasing the amount of time required to acquire the intensity spectra. Currently the spectrometer acquires each interferogram and

Fourier transforms it while the rotation stages are moving. If faster rotation stages were used and the interferograms were Fourier transformed after all spectra were acquired, the time between the acquisition of each spectrum and consequently the time to acquire all spectra would be reduced. The amount of instrumental drift and its effect on the reduced data would therefore be reduced.

In Chapter IV, the rotating sample and dual rotating retarder polarimeters were compared. The rotating sample polarimeter is simpler, i.e. it uses fewer polarization elements, fewer rotation stages, and the data reduction is less complex. It's major disadvantage is that it measures only linear diattenuation and linear retardance. The dual rotating retarder polarimeter is complete, i.e. it measures all sixteen elements of the Mueller matrix including linear polarization, circular polarization, and depolarization. However, calibration and operation of a dual rotating retarder is far more complex than for the rotating sample polarimeter and there are many more potential sources of error. Based on the experience gained in performing experiments and analyzing calibration data, the dual rotating retarder is less accurate. An interesting area for research would be to examine in detail the two polarimeters and compare their accuracy for common systematic errors. A natural extension of this work would be to determine the most accurate polarimeter to measure, for example, linear diattenuation or particular elements of the Mueller matrix.

2. Theoretical Development of the Mueller Calculus

The Mueller matrix provides the most complete characterization of the polarization properties of optical elements, including linear diattenuation, linear retardance, circular diattenuation, circular retardance, and depolarization. The polarization properties are not easily extracted from the Mueller matrix, however, except in a few special cases when one or two polarization properties are present.

Algorithms are required to extract useful information on polarization properties from the Mueller matrix. A detailed analysis of the Mueller calculus is currently underway to derive explicit expressions for calculating the diattenuation and retardance of an arbitrary Mueller matrix [107]. This work should establish important relationships between physically meaningful quantities such as depolarization, diattenuation, and retardance and experimentally determined Mueller matrix data and the physical realizability of Mueller matrix data.

The Mueller matrix includes information on the depolarization of the optical element. The amount of depolarization in polarization devices will become an increasingly important quantity to measure and control as optical instruments require continuing improvements in the accuracy and control of polarized light. Depolarization will be an important consideration in the development of polarization devices such as liquid crystal modulators for the infrared.

Currently there are figures of merit to characterize the amount of depolarization in optical elements. The sources of depolarization and how different types of depolarization appear in the Mueller matrix are not well understood, however. There may be nine types of depolarization corresponding to the additional degrees of freedom in the Mueller matrix beyond what is required to characterize the polarization properties. The physical origins of depolarization and how they appear in the Mueller matrix should be determined in order to more completely understand these effects on optical systems.

3. Future Measurements

There is great potential for the infrared spectropolarimeter to provide calibration spectra for a large number of infrared devices and to give insight into the fun-

damental physical properties of infrared materials. This section describes a few of the measurements that should be made in the short term on infrared polarization devices and materials.

The need for calibration of infrared polarization devices has been established in this research. A spectrum of the retardance in a wire grid polarizer and misalignment of multiple plate retarders were demonstrated. A data base of polarization properties and calibration spectra of commercially available infrared polarization elements would contribute to the development of other infrared polarimeters and would encourage the improvement of polarization devices. Materials currently used in the visible for polarization devices, such as sheet polaroid and mica, may have use in the infrared as well.

Photo-elastic modulators hold promise for application in military tracking systems. These polarimetric tracking systems target the hardbody rather than the plume by using the polarized light emitted from aerodynamically heated missiles. These systems are inherently broad spectral band and require proper calibration of the photo-elastic modulator and other polarization elements. The calibration of the photo-elastic modulator should include measurements of residual birefringence in the photo-elastic modulator and measurements of retardance as a function of wavelength and driving voltage.

The liquid crystal samples described in Chapter V hold promise for modulation devices in the infrared. Liquid crystals' chief advantage is the low voltage required for producing modulation in the visible. The significant birefringence presented in Chapter V suggests that this advantage may apply in the infrared as well. Liquid crystals are known to be relatively slow and have low contrast in the visible, however, and these characteristics must be examined in the infrared. There

may be some portions of the infrared that are more suitable than others for modulator applications, and the spectropolarimeter is ideally suited to find these spectral bands. An additional concern is the depolarization that may be present due to scattering from the large molecules. Large amounts of depolarization would affect the modulator applications of liquid crystals. Liquid crystal materials must therefore be examined with applied voltages in the spectropolarimeter to determine their polarization characteristics. These measurements should produce recommendations for optimum voltages and spectral bands for modulator applications. The depolarization as a function of voltage and wavelength must also be examined. These and other materials measurements hold the key to development of polarization devices for the polarization critical optical systems of the future.

APPENDICES

Appendix A

Fourier Transform Spectroscopy

Infrared spectroscopy is a broad subject. We will discuss here only the basics of Fourier Transform Infrared Spectroscopy, or FTIR, which are applicable to the spectropolarimetry of crystalline materials. The goal common to all spectroscopic applications is to obtain a plot of radiation intensity versus frequency. One method of spectral measurement is the conventional dispersive spectrometer. A dispersive spectrophotometer would be difficult to convert to a precision spectropolarimeter because of the large polarization effects which arise from the diffraction grating and which change rapidly with wavelength. The Fourier transform spectrometer is a more suitable spectroscopic instrument to adapt for polarization measurements.

FTIR uses a Michelson interferometer to encode frequency information. A collimated beam is partially reflected and partially transmitted by the beamsplitter. The reflected beam is reflected from the fixed mirror while the transmitted beam is reflected from the moving mirror. The beams are recombined at the beamsplitter and are passed on to the sample compartment and detector.

If the incoming beam were monochromatic, the output of the interferometer would be a sinusoidal intensity variation resulting from the alternate constructive and destructive interference of the two beams as the optical path difference

changes. The sine wave is the interference pattern or interferogram of this frequency of incoming light. A Fourier transform relates the interferogram to the optical frequency when more than one modulation frequency is present in the interferogram. The Fourier transform of the resulting interferogram is the familiar frequency spectrum.

All the spectroscopic information is present in the interferogram. The Fourier transform process simply converts the information into the familiar form. Also, the frequency of the interferogram is a function of both the frequency of the source radiation and the velocity of the moving mirror. By changing these parameters the optimal signal for a given detector may be found.

Accuracy in FTIR is highly dependent upon the accuracy in the distance scale of the interferogram. This accuracy is maintained in the Nicolet 6000 by monitoring the output of a reference laser through the interferometer. The distance between each zero crossing of the reference laser interferogram is just one-half the wavelength of the laser. This signal is used to improve the distance scale of the interferogram.

These reference zero crossings are used as a signal to take data points. The bandwidth sampled depends on the number of the zero crossings that are skipped. According to the sampling theorem, a data must be taken at least twice every wavelength in order to measure a given frequency. If a data point is taken every zero crossing of the laser, a bandwidth equal to the laser frequency of 15798 cm^{-1} is achieved.

The closer two frequencies are to each other, the further from the zero path difference it takes for them to destructively interfere with each other and produce a fringe node. To achieve greater spectral resolution in the interferogram, a greater

optical path difference is necessary. This is accomplished by increasing the length of mirror travel which increases the number of data points taken. It can be shown that under certain conditions the resolution is just the inverse of the maximum optical path difference or distance of mirror travel. Thus for 16 cm of mirror travel, the resolution is 0.06 wavenumbers. The normal mode of operation for the Nicolet spectrometer and the spectropolarimetric measurements taken here is 4 cm^{-1}

The signal-to-noise ratio (S/N) is a function of several parameters. The S/N improves as the square root of the number of scans of the Michelson interferometer that are averaged to produce one transmission spectrum. Thus to improve the S/N by a factor of two, four times as many scans must be taken. S/N is approximately proportional to the square root of resolution as well since smaller (higher) resolution implies less photons per resolution element. Thus, a spectrum with a resolution of 1 cm^{-1} would be approximately twice as noisy as a 4 cm^{-1} spectrum. In addition, the higher resolution spectrum takes longer to collect, as discussed above. Signal-to-noise is also a function of mirror velocity due to the time constant of the detector.

A. Hardware

The Nicolet 6000 Fourier Transform Infrared Spectrometer may be separated into four main units: the interferometer and optics bench, the interferometer control electronics, the data system, and the controlling program, FTIR. The instrument is versatile and may be adapted for many applications with minimal hardware alterations.

The optics bench and interferometer are detailed here. Choices for source, beamsplitter, and detector for the spectral range 400-4000 wavenumbers are the following: water cooled Globar source, KBr beamsplitter, and a long wavelength Mer-

cury Cadmium Telluride liquid nitrogen cooled detector. Other components for different spectral ranges are commercially available. The two infrared beams from the beamsplitter are modulated by a high resolution interferometer consisting of a fixed mirror, moving mirror assembly, and the beamsplitter. The fixed mirror is mounted on wedges, providing the fine tuning required to optimize the IR signal. The moving mirror assembly is mounted on dual air bearings to reduce friction and the corresponding friction-induced fluctuations of velocity. The dual air bearings also prevent any appreciable mirror tilt allowing resolutions up to 0.06 cm^{-1}. The assembly is driven by a linear induction motor. The large field strength of this motor allows only ±0.3 % velocity error. This error is decreased further by use of the He-Ne reference laser. This laser runs the same path through the interferometer as the IR signal. The He-Ne interference pattern allows extremely accurate measurement of the distance traveled by the moving mirror. A control servo loop uses the zero crossings of the laser to calculate and correct for variations in the velocity. These zero crossings are also used as a signal for the computer to take a data point. There is also a white light source whose interference pattern gives a spike at the point of zero optical path difference. This spike is used as a trigger to begin the sampling. The aperture and the variable position mirrors are computer controlled.

The interferometer control electronics take the signal from the interferometer's preamplifiers, amplifiers, and filters, digitizes the signal, and transmits the signal to the data system. The control electronics consist of an interferometer control, digital interface, and beam path control. The interferometer control and digital interface make the analog to digital conversion for the various signals. The amplified analog and digital signals from the laser, white light, and infrared beams as well

as other signals may be directly read from the digital interface. This facilitates alignment and allows the operator to monitor the instrument in real time. The digital interface also has hardwired switches for the various parameters involved in data collection. These allow testing of the interferometer independently of the data system and are rarely used. The beam path control also has various hardwired switches that change the positions of the variable mirrors and the aperture. These are useful in aligning the optics and making adjustments independent of the computer. Separate power supplies for the signal electronics (e.g. preamps, detector) and optical isolators are employed to eliminate noise and cross-talk on the various signals.

B. Software

The data system consists of the main processor, a computer interface, front control panel, and various peripheral devices, such as teletype, raster display and hard disk.

The controlling program for the spectrometer, named FTIR, allows software control of all aspects of data collection and manipulation. The large number of commands gives the operator a wide variety of ways in which to custom design each experiment. For example, data may be collected and processed in one command, or, commands for each step of processing, such as Fourier transformation or apodization, may be executed one at a time so that the effects of various parameter changes may be seen.

After the data is initially processed, it may be manipulated in any number of ways. Arithmetic functions as well as differentiation and integration of spectra are one-command routines. Conversions from absorbance to transmittance, wavenumbers to wavelength, and vice-versa are easily made. A number of routines are avail-

able for data comparison. These routines allow the operator to search any of a number of commercially available libraries and find close matches of known spectra and the sample spectrum. A variety of display and plot commands are also implemented.

Several software routines may be used to perform what is known as spectral stripping or difference spectroscopy. These routines allow the operator to optimize a subtraction between two spectra interactively. This technique is a powerful tool for determining small changes in samples with different treatments, e.g. a varying electric field.

Some fifty parameters may be changed as needed. These include data collection parameters and data manipulation parameters. The former deal with such variables as resolution, bandwidth, spectral range, and gain levels. These may be varied to optimize signal-to-noise, increase resolution, or maximize file storage space. Data manipulation parameters deal with basic bookkeeping for the various data manipulation routines, such as plotting and displaying the data.

Appendix B

Polarization Calibration and Measurement Sequence

In this Appendix, a specific measurement sequence and polarimeter configuration is described for the polarimetric data reduction algorithm given in Chapter VIII. The measurement sequence and data reduction proposed here is suitable for calibration of the polarimetric measurement matrix in the infrared spectropolarimeter.

Recall the iterative measurement sequence described in Section A.3 of Chapter VIII in which the polarization state generator and analyzer are stepped through eight settings each. The polarization state analyzer is held fixed while intensity measurements are made for each of the eight polarization state generator settings. The analyzer is incremented to its next position and the process is repeated. This is continued until a total of 64 measurements have been made with both generator and analyzer in all eight settings. Table B-1 explicitly lists the settings of the polarization state generator and analyzer for the sequence of 64 measurements.

The iterative measurement sequence described in Chapter VIII and the calculation of the polarimetric measurement matrix are now described in detail. Consider the polarization state generator to consist of a linear polarizer at an angle θ

and a quarter wave linear retarder at an angle ϕ, both of which are allowed to rotate. The eight settings of the polarization state generator are indexed by the quantity $\beta = 0, 1, \ldots, 7$. The polarization state generator vector $\vec{S}_\beta$ for the β setting of the linear polarizer at orientation θ_β with respect to the x-axis and a linear quarter wave retarder at ϕ_β is

$$\vec{S}_\beta = \frac{1}{2}\begin{pmatrix} 1 \\ \cos 2\theta_\beta \cos^2 2\phi_\beta + \sin 2\theta_\beta \sin 2\phi_\beta \cos 2\phi_\beta \\ \cos 2\theta_\beta \sin 2\phi_\beta \cos 2\phi_\beta + \sin 2\theta_\beta \sin^2 2\phi_\beta \\ \cos 2\theta_\beta \sin 2\phi_\beta - \sin 2\theta_\beta \cos 2\phi_\beta \end{pmatrix}. \tag{B-1}$$

The source is assumed to be unpolarized. The polarization state analyzer consists of a quarter wave linear retarder and a linear polarizer. Its eight settings are indexed by the quantity $\alpha = 0, 1, \ldots, 7$. The polarization state analyzer vector $\vec{A}_\alpha$ for the quarter wave linear retarder at angle ϕ_α followed by the linear retarder at θ_α and a polarization insensitive detector is

$$\vec{A}_\alpha = \frac{1}{2}\begin{pmatrix} 1 \\ \cos 2\theta_\alpha \cos^2 2\phi_\alpha + \sin 2\theta_\alpha \sin 2\phi_\alpha \cos 2\phi_\alpha \\ \cos 2\theta_\alpha \sin 2\phi_\alpha \cos 2\phi_\alpha + \sin 2\theta_\alpha \sin^2 2\phi_\alpha \\ \cos 2\theta_\alpha \sin 2\phi_\alpha - \sin 2\theta_\alpha \cos 2\phi_\alpha \end{pmatrix}. \tag{B-2}$$

Table B-1 lists the sequence of measurements and the settings for $\vec{S}_\beta$ and $\vec{A}_\alpha$.

A Mueller matrix is determined by making a series of Q measurements i_q with the polarization state analyzer and generator in the prescribed sequence. The relationship between the set of measured intensities, the sample Mueller matrix, and the polarizing and analyzing optics for Q measurements is then

Table B-1: Sequence of measurements for $\vec{S}_\beta$ and $\vec{A}_\alpha$.

Measurement q	Analyzer vector index α	Generator vector index β
0	0	0
1	0	1
2	0	2
.	.	.
.	.	.
.	.	.
7	0	7
8	1	0
9	1	1
.	.	.
.	.	.
.	.	.
$q = 8\alpha + \beta$	α	β
.	.	.
.	.	.
.	.	.
63	7	7

$$\vec{I} = \mathrm{W}\vec{M}, \tag{B-3}$$

where the element $w_{i,j}$ of W is given by

$$w_{i,j} = a_{\alpha,k} s_{\beta,l}, \tag{B-4}$$

for $i = 8\alpha + \beta$ and $j = 4k + l$. The polarimetric measurement matrix W takes the form

$$\begin{pmatrix} a_{0,0}s_{0,0} & a_{0,0}s_{0,1} & a_{0,0}s_{0,2} & a_{0,0}s_{0,3} & a_{0,1}s_{0,0} & a_{0,1}s_{0,1} & a_{0,1}s_{0,2} & \cdots \\ a_{0,0}s_{1,0} & a_{0,0}s_{1,1} & a_{0,0}s_{1,2} & a_{0,0}s_{1,3} & a_{0,1}s_{1,0} & a_{0,1}s_{1,1} & a_{0,1}s_{1,2} & \cdots \\ \vdots & & & & & & & \\ a_{\alpha,0}s_{\beta,0} & a_{\alpha,0}s_{\beta,1} & a_{\alpha,0}s_{\beta,2} & a_{\alpha,1}s_{\beta,3} & a_{\alpha,0}s_{\beta,0} & a_{\alpha,1}s_{\beta,1} & a_{\alpha,1}s_{\beta,2} & \cdots \\ \vdots & & & & & & & \\ a_{7,0}s_{6,0} & a_{7,0}s_{6,1} & a_{7,0}s_{6,2} & a_{7,0}s_{6,3} & a_{7,1}s_{6,0} & a_{7,1}s_{6,1} & a_{7,1}s_{6,2} & \cdots \\ a_{7,0}s_{7,0} & a_{7,0}s_{7,1} & a_{7,0}s_{7,2} & a_{7,0}s_{7,3} & a_{7,1}s_{7,0} & a_{7,1}s_{7,1} & a_{7,1}s_{7,2} & \cdots \end{pmatrix}$$

$$\begin{pmatrix} \cdots & a_{0,3}s_{0,2} & a_{0,3}s_{0,3} \\ \cdots & a_{0,3}s_{1,2} & a_{0,3}s_{1,3} \\ & \vdots & \\ \cdots & a_{\alpha,3}s_{\beta,2} & a_{\alpha,3}s_{\beta,3} \\ & \vdots & \\ \cdots & a_{7,3}s_{6,2} & a_{7,3}s_{6,3} \\ \cdots & a_{7,3}s_{7,2} & a_{7,3}s_{7,3} \end{pmatrix} \qquad \text{(B-5)}$$

The eight analyzing and generating polarization states must be chosen such that the columns of the polarimetric measurement matrix are linearly independent. Given this requirement, it seems appropriate to select eight states that are spaced evenly over all possible elliptical states. With this choice, the measurement sequence is equally sensitive to an arbitrary polarization state. The Poincare sphere is useful in selecting these states. The Poincare sphere is described in many references on polarization [11],[15],[16],[17].

The Poincare sphere is shown in Figure B-1. Each point on the sphere represents a polarization state of azimuth α and ellipticity $b/a = \tan|\omega|$. The point P is given by the angles 2α and 2ω which correspond to the longitude and latitude. Points representing linearly polarized light lie along the equator, and left and right circularly polarized light are at the top and bottom respectively. Points in between represent elliptically polarized light.

The suggested eight generated and analyzed polarization states are the states that are equally spaced about the Poincare sphere. Eight equally spaced points on a sphere are the points where the corners of an inscribed cube lie on the surface of the sphere. If the cube is placed such that corners on the ends of a body diagonal are placed at the vertically and horizontally polarized states and two other states are chosen to be linear as shown in Figure B-2, the other corners are easily determined in terms of the angles α and ω. These angles are in turn related to the orientations of a linear polarizer and a linear quarter wave retarder for the polarization state generator. The orientations for the linear polarizer and the fast axis of the quarter wave retarder from horizontal for the appropriate point on the Poincare sphere are given in Table B-2. The orientation of the linear retarder and polarizer for the polarization state analyzer are chosen to be the same as for the generator.

This measurement sequence and generator and analyzer configuration can be used in a polarimeter whose polarization elements are ideal and has no instrumental polarization. This sequence is also suitable for calibration of the polarization state generator vector $\vec{S}$ and analyzer vector $\vec{A}$ as described in Section B of Chapter VIII. If this measurement sequence is used in a polarimeter where there is systematic error, these settings for the polarization state generator and analyzer can be used as the initial guess in a calibration procedure described in Chapter VIII

Section B.

Table B-2: Orientations of a linear polarizer and quarter wave retarder for eight points on the Poincare sphere.

Point on Poincare sphere α, β	Linear polarizer orientation θ_n (degrees)	Quarter wave linear retarder ϕ_n (degrees)
0	0	0
1	35.264	35.264
2	62.632	35.264
3	62.632	90
4	90	90
5	125.264	125.264
6	152.632	125.264
7	152.632	180

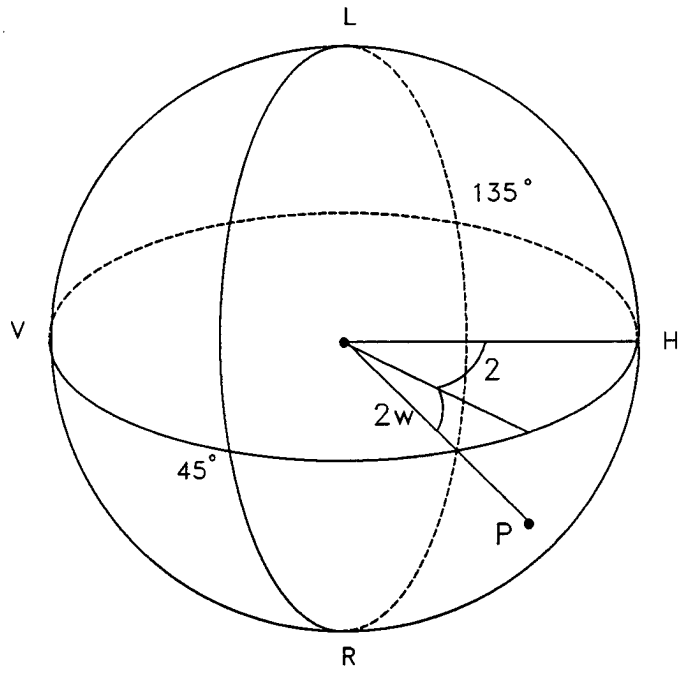

Figure B-1 Poincare sphere.

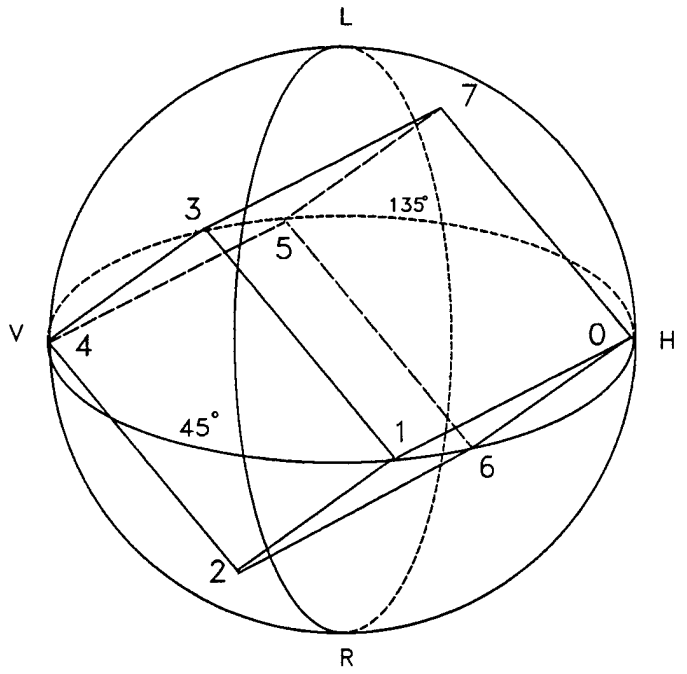

Figure B-2 Proposed measurements on Poincare sphere.

Appendix C

Achromatic Retarder Patent

United States Patent [19]

Chipman et al.

[11] **Patent Number: 4,961,634**

[45] **Date of Patent: Oct. 9, 1990**

[54] **INFRARED ACHROMATIC RETARDER**

[75] Inventors: **Russell Chipman**, Madison; **David Chenault**, Huntsville, both of Ala.

[73] Assignee: **The University of Alabama in Huntsville**, Huntsville, Ala.

[21] Appl. No.: **365,795**

[22] Filed: **Jun. 14, 1989**

[51] **Int. Cl.**[5] **G02B 5/30**

[52] **U.S. Cl.** **350/403**; 350/406; 350/407; 350/1.1

[58] **Field of Search** ..... 350/1.1, 1.4, 403, 404, 350/405, 406, 407, 311, 316; 250/504 R

[56] **References Cited**

U.S. PATENT DOCUMENTS

4,229,073	10/1980	Lotspeich	350/400
4,500,178	2/1985	Yeh	350/404
4,548,479	10/1985	Yeh	350/404
4,772,104	9/1988	Buhrer	350/403

Primary Examiner—Rodney B. Bovernick
Assistant Examiner—R. D. Shafer

Attorney, Agent, or Firm—Oblon, Spivak, McClelland, Maier & Neustadt

[57] **ABSTRACT**

An infrared achromatic waveplate structure having a cadmium sulfide (CdS) plate and a cadmium selenide (CdSe) plate aligned with each other so that the fast axis of the plates are perpendicular to each other, this structure provides a desired retardance of a first orthogonal polarization component with respect to a second orthogonal polarization component of an incident light beam. The thickness of the plates are in a ratio between 0.8:1 and 0.9:1 (CdSe:CdS), an achromatic response with a substantially constant retardance is provided in a wavelength range from 3 to 11 microns. A desired amount of retardance is available by adjusting the thickness of the two plates as long as the ratio of the thicknesses is maintained within the recited value. In particular a quarter wave net retardance of an incident light beam operating between 3 and 11 microns is provided when the cadmium sulfide plate is 1.25 millimeters and the cadmium selenide plate is 1.0666 millimeters.

4 Claims, 1 Drawing Sheet

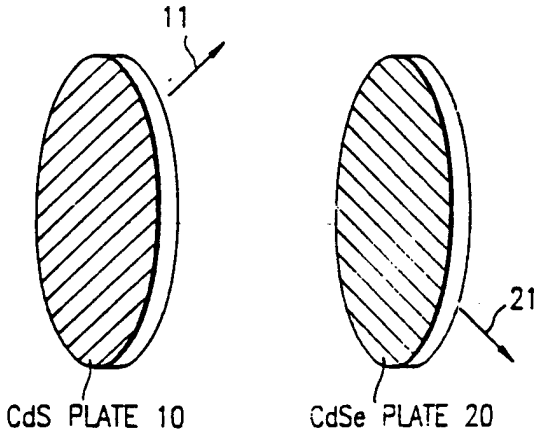

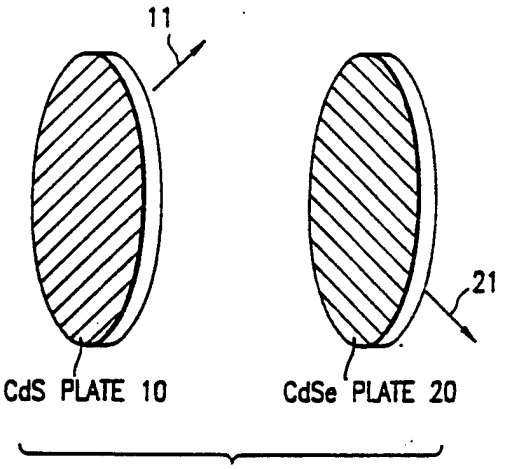
11
21
CdS PLATE 10
CdSe PLATE 20

FIG. 1

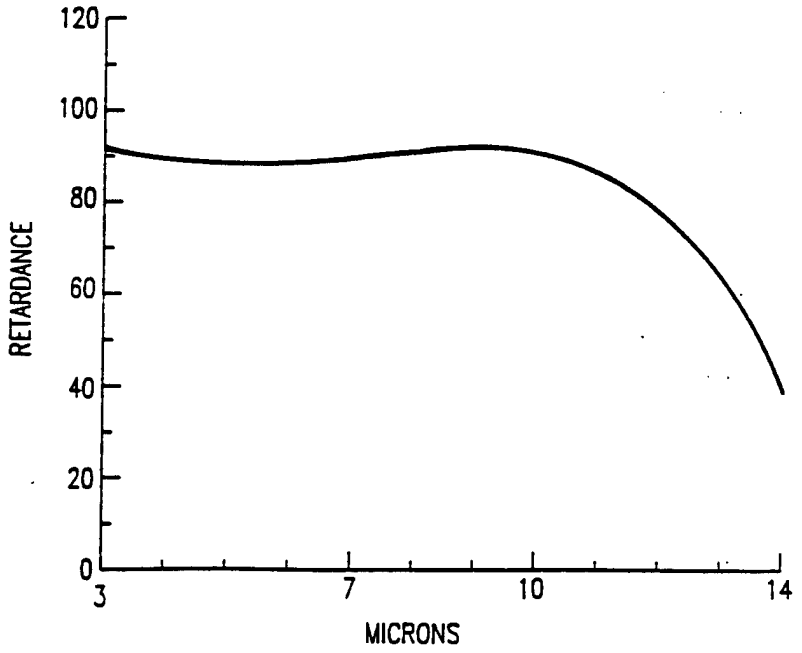
120
100
80
60
40
20
0
RETARDANCE
3
7
10
14
MICRONS

FIG. 2

INFRARED ACHROMATIC RETARDER

BACKGROUND OF THE INVENTION

1. Field of the Invention

The present invention relates to an infrared achromatic waveplate capable of improved response as a function of wavelength in a simple, small and inexpensive configuration of waveplates.

2. Discussion of Background

Many optical systems including those for spectropolarimetry, laser polarimetry, laser spectroscopy, and ellipsometry have a need for converting light between polarization states and a need to analyze polarized light. The design of polarimeters requires polarization elements whose properties satisfy a number of criteria including the very important criteria that the polarization properties need to be substantially constant over a range of wavelength of interest. Additional constraints in this area include a reasonable element size and proper positioning of the light beam exiting from the element and of course the cost of the element.

Liquids and amorphous solids such as glass and crystalline solids have a cubic symmetry which normally show a behavior whereby the speed of light and the index of refraction is independent of the direction of propagation in the medium and is independent of the state of the polarization of the light. These types of elements are said to be optically isotropic. Other crystalline solids, which induce birefringent behavior, are optically anisotropic. Of course, solids may be anisotropic in many of their properties, but it is the optical anisotropy of a material which is used in order to provide the "double refraction" of a beam. The two emerging beams from an optically anisotropic material are plane-polarized beams with their planes of vibration at right angles to each other.

The conversion of light between polarization states and the analysis of polarized light has traditionally involved the use of birefringent materials wherein a light beam incident on a birefringent material is divided into two orthogonal polarization components. A retarder can then shift the phase or in other words retard the phase of one of these two orthogonal polarization components with respect to the other component. In a birefringent material, the index of refraction depends on the polarization state of the light beam.

The most appropriate way that these anisotropic or birefringent materials are used involves the exploiting of the dependency of the index of refraction on the polarization state of the incoming light beam. A phase shift is introduced between the polarization state aligned with the fast axis of the birefringent material, where the index of refraction is the smallest and the polarization state aligned along the slow axis of the material, where the index of refraction is at its highest value.

When plane-polarized light falls at normal incidence on a slab or piece of anisotropic material so that the optic axis is parallel to the face of the slab, the two waves which emerge are plane-polarized at right angles to each other. Because the waves travel through the material at different speeds, there will be a phase difference between the two waves when they emerge from the material. If the material thickness is chosen so that for a particular frequency of light the phase angle or "phase change between the two waves" is 90°, the slab or piece of material is called a quarter-waveplate. If

linearly polarized light is incident on this quarter waveplate with its plane of polarization oriented at ±45° to the fast axis, the emerging light is said to be circularly polarized.

Traditionally then, the proper thickness of the material was chosen in order to obtain the desired retardance. However, these prior art designs are very sensitive to small changes in wavelength of the incident beam and thus are not suitable for many optical systems where broadband light is used.

While other designs have better response as a function of wavelength, they involve complicated, large and expensive devices as for example in a design utilizing a modified Fresnel rhomb which is 4 inches long which of course exceeds the requirements for size.

Still other designs cause the exit beam to be shifted from the path of the incident beam which also makes these designs not appropriate for such polarimeter usage.

Thus, there is a specific need for an achromatic infrared retarder in which the polarization properties of the element is substantially constant over a particular range of wavelength and wherein the elements are small in size and produce a light beam which is properly positioned upon emergence from the element.

SUMMARY OF THE INVENTION

It is the object of the present invention to provide a configuration of two plates made of cadmium sulfide and cadmium selenide respectively with the fast axis of the materials at right angles to each other in order to produce polarization of incident light which is substantially constant over a range of wavelengths.

It is another object of the present invention to provide a retarder which can shift the phase or retard the phase of one of two orthogonal polarization components in such a way that the resultant device is inexpensive, insensitive to changes in wavelength and easy to manufacture.

The structure which accomplishes these objects involves a Cadmium Sulfide (CdS) plate and a Cadmium Selenide (CdSe) plate oriented so that the fast axis of the plates are perpendicular to each other in order to provide a positive retardance from one plate and a negative retardance from the other plate with the net effect providing a desired retardance.

The device according to the present invention provides achromatic response in the wavelength range of from 3–11 microns when the thickness of the plates have a ratio of between 0.8:1 and 0.9:1 (CdSe:CdS).

BRIEF DESCRIPTION OF THE DRAWINGS

A more complete appreciation of the invention and many of the attendant advantages thereof will be readily obtained as the same becomes better understood by reference to the following detailed description when considered in connection with the accompanying drawings, wherein:

FIG. 1 illustrates the structure of the two plates having their fast axis at right angles to each other;

FIG. 2 graphically illustrates the retardance as a function of wavelength of the achromatic retarder of the present invention.

DESCRIPTION OF THE PREFERRED EMBODIMENTS

Referring now to the drawings, and more particularly to FIG. 1 thereof, there is shown an orientation of two plates 10 and 20. The plate 10 is made of Cadmium Sulfide (CdS) and plate 20 is made of Cadmium Selenide (CdSe). These plates have similar birefringent properties as a function of wavelength and the orientation of the two plates is such that the fast axis 11 of plate 10 is at a right angle with respect to the fast axis 21 of plane 20. One of the plates produces a retardance of one polarization state (state 1) with respect to the other state (state 2) while the second plate retards state 2 with respect to state 1. The first plate 10 produces a positive retardance and the second plate 20 produces a negative retardance with the net result being a substantially constant retardance over a broad wavelength range.

By choosing the proper thickness for each plate, a quarter wave retardance occurs over a broad wavelength range as illustrated in FIG. 2. Given the achromatic response for one quarter wavelength retardance, the ratio between the thicknesses of the two plates is computed. Waveplates of other retardances may be constructed by varying the thickness of the plates with the ratio being kept constant.

In order to obtain retardances for various thickness, numerous experiments may be conducted or a program may be utilized to calculate the retardances of birefringent plates with the material properties of CdS and CdSe being entered into the program. For a net retardance of one quarter wave, the thickness of the CdS plate is 1.25 millimeters and the thickness of the CdSe plate is 1.0666 millimeters. This provides a ratio of the CdSe to CdS of 0.853.

The thickness of each of these plates is ideal for fabrication because the single crystals of this size can be grown. Furthermore, the plates are thick enough to retain structural strength.

This design utilizes the materials CdS and CdSe and is specifically used in the mid-infrared region. As a result the device, which is used as a retarder, is an optical component which converts light between the polarization states and by varying the thickness of the plates, while holding the ratio constant, the retardance of a quarter-or half-wave or of any arbitrary value may be fabricated.

The response of these two materials, cadmium sulfide and cadmium selenide, when used together in this manner provided a remarkable improvement in the formation of an achromatic waveplate over a very broad wavelength range. The particular embodiment wherein the ratio of the thickness of the plates is between 0.8:1 and 0.9:1 (CdSe:CdS) provided achromatic response in the wavelength range from 3 to 11 microns.

Although the discussed embodiment utilizes 100% cadmium sulfide and cadmium selenide respectively, composite materials having doped cadmium sulfide or doped cadmium selenide could be used. Materials such as zinc selenide, galium arsenide, mercury, indium, galium, arsenic and zinc could be utilized as additive

materials to either or both of the cadmium sulfide and cadmium selenide waveplates. The criteria for selection and addition of additive materials is controlled by the birefringent characteristics of the resultant composite material. In other words, any material may be added in small amounts as a doping in order to form a composite material for the first and second waveplate as long as the birefringent characteristics of the resulting composite materials is substantially the same as cadmium sulfide alone or cadmium selenide alone for the first or second waveplates.

In order to avoid any reflection losses which occur due to the passage of the light through the four surfaces of the two plates, an anti-reflection coating ma be applied to each of the surfaces of the plates 10 and 20.

Furthermore, a computer program may be substituted for experimentation in order to calculate the retardances of the birefringent plates. The material properties of CdS and CdSe are entered into the program and the various retardances calculated for each material as a function of wavelength.

Obviously, numerous modifications and variations of the present invention are possible in light of the above teachings. It is therefore to be understood that within the scope of the appended claims, the invention may be practiced otherwise then as specifically described herein.

What is claimed as new and desired to be secured by Letters Patent of the United States is:

1. An achromatic retarder for shifting two orthogonal polarization components, with respect to each other, of an incident light beam;

a first waveplate made of substantially cadmium sulfide having a fast axis;

a second waveplate made of substantially cadmium selenide having a fast axis wherein said first and second plates are oriented so that said fast axis of said first plate is at a right angle with respect to said fast axis of said second plate and wherein said first plate produces a retardance of a first polarization state with respect to a second polarization state while said second plate produces a retardance of said second polarization state with respect to said first polarization state to produce a net retardance which has a substantially constant value over a range of wavelength values of interest for said light beam.

2. The retarder according to claim 1 wherein the ratio of the thickness of said second plate with respect to said first plate is in a range of between 0.8:1 and 0.9:1 in order to provide achromatic response in the wavelength range from 3 to 11 microns.

3. The retarder according to claim 1 wherein the thickness of said first plate is 1.25 millimeters and the thickness of said second plate is 1.0666 millimeters and wherein said net retardance of said retarder is one quarter of the wavelength of said incident light beam.

4. The retarder according to claim 1 further comprising anti-reflection coatings provided on both a first and a second surface of each of said first and second plates.

* * * * *

REFERENCES

1. U. Efron, "SLMs key to optical information processing, displays," Optics & Photonics News, Vol. 1 (8), 31 (1990).

2. A. D. Fisher and J. N. Lee, "The current status of two-dimensional spatial light modulator technology," in Optical and Hybrid Computing, H. H. Szu and R. F. Potter eds., Proc. SPIE 634, 352-371 (1986).

3. C. Warde and U. Efron, "Guest editorial: materials and devices for optical information processing," Opt. Eng. 25 (2), 197 (1986).

4. A. A. Ballman et. al., "Research on nonlinear optical materials: an assessment - V. Inorganic materials for frequency conversion," Appl. Opt. 26 (2), 224-227 (1987).

5. Molectron Detector, Inc. for example provides principal transmission spectra.

6. N. A. Clark and S. T. Lagerwald, "Submicrosecond Bistable Electro-optic Switching in Liquid Crystals," Appl. Phys. Letts. 36, 899-901 (1980).

7. K. M. Johnson, M. A. Handschy, and L. A. Pagano-Stouffer, "Optical Computing and Image Processing with Ferroelectric Liquid Crystal," Opt. Eng. 26, 385-391 (1987).

8. M. R. Meadows, M. A. Handschy, and N. A. Clark, "Electro-optic switching using total internal reflection by a ferroelectric liquid crystal," Appl. Phys. Lett. 54 (15), 1392-1396 (1989).

9. R. M. A. Azzam, "Perspectives on Ellipsometry," Ellipsometry: Proc. of Third International Conf. on Ellipsometry, N. M. Bashara, and R. M. A. Azzam eds., North-Holland, Amsterdam, 6-18 (1976).

10. D. H. Goldstein, "Polarization modulation in infrared electro-optic materials," Ph.D. Thesis, University of Alabama in Huntsville (1990).

11. R. M. A. Azzam and N. M. Bashara, Ellipsometry and Polarized Light, North-Holland, Amsterdam (1977).

12. R. A. Chipman, "Polarization analysis of optical systems," Opt. Eng. 28 (2), 90-99 (1989).

13. R. A. Chipman, "Polarization analysis of optical systems II," in Polarization Considerations for Optical Systems II, SPIE 1166, R. A. Chipman ed., 79-94 (1990).

14. D. H. Goldstein, R. A. Chipman, D. B. Chenault, "Spectropolarimetry of Electro-Optical Materials," Polarization Considerations for Optical Systems, SPIE 891, R. A. Chipman ed., 56-73 (1988).

15. W. A. Shurcliff, Polarized Light, Harvard University Press, Cambridge, MA (1961).

16. P. S. Theocaris and E. E. Gdoutos, Matrix Theory of Elasticity, Springer-Verlag, Berlin (1979).

17. D. S. Kliger, J. S. Lewis, C. E. Randall, Polarized Light in Optics and Spectroscopy, Academic Press, New York (1990).

18. A. Yariv and P. Yeh, Optical Waves in Crystals, Wiley and Sons, New York (1984).

19. A. Yariv, Optical Electronics, Holt, Rinehart, and Winston, New York (1985).

20. N. Gerrard, and J. M. Burch, Introduction to Matrix Methods in Optics, John Wiley and Sons, London (1975).

21. E. Hecht and A. Zajac, Optics, Addison-Wesley, Reading, MA (1974).

22. R. A. Chipman, Polarization Aberrations, dissertation, University of Arizona (1987).

23. P. S. Hauge, "Recent Developments in Instrumentation in Ellipsometry," Ellipsometry: Proc. of Fourth International Conf. on Ellipsometry, R. H. Muller, R. M. A. Azzam, and D. E. Aspnes eds., North-Holland, Amsterdam, 108-140 (1980).

24. L. A. Nafie, Nam-Soo Lee, G. Paterlini, and T. B. Freedman, "Polarization Modulation Fourier Transform Infrared Spectroscopy," Mikrochim. Acta, 111, 93-104 (1987).

25. J. Michl and E. W. Thulstrup, Spectroscopy with Polarized Light, VCH Publishers, New York (1986).

26. A. L. Fymat, "High-Resolution Spectropolarimetry: A New Atmospheric Remote Sensor," in Optical Polarimetry: Instrumentation and Applications, R. M. A. Azzam and D. L. Coffeen eds., Proc. SPIE 112, 16-27 (1977).

27. J. O. Stenflo, "The Measurement of Solar Magnetic Fields," Rep. Prog. Phys. 41, 865-907 (1978).

28. J. C. Kemp, "Photoelastic-modulator Polarimeters in Astronomy," in Polarizers and Applications, G. P. Trapani ed., Proc. SPIE 307 (1981).

29. A. L. Fymat, "An Interferometric Approach to the Measurement of Optical Polarization," App. Opt. 9 (5), 1075-1081 (1970).

30. E. B. Hodgdon, "Theory, Design, and Calibration of a uv Spectophotopolarimeter," App. Opt. 4 (11), 1479-1483 (1965).

31. T. G. Baur, L. L. House, and H. K. Hull, "A Spectrum Scanning Stokes Polarimeter," Solar Physics 65, 111-146 (1980).

32. J. C. Kemp, G. D. Henson, C. T. Steiner, and E. R. Powell, "The Optical Polarization of the Sun Measured at a Sensitivity of Parts in Ten Million," Nature 326 (6110), 270-273 (1987).

33. J. O. Stenflo, "Stokes Polarimetry," Proc. Workshop on Small Magnetic Flux Concentrations in the Solar Photosphere, Gottingen, October 1985.

34. J. O. Stenflo, "Measurement of Magnetic Fields and the Analysis of Stokes Profiles," Solar Physics 100, 189-208 (1985).

35. R. W. Lindgren, and T. D. Tarbell, "Video Image Processor on the Spacelab 2 Solar Optical Universal Polarimeter (SL2 SOUP)," in Shuttle Pointing of Electro-optical Experiments, W. Jerkovsky ed., Proc. SPIE 265 (1981).

36. D. P. Gonatas, X. D. Wu, G. Novak, and R. H. Hildebrand, "Systematic Effects in the Measurement of Far-infrared Linear Polarization," App. Opt. 28 (5), 1000-1006 (1989).

37. J. D. Goguen, and W. M. Sinton, "Characterization of Io's Volcanic Activity by Infrared Polarimetry," Science 230, 65-69 (1985).

38. M. Elhanine, R. Farrenq, G. Guelachvili, "Polarization modulation high resolution Fourier transform spectroscopy," App. Opt. 28 (18), 4024-4029 (1989).

39. R. Hilbst, and H. H. Bukow, "Intensity Calibration of an EUV Polarizer Spectrometer Detector System," App. Opt. 28 (10), 1806-1812 (1989).

40. J. P. Krumme, V. Doormann, and C. P. Klages, "Measurement of the magnetooptic properties of bismuth-substituted iron garnet films using piezobirefringent modulation," App. Opt. 23 (8), 1184-1192 (1984).

41. R. Teets, R. Feinberg, T. W. Hansch, and A. L. Schawlow, "Simplification of Spectra by Polarization Labeling," Phys. Rev. Letts. 37 (11), 683-686 (1976).

42. H. Ishida, et. al., "Polarization Modulation FT-IR Reflection Spectroscopy Using a Polarizing Michelson Interferometer," App. Spect. 41 (8), 1288-1294 (1987).

43. H. Seki, K. Kunimatsu, and W. G. Golden, "A Thin-Layer Electrochemical Cell for Infrared Spectroscopic Measurements of the Electrode/Electrolyte Interface," App. Spect. 39 (3), 437-443 (1985).

44. S. T. Wu, U. Efron, and L. D. Hess, "Birefringence measurements of liquid crystals," App. Opt. 23 (21), 3911-3915 (1984).

45. R. M. A. Azzam, "Photopolarimetric measurement of the Mueller matrix by Fourier analysis of a single detected signal," Opt. Lett. 2 (6), 148-150 (1978).

46. P. S. Hauge, "Mueller matrix ellipsometry with imperfect compensators," JOSA 68 (11), 1519-1528 (1978).

47. P. S. Hauge and F. H. Dill, "A Rotating-Compensator Fourier Ellipsometer," Opt. Comm. 14 (4), 431-437 (1975).

48. R. M. A. Azzam, "A simple Fourier photopolarimeter with rotating polarizer and analyzer for measuring Jones and Mueller matrices," Opt. Comm. 25 (2), 137-140 (1978).

49. L. Y. Chen and D. W. Lynch, "Scanning ellipsometer by rotating polarizer and analyzer," Appl. Opt. 26 (24), 5221-5228 (1987).

50. R. M. A. Azzam, "NIRSE: Normal-incidence rotating-sample ellipsometer," Opt. Comm. 20 (3), 405-408 (1977).

51. D. B. Chenault and R. A. Chipman, "Linear diattenuation and retardance measurements in an IR rotating sample spectropolarimeter," submitted to Appl. Opt. (1992).

52. D. E. Aspnes, "Photometric ellipsometer for measuring partially polarized light," JOSA 65 (11), 1274-1278 (1975).

53. G. P. Tolstov, Fourier Series, Richard A. Silverman trans., Dover, New York (1962).

54. M. V. Klein and T. E. Furtak, Optics, 2nd ed., John Wiley and Sons, New York (1986).

55. F. A. Jenkins and H. E. White, Fundamentals of Optics, 4th Edition, McGraw-Hill, New York (1976).

56. S. D. Stearns, Digital Signal Analysis, Hayden Book Co., New Jersey (1975).

57. R. W. Boyd, Radiometry and the Detection of Optical Radiation, Wiley and Sons, New York (1983).

58. Burle Industries, Inc., Electro-Optics Handbook, Burle Technologies, Inc., Lancaster, PA (1974).

59. D. H. Goldstein and R. A. Chipman, "Error Analysis of Mueller Matrix Polarimeters," JOSA A 7 (4), 693-700 (1990).

60. J. C. Zwinkels and C. X. Dodd, "Determination of spectrophotometer polarization and its use in rapid accurate polarized transmission measurements," Appl. Opt. 28 (12), 2381-2388 (1989).

61. D. E. Aspnes, "Effects of component optical activity in data reduction and calibration of rotating-analyzer ellipsometers," JOSA 64 (6), 812-819 (1974).

62. J. B. Breckenridge, "Polarization Properties of a Grating Spectrograph," Appl. Opt. 10, 286 (1971).

63. J. E. Stewart, Infrared Spectroscopy, Experimental methods and techniques, Marcel Decker, Inc., New York (1970).

64. R. J. Bell, Introductory Fourier Transform Spectroscopy, Academic Press, New York (1972).

65. V. Chandrasekharan and H. Demany, "Birefringence of Sapphire, Magnesium Fluoride, and Quartz in the Vacuum Ultraviolet, and Retardation Plates," Appl. Opt. 7 (5), 939-941 (1968).

66. I. Filinski and T. Skettrup, "Achromatic optical compensator-modulator," Appl. Opt. 28 (9), 1720-1726 (1989).

67. P. D. Hale and G. W. Day, "Stability of birefringent retarders," Appl. Opt. 27 (24), 5146-5153 (1988).

68. Carl F. Buhrer, "High-order achromatic quarterwave combination plates and tuners," Appl. Opt. 27 (15), 3166-3169 (1988).

69. R. A. Chipman and D. B. Chenault, U.S. Patent #4,961,634, "Infrared achromatic retarder," October, 1990.

70. J. M. Bennett, "A Critical Evaluation of Rhomb-Type Quarterwave Retarders," Appl. Opt. 9 (9), 2123-2129 (1970).

71. P. A. Clapham, M. J. Downs, and R. J. King, "Some Applications of Thin Films to Polarization Devices," Appl. Opt. 8 (10), 1965-1974 (1969).

72. D. H. Goldstein, R. A. Chipman, D. B. Chenault, "Infrared spectropolarimetry," Opt. Eng. 28 (2), 120-125 (1989).

73. D. B. Chenault and R. A. Chipman, "Infrared spectropolarimetry," in Polarization Considerations for Optical Systems II, R. A. Chipman ed., Proc. SPIE 1166, 254-266 (1989).

74. D. B. Chenault, R. A. Chipman, K. M. Johnson, and D. Doroski, "Infrared linear diattenuation and birefringence spectra of ferroelectric liquid crystals," Appl. Opt. 17 (6), 447-449 (1992).

75. S. G. Lipson and H. Lipson, Optical Physics, Cambridge University Press (1969).

76. R. A. Chipman, "Polarimetric impulse response and polarimetric transfer function for time-sequential polarimeters," in Polarimetry: Radar, Infrared, Visible, Ultraviolet, and X-ray, R. A. Chipman and J. W. Morris eds., Proc. SPIE 1317, 223-241 (1990).

77. I. Abdulhalim, G. Moddel, and K. M. Johnson, "High-speed analog spatial light modulator using a hydrogenated amorphous silicon photosensor and an electroclinic liquid crystal," Appl. Phys. Lett 55 (16), 1603-1605 (1989).

78. British Drug House FLC mixtures available from EM Industries, Inc., 5 Skyline Drive, Hawthorne, NY 10532.

79. S. T. Wu, "Infrared properties of nematic liquid crystals: an overview", Opt. Eng. 26 (2), 120-128 (1987).

80. M. Hareng, G. Assouline, and E. Leiba, "Electrically controlled birefringence in nematic liquid crystals," Appl. Opt. 11, 2920 (1972).

81. R. Chang, "Application of polarimetry and interferometry to liquid crystal research," Mater. Res. Bull. 7, 267 (1972).

82. S. T. Wu, U. Efron, and L. D. Hess, "Infrared birefringence of liquid crystals," Appl. Phys. Lett. 44, 1033-1035 (1984).

83. G. Anderson, I. Pahl, and P. Kells, "Submicrosecond electro-optic switching in the liquid crystal smectic A phase," Appl. Phys. Lett. 51, 640-642 (1987).

84. D. Y. Smith, "Comments on the dispersion relations for the complex refractive index of circularly and elliptically polarized light," JOSA 66 (5), 454-460 (1976).

85. E. M. Aver'yanov et al., "Splitting of polarization absorption bands with a complex vibron structure in the spectra of impurity liquid crystals," Sov. Phys. JETP 63 (1), 57-62 (1986).

86. R. Weil and D. Neshmit, "Temperature coefficients of the indices of refraction and of the birefringence in cadmium sulphide," JOSA 67 (2), 190 - 195 (1977).

87. S. J. Czyzak, R. C. Crane, and T. M. Bieniewski, "Dichroism in essentially pure and activated cadmium sulfide single crystals," JOSA 49 (5), 485 - 488 (1959).

88. T. M. Bieniewski and S. J. Czyzak, "Refractive indices of single hexagonal ZnS and CdS crystals," JOSA 53, 496 - 497 (1963).

89. D. H. Goldstein and R. A. Chipman, "Error Analysis of Mueller Matrix Polarimeters," JOSA A 7 (4), 693 - 700 (1990).

90. Cleveland Crystals, Inc. Data Sheet, Cleveland, Ohio, May 1984.

91. G. C. Bhar, "Refractive index interpolation in phase-matching," Appl. Opt. 15 (2), 305 - 307 (1976).

92. S. A. Abagyan, G. A. Ivanov, A. A. Kartuchina, and G. A. Koroleva, "Spectral dependence of birefringence of CdSe," Sov. Phys. Semi. 5 (8), 1425 - 1426 (1972).

93. S. A. Abagyan, G. A. Ivanov, E. V. Markov, G. A. Koroleva, and N. N. Pogorelova, "Optical properties of CdS with an improved structure," Sov. Phys. Semi. 5 (10), 1751 - 1752 (1972).

94. SigmaPlot, Jandel Scientific (1991).

95. G. C. Bhar and G. Ghosh, "Temperature-dependent Sellmeier coefficients and coherence lengths for some chalcopyrite crystals," JOSA 69 (5), 730 - 733 (1979).

96. B. Jensen and A. Torabi, "Refractive index of hexagonal II-VI compounds CdSe, CdS, and $CdSe_xS_{1-x}$," JOSA B 3 (6), 857 - 863 (1986).

97. Stephen C. McClain, "Birefringent polarization ray tracing: theory and applications," Ph.D. thesis, Cornell University (1992).

98. Herman E. Reedy, II-VI, Inc., personal communication, October, 1992.

99. A. G. DeBell, E. L. Dereniak, J. Harvey, J. Nissley, J. Palmer, A. Selvarajan, and W. L. Wolfe, "Cryogenic refractive indices and temperature coefficients of cadmium telluride from 6 μm to 22 μm," Appl. Opt. 18 (18), 3114-3115 (1979).

100. C. J. Johnson, G. H. Sherman, and R. Weil, "Far infrared measurements fo the dielectric properties of GaAs and CdTe at 300K and at 8K," Appl. Opt. 8, 1667 (1969).

101. Gary L. Herrit and Herman E. Reedy, "Electro-optic coefficient for gallium arsenide and cadmium telluride modulator rods," in Optical Materials: Processing and Science, C. Ortiz and D. B. Poker eds. Proc. Mat. Res. Soc. 152 (1989).

102. G. L. Herrit and H. E. Reedy, "Methods for reducing stress birefringence in cadmium telluride electro-optic modulators," J. Appl. Phys. 65 (1), 393-395 (1989).

103. G. L Herrit, II-VI, Inc., personal communication, October, 1992.

104. Gilbert Strang, Linear Algebra and Its Applications, Academic Press, New York (1980).

105. Philip R. Bevington, Data Reduction and Error Analysis for the Physical Sciences, McGraw-Hill, New York (1969).

106. Tod. F. Schiff, J. C. Stover, Brent D. Swimley, and Donald R. Bjork, "Mueller matrix measurements of scattered light," in Polarization Analysis and Measurement, Dennis H. Goldstein and Russell A. Chipman eds., Proc. SPIE 1746, in press (1992).

107. S. Y. Lu and R. A. Chipman, "Generalized diattenuation and retardance for inhomogeneous polarization elements," in Polarization Analysis and Measurement, D. H. Goldstein and R. A. Chipman eds., Proc. SPIE 1746, in press (1992).

11/17/92

Dr. Warren Peele
Program Director
Air Force Laboratory Graduate Fellowship Program
SCEEE
11th & Massachesetts Ave.
St. Cloud, FL 34769

Dr. Dr. Peele:

I have completed my dissertation and my doctoral program. I will receive my doctorate on December 13th from the University of Alabama in Huntsville. I am pleased to enclose my dissertation and a copy of a paper that has been accepted for publication in Applied Optics. I would like to thank you and express my appreciation to the Air Force for their support of my doctoral research program.

I have accepted a postdoctoral fellowship through the Office of Naval Technology and will begin by postdoc at the Naval Research Laboratory on December 1st. My new address is given below. If you have any questions or comments, don't hesitate to get in touch with me there. Thank you.

Sincerely,

David Chenault

David Chenault
Code 6522
Optical Sciences Division
Naval Research Laboratory
Washington, DC 20375-5000

after December 1, 1992

NOV 23 1992